



Search for higgsinos in compressed mass spectra using low-momentum tracks in pp collisions at $\sqrt{s} = 13$ TeV with the ATLAS detector

The ATLAS Collaboration

This paper presents two searches for the electroweak production of higgsinos with compressed mass spectra using 140 fb^{-1} of $\sqrt{s} = 13$ TeV proton–proton collision data collected by the ATLAS experiment at the Large Hadron Collider. Events are required to feature an energetic jet, large missing transverse momentum, and at least one low-momentum charged particle that serves as a candidate higgsino decay product. In the first search, targeting higgsino mass splittings in the range of 0.3–1 GeV, the higgsinos are expected to predominantly decay into pions that are identified as low-momentum charged particles with large transverse impact parameters due to the long higgsino lifetime ($c\tau \approx O(0.1\text{--}1 \text{ mm})$). The second search targets larger mass splittings in the range of 1–3 GeV, where the higgsinos are expected to decay promptly into low-momentum leptons, one of which is identified by dedicated low-momentum electron or muon taggers based on neural networks utilising tracking and calorimeter information. No significant excess above the Standard Model prediction is observed in either search and the results are used to set lower limits on the masses of the higgsino-like charginos and neutralinos within a simplified model. Together, these searches exclude chargino masses below 126 GeV at 95% confidence level for mass splittings between the chargino and lightest neutralino in the range of 0.3–2 GeV, representing the first ATLAS constraints in this parameter space and surpassing the limits previously set by the LEP experiments.

1 Introduction

Supersymmetry (SUSY) [1–6] proposes a symmetry between bosons and fermions, thus predicting new particles that have identical quantum numbers as their Standard Model (SM) partners except for spin: SM fermions have bosonic superpartners and SM bosons have fermionic superpartners. In SUSY models with R -parity conservation [7], the lightest SUSY particle (LSP) must be stable and, if electrically neutral and weakly interacting, can be a viable dark matter candidate [8, 9]. In addition, SUSY has the potential of providing gauge coupling unification [10–13] and a solution to the fine-tuning problem of the Higgs boson mass [14, 15] and remains as a leading candidate of physics beyond the SM.

In the minimal supersymmetric extension of the SM (MSSM) [16, 17], the bino, wino, and higgsino fields are the fermionic partners of the $SU(2) \times U(1)$ gauge fields in the SM and the two complex scalar Higgs doublets, respectively. The bino, wino, and higgsino fields are collectively referred to as ‘electroweakinos,’ which mix to form mass eigenstates known as neutralinos $\tilde{\chi}_i^0$ ($i = 1, 2, 3, 4$) and charginos $\tilde{\chi}_j^\pm$ ($j = 1, 2$) with the subscripts indicating increasing mass. The masses of the bino, wino, and higgsino fields are parameterised in terms of M_1 , M_2 , and μ , respectively. For large values of $\tan\beta$, representing the ratio between the vacuum expectation values of the two Higgs doublets, the phenomenology of the electroweakinos is driven by these three mass parameters.

This paper presents searches targeting SUSY scenarios in which the masses of the higgsino states are much smaller compared with the masses of the bino and wino states (i.e. $|\mu| \ll M_1, M_2$). Such scenarios are motivated by the role of μ in naturalness arguments [14, 15], which favour values of $|\mu|$ near the weak scale [18–21]. In these scenarios, the lightest SUSY particles are a triplet of higgsino-like states ($\tilde{\chi}_1^0, \tilde{\chi}_1^\pm, \tilde{\chi}_2^0$) having ‘compressed mass spectra’, with minimal mass splittings of about 300 MeV due to radiative corrections. Larger mass splitting values of a few GeV can be generated depending on the values of M_1 and M_2 relative to μ . Hereinafter, the LSP is assumed to be the lightest neutralino ($\tilde{\chi}_1^0$) and the higgsino-like mass eigenstates are referred to as ‘higgsinos’ for simplicity.

Various ATLAS and CMS searches were conducted to explore this regime of compressed mass spectra, primarily with the use of ‘tracks’ that represent the reconstructed trajectories of charged particles in the inner detector. Highly compressed scenarios with $\Delta m(\tilde{\chi}_1^\pm, \tilde{\chi}_1^0) \lesssim 300\text{--}400$ MeV were searched for using the ‘disappearing track’ signature that targets the long-lived ($c\tau > \mathcal{O}(10$ mm)) $\tilde{\chi}_1^\pm$. In these scenarios, a significant fraction of the produced $\tilde{\chi}_1^\pm$ particles can traverse several silicon layers of the inner detector before decaying into an invisible $\tilde{\chi}_1^0$ and a low-momentum (‘soft’) charged pion (i.e. $\tilde{\chi}_1^\pm \rightarrow \tilde{\chi}_1^0 \pi^\pm$) that is not reconstructed, leading to the distinct signature of a charged particle track disappearing within the inner detector [22–25]. Scenarios with $\Delta m(\tilde{\chi}_1^\pm, \tilde{\chi}_1^0) \approx 300\text{--}900$ MeV, and thus shorter $\tilde{\chi}_1^\pm$ lifetimes ($c\tau \approx \mathcal{O}(0.1\text{--}1$ mm)), were searched for using a ‘mildly displaced track’ signature [26], in which the $\tilde{\chi}_1^\pm$ decay occurs before reaching the tracking detector and instead, the charged pion is reconstructed as a soft track with a large transverse impact parameter [27], denoted by d_0 and defined as the shortest distance between the track and the beam line in the transverse plane. Scenarios with mass splittings larger than approximately 1.5 GeV, corresponding to $c\tau < \mathcal{O}(0.1$ mm), were explored by searches targeting low-momentum prompt lepton¹ signatures from $\tilde{\chi}_2^0 \rightarrow \tilde{\chi}_1^0 Z^* \rightarrow \tilde{\chi}_1^0 \ell^+ \ell^-$ [28–32]. Despite these efforts, the strongest constraints on scenarios with $\Delta m(\tilde{\chi}_1^\pm, \tilde{\chi}_1^0) \approx 0.9\text{--}1.5$ GeV are still set by the LEP experiments [33]. Additionally, ATLAS has performed a scan of the electroweak sector of the phenomenological MSSM [34, 35] that highlights the continued viability of higgsinos in this mass regime after accounting for constraints

¹ The term ‘lepton’ in this paper refers to electrons or muons and does not include neutrinos and τ -leptons unless otherwise specified.

from previous Run-2 searches, flavour physics observables, precision electroweak measurements, and the observed dark matter relic density [36].

The searches in this paper use 140 fb^{-1} of proton–proton (pp) collision data at a centre-of-mass energy $\sqrt{s} = 13 \text{ TeV}$, collected by the ATLAS experiment [37] from 2015 to 2018 at the CERN Large Hadron Collider (LHC). The pair production of higgsinos via electroweak interactions is assumed, with subsequent decays into a stable $\tilde{\chi}_1^0$, the LSP, and SM particles. Simplified SUSY models [38–40] are used to optimise the searches and interpret the results.

Two searches are designed to identify at least one of the higgsino decay products as a low-momentum track using machine learning techniques, which are adopted to search a range of mass splitting scenarios of the higgsinos. The first search targets smaller mass splittings ($\Delta m(\tilde{\chi}_1^\pm, \tilde{\chi}_1^0) \approx 0.3\text{--}1 \text{ GeV}$) using event signatures similar to the one employed in Ref. [27], where soft pion tracks with large d_0 are identified as the long-lived higgsino decay product candidates. In contrast to this previous search, the sensitivity is enhanced using two dedicated neural-network classifiers: one exploiting the kinematic information of individual tracks (referred to as the ‘track-level’ neural network) and the other exploiting global kinematic observables of the event (referred to as the ‘event-level’ neural network) to provide discrimination between signal and SM background processes. The second search targets slightly larger mass splittings ($\Delta m(\tilde{\chi}_1^\pm, \tilde{\chi}_1^0) \approx 1\text{--}3 \text{ GeV}$) by using dedicated neural-network-based soft-electron and -muon identification algorithms, or ‘taggers’, to identify the leptons from the $\tilde{\chi}_2^0 \rightarrow Z^*(\rightarrow \ell^+\ell^-)\tilde{\chi}_1^0$ decays. These advanced soft-lepton taggers extend the identification of electrons and muons to lower transverse momenta than what is achievable with the existing ATLAS algorithms, granting the ability to search for new physics in this regime of mass splittings.

The paper is structured as follows: Section 2 highlights the analysis strategies of the two searches in further detail. Section 3 provides a brief overview of the ATLAS detector. Details of the data and simulated event samples used in the analyses are given in Section 4. The object reconstruction and identification methods are presented in Section 5. The event selection strategies and signal region definitions are outlined in Section 6. The background estimation methods are discussed in Section 7, followed by a summary of systematic uncertainties in Section 8. Finally, the search results and their statistical interpretations are presented in Section 9, followed by the conclusion in Section 10.

2 Analysis strategy

Two search strategies are employed in this paper to search for the direct production of higgsinos that feature small mass splittings between the $\tilde{\chi}_1^0$ LSP and the slightly heavier $\tilde{\chi}_2^0$ and $\tilde{\chi}_1^\pm$ particles. They are referred to as the ‘displaced track’ and the ‘one-lepton and one-track (1 ℓ 1T).’ In this regime, the transverse momenta (p_T) of the SM particles arising from the $\tilde{\chi}_2^0$ and $\tilde{\chi}_1^\pm$ decays are well below the ATLAS trigger thresholds. Additionally, the signal processes are expected to result in two undetected $\tilde{\chi}_1^0$ particles that are typically back-to-back in the transverse plane, therefore producing only a small amount of missing transverse momentum (with magnitude denoted by E_T^{miss}), defined as the negative vector sum of the transverse momenta of all reconstructed particles in the event. In such cases, the missing transverse momentum triggers remain inefficient. Both of the searches therefore target events in which the higgsinos are produced in association with a high- p_T jet from initial-state radiation (ISR), which provides a boost to the higgsinos in the direction opposite to that of the ISR jet in the transverse plane. While reducing the signal acceptance, the boost from the ISR jet serves to increase the p_T of the two $\tilde{\chi}_1^0$ particles and align their directions in the transverse plane, thereby increasing the E_T^{miss} in the event. The large E_T^{miss} then

allows the E_T^{miss} trigger to be highly efficient and provides important discrimination between the signal and SM background processes.

In addition to this common selection, each search attempts to reconstruct the soft SM particles from the $\tilde{\chi}_2^0$ and $\tilde{\chi}_1^\pm$ decays to further reduce the large SM backgrounds. In contrast to previous ATLAS searches for higgsino-like LSPs with compressed mass spectra, the identification of these soft decay products, and the discrimination between signal and SM background processes, are performed using several dedicated neural network classifiers.

The first, ‘displaced track’ search, targets models in which $\Delta m(\tilde{\chi}_1^\pm, \tilde{\chi}_1^0) \approx 0.3\text{--}1$ GeV, where the dominant decay mode of the charged higgsino is expected to be $\tilde{\chi}_1^\pm \rightarrow \pi^\pm \tilde{\chi}_1^0$ [41] and the decay length of this particle is $\mathcal{O}(0.1\text{--}1$ mm), i.e. well before reaching the ATLAS tracking detector. The charged pions from these decays can be identified as low-transverse-momentum tracks, typically having $p_T < 5$ GeV, with moderately large $|d_0|$ relative to the beam line. An example diagram showing $\tilde{\chi}_1^\pm \tilde{\chi}_1^0$ production in association with an ISR jet is shown in Figure 1(a), where the $\tilde{\chi}_1^\pm$ decays into a charged pion and the $\tilde{\chi}_1^0$ LSP. The displaced track search leverages two fully connected neural networks to discriminate between the signal and SM background processes. The first network uses tracking information to identify tracks that are consistent with arising from the decay of a moderately long-lived $\tilde{\chi}_1^\pm$, while the second network uses event-level information such as the jet kinematics and missing transverse momentum to provide additional discriminating power. The output scores of these networks are used to define the analysis regions, as described in Section 6.1. The estimate of the SM backgrounds, which are largely represented by $Z(\rightarrow \nu\bar{\nu}) + \text{jets}$ and $W^\pm(\rightarrow \tau^\pm\nu_\tau) + \text{jets}$ processes, is performed using simulation, with the normalisations of the dominant backgrounds being constrained in dedicated control regions, as described in Section 7.1.

The second, ‘1 ℓ 1T’ search, is designed to have sensitivity to models with larger mass splittings where $2 \text{ GeV} \lesssim \Delta m(\tilde{\chi}_2^0, \tilde{\chi}_1^0) = 2\Delta m(\tilde{\chi}_1^\pm, \tilde{\chi}_1^0) \lesssim 5$ GeV. Here, the $\tilde{\chi}_1^\pm$ and $\tilde{\chi}_2^0$ are assumed to decay promptly into off-shell SM gauge bosons and the $\tilde{\chi}_1^0$ LSP: $\tilde{\chi}_1^\pm \rightarrow W^{*\pm} \tilde{\chi}_1^0$ and $\tilde{\chi}_2^0 \rightarrow Z^* \tilde{\chi}_1^0$. The search targets events featuring two electrons or muons with opposite electric charges from the Z^* decay, where one of the leptons is identified using the standard ATLAS identification algorithms, defined in Section 5, and the other is identified using dedicated soft-electron and soft-muon taggers based on deep neural networks that were developed for this search. These taggers use charged particle tracks and energy deposits in the electromagnetic calorimeter to significantly increase the identification efficiency for electrons and muons with $p_T \in [0.5, 5]$ GeV relative to standard identification methods, as described in Section 5.1. Figure 1(b) shows an example diagram of $\tilde{\chi}_1^\pm \tilde{\chi}_2^0$ production in association with an ISR jet where the heavier higgsinos decay into an off-shell W/Z boson and the $\tilde{\chi}_1^0$ LSP. To further enhance the sensitivity to higgsino production, the search employs a parameterised neural network (pNN) [42] to provide discrimination between the signal and SM background processes. The parameterisation is performed relative to $\Delta m(\tilde{\chi}_2^0, \tilde{\chi}_1^0)$, the parameter of the benchmark scenarios that has a significant impact on the signal event kinematics. The details of the event selection are given in Section 6.2. The dominant SM backgrounds in which the lepton-tagged track is not a real lepton, dominated by $W^\pm + \text{jets}$ processes, are determined by data-driven methods, while the residual SM backgrounds featuring a real lepton-tagged track are estimated by using simulation, as described in Section 7.2.

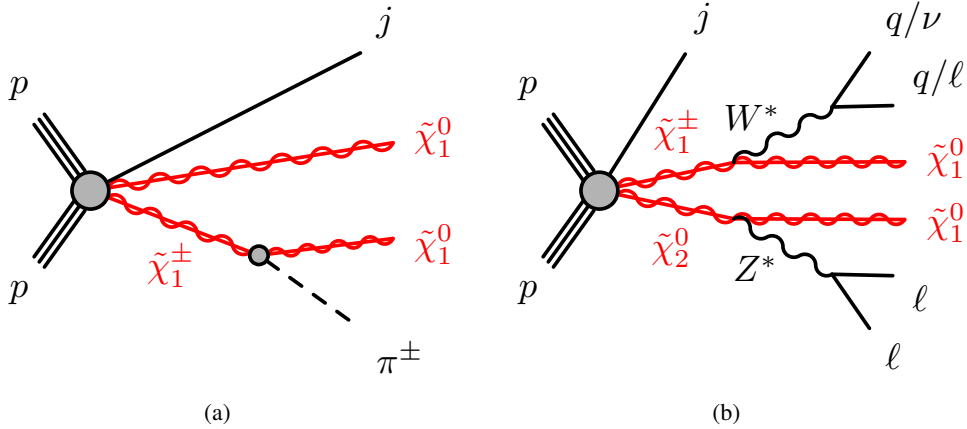


Figure 1: Example diagrams for the targeted signal processes featuring a jet (j) from initial-state radiation for (a) the displaced track search and (b) the $1\ell 1T$ search. While only the $\tilde{\chi}_1^0\tilde{\chi}_1^\pm$ ($\tilde{\chi}_2^0\tilde{\chi}_1^\pm$) diagram is shown for the displaced track ($1\ell 1T$) search, the additional production processes described in Section 4 are considered as well.

3 ATLAS detector

The ATLAS detector [37] at the LHC covers nearly the entire solid angle around the collision point.² It consists of an inner tracking detector surrounded by a thin superconducting solenoid, electromagnetic and hadronic calorimeters, and a muon spectrometer incorporating three large superconducting air-core toroidal magnets.

The inner-detector system is immersed in a 2 T axial magnetic field and provides charged-particle tracking in the range of $|\eta| < 2.5$. It consists of a high-granularity silicon pixel detector, a silicon microstrip detector (SCT), and a transition radiation straw-tube tracker (TRT), each spanning a sensitive radial distance from the interaction point of 33–150 mm, 299–560 mm, and 563–1066 mm, respectively [43]. The barrel (each endcap) consists of four (three) pixel layers, four (nine) double-layers of single-sided silicon microstrips, and 73 (160) layers of TRT straws. The pixel detector covers the vertex region and typically provides four measurements per track, the first hit generally being in the insertable B-layer (IBL) installed before Run 2 [44, 45]. The smaller radius and the reduced pixel size of IBL results in improvements of both the transverse and longitudinal impact parameter resolutions. The d_0 resolution reaches ~ 0.09 mm for tracks with $p_T = 1$ GeV [46]. The SCT usually provides eight measurements, each corresponding to a single side of the double-layered strips, per track. The TRT enables radially extended track reconstruction up to $|\eta| = 2.0$. As electrons tend to have higher relativistic gamma factors and thus higher probabilities of inducing transition radiation compared with other particles, the TRT is also capable of providing electron identification information based on the fraction of hits (typically 30 in total) above a higher energy-deposit threshold.

The calorimeter system covers the pseudorapidity range $|\eta| < 4.9$. Within the region $|\eta| < 3.2$, electromagnetic calorimetry is provided by barrel and endcap high-granularity lead/liquid-argon (LAr)

² ATLAS uses a right-handed coordinate system with its origin at the nominal interaction point (IP) in the centre of the detector and the z -axis along the beam pipe. The x -axis points from the IP to the centre of the LHC ring, and the y -axis points upwards. Polar coordinates (r, ϕ) are used in the transverse plane, ϕ being the azimuthal angle around the z -axis. The pseudorapidity is defined in terms of the polar angle θ as $\eta = -\ln \tan(\theta/2)$ and is equal to the rapidity $y = \frac{1}{2} \ln \left(\frac{E+p_z}{E-p_z} \right)$ in the relativistic limit. Angular distance is measured in units of $\Delta R \equiv \sqrt{(\Delta y)^2 + (\Delta\phi)^2}$.

calorimeters, with an additional thin LAr presampler covering $|\eta| < 1.8$ to correct for energy loss in material upstream of the calorimeters. Hadronic calorimetry is provided by the steel/scintillator-tile calorimeter, segmented into three barrel structures within $|\eta| < 1.7$, and two copper/LAr hadronic endcap calorimeters. The solid angle coverage is completed with forward copper/LAr and tungsten/LAr calorimeter modules optimised for electromagnetic and hadronic energy measurements, respectively. The electromagnetic calorimeters consist of three main layers and the presampler layer. The hadronic calorimeters consist of three (four) layers in the barrel (endcap) regions, providing sufficient containment of hadronic showers.

The muon spectrometer comprises separate trigger and high-precision tracking chambers measuring the deflection of muons in a magnetic field generated by the superconducting air-core toroidal magnets. The field integral of the toroids ranges between 2.0 and 6.0 T m across most of the detector. Three layers of precision chambers, each consisting of layers of drift tubes, cover the region $|\eta| < 2.7$, complemented by cathode-strip chambers in the forward region, where the background is highest. The muon trigger system covers the range $|\eta| < 2.4$ with resistive-plate chambers in the barrel, and thin-gap chambers in the endcap regions.

The luminosity is measured mainly by the LUCID-2 [47] detector that records Cherenkov light produced in the quartz windows of photomultipliers located close to the beampipe.

Events are selected by the first-level trigger system implemented in custom hardware, followed by selections made by algorithms implemented in software in the high-level trigger [48]. The first-level trigger accepts events from the 40 MHz bunch crossings at a rate below 100 kHz, which the high-level trigger further reduces to record complete events to disk at about 1.25 kHz.

A software suite [49] is used in data simulation, in the reconstruction and analysis of real and simulated data, in detector operations, and in the trigger and data acquisition systems of the experiment.

4 Data and simulated event samples

The considered data sample amounts to 140 fb^{-1} of $\sqrt{s} = 13 \text{ TeV}$ pp collision data recorded by the ATLAS detector from 2015–2018 with an uncertainty of 0.83% in the integrated luminosity [50]. The average number of interactions per bunch-crossing in the data sample is 33.7 [51]. The data are selected using missing transverse momentum triggers [52] that use different trigger thresholds depending on the data-taking periods, resulting in an efficiency of more than 95% for events with offline-calibrated $E_{\text{T}}^{\text{miss}}$ greater than 200 GeV. Additionally, single-electron and single-muon triggers [53, 54] are employed to collect a sample of events that are used to constrain SM backgrounds involving the production of W^{\pm} or Z bosons, as described in Section 7.1.

Monte Carlo (MC) simulation samples are produced for the signal and SM background processes to estimate their event yields and associated systematic uncertainties. The SM backgrounds in the searches are determined from both the data-driven methods and the MC simulation, as described in Section 7. While the details of the signal and SM background MC simulation are given below, both of the sets of samples undergo the same procedure to include the effects of multiple pp interactions in the same and neighbouring bunch crossings (pile-up). In each case, the simulated hard-scattering events are overlaid with inelastic pp collision events generated with PYTHIA 8.186 [55] using the NNPDF2.3LO set of parton distribution functions (PDF) [56] and the A3 set of tuned parameters [57]. Weights are then applied to the simulated events to match the pile-up distribution observed in the data and the detector response is simulated using the ATLAS simulation framework [58] based on GEANT4 [59]. The full detector simulation is used for the

SM background samples, while the signal samples use either this full detector simulation or the ATLAS fast simulation that relies on a parameterisation of the calorimeters, as detailed below.

Dedicated signal MC samples consisting of direct higgsino production are simulated for the displaced track and $1\ell 1T$ searches to optimise the event selections and interpret the results in the context of the simplified model. Since the $1\ell 1T$ search targets the soft leptons from the $\tilde{\chi}_2^0 \rightarrow Z^*(\rightarrow \ell^+\ell^-)\tilde{\chi}_1^0$ decays, the $\tilde{\chi}_2^0\tilde{\chi}_1^\pm$ and $\tilde{\chi}_2^0\tilde{\chi}_1^0$ production modes are simulated, while the samples used for the displaced track search also include the $\tilde{\chi}_1^0\tilde{\chi}_1^\pm$ and $\tilde{\chi}_1^+\tilde{\chi}_1^-$ processes. In each case, the $\tilde{\chi}_1^0\tilde{\chi}_1^0$ and $\tilde{\chi}_2^0\tilde{\chi}_2^0$ production modes are ignored due to their negligible production cross-sections when the $\tilde{\chi}_1^0$ and $\tilde{\chi}_2^0$ are higgsino-like states. In the simplified model considered here, the $\tilde{\chi}_1^\pm$ mass is set to be halfway between the neutralino masses, such that $\Delta m(\tilde{\chi}_2^0, \tilde{\chi}_1^0) = 2\Delta m(\tilde{\chi}_1^\pm, \tilde{\chi}_1^0)$. The MC samples are generated at leading-order (LO) with MADGRAPH5_AMC@NLO 2.9.5 [60] for the displaced track search and version 2.9.3 for the $1\ell 1T$ search using the NNPDF2.3LO [56] PDF set and including up to two additional partons in the matrix element calculation. The simulated events for the displaced track search and the $1\ell 1T$ search are then interfaced with PYTHIA 8.306 [61] and PYTHIA 8.245 [62], respectively, to model the parton shower, hadronisation, and underlying event using the A14 set of tuned parameters [63]. Matching between the matrix element and parton shower jets is performed using the CKKW-L scheme [64] with the matching scale set to 15 GeV. At least one parton in the final state is required to have a transverse momentum greater than 50 GeV to enforce the ISR topology targeted by both of the searches. The decays of b - and c -hadrons are modelled by EVTGEN 1.7.0 [65].

For the signal samples used by the $1\ell 1T$ search, the branching fractions for the $\tilde{\chi}_2^0 \rightarrow Z^*\tilde{\chi}_1^0$ and $\tilde{\chi}_1^\pm \rightarrow W^{\pm*}\tilde{\chi}_1^0$ are set to 100% and the higgsinos are decayed with MADSPIN [66] to account for spin correlations effects. The leptonic branching fractions of the $\tilde{\chi}_2^0 \rightarrow Z^*\tilde{\chi}_1^0$, typically 5% each for $\tilde{\chi}_2^0 \rightarrow e^+e^-\tilde{\chi}_1^0$ and $\tilde{\chi}_2^0 \rightarrow \mu^+\mu^-\tilde{\chi}_1^0$, are calculated with SUSY-HIT [67] for different $\Delta m(\tilde{\chi}_2^0, \tilde{\chi}_1^0)$ values and incorporated in the signal yield calculation. The higgsino branching fractions in the samples used by the displaced track search are calculated following the prescription in Ref. [41], which accounts for the mass splitting between the heavier $\tilde{\chi}_2^0/\tilde{\chi}_1^\pm$ and the $\tilde{\chi}_1^0$. For $\Delta m(\tilde{\chi}_1^\pm, \tilde{\chi}_1^0) = 0.5$ GeV, the branching fraction for $\tilde{\chi}_1^\pm \rightarrow \pi^\pm\tilde{\chi}_1^0$ is approximately 80%, with the remaining 20% corresponding to $\tilde{\chi}_1^\pm \rightarrow e^\pm/\mu^\pm\nu\tilde{\chi}_1^0$. In the simplified model, this corresponds to $\Delta m(\tilde{\chi}_2^0, \tilde{\chi}_1^0) = 1$ GeV, for which the dominant branching fractions are approximately 30% for each of the $\tilde{\chi}_2^0 \rightarrow \pi^0\tilde{\chi}_1^0$, $\tilde{\chi}_2^0 \rightarrow \pi^+\pi^-\tilde{\chi}_1^0$, and $\tilde{\chi}_2^0 \rightarrow \nu\bar{\nu}\tilde{\chi}_1^0$ processes. In addition to the branching fractions, the mass splitting between the higgsinos determines the $\tilde{\chi}_1^\pm$ and $\tilde{\chi}_2^0$ lifetimes, where smaller mass splittings result in longer lifetimes and flight lengths. The higgsino decays for these samples are performed using PYTHIA and the higgsino lifetimes are determined by the mass splitting according to the prescription in Ref. [41].

The higgsino production cross-sections and uncertainties are calculated using RESUMMINO 2.0.1 at NLO+NLL precision [68–75] using an envelope of the CTEQ6.6 [76] and MSTW2008nlo90cl [77] PDF sets. The uncertainties originate primarily from QCD renormalisation and factorisation scales. Taking an example with $m(\tilde{\chi}_2^0) = 102$ GeV, $m(\tilde{\chi}_1^\pm) = 101$ GeV, and $m(\tilde{\chi}_1^0) = 100$ GeV, the cross-section values are 5.3 ± 0.2 pb, 3.2 ± 0.1 pb, 5.5 ± 0.2 pb and 2.9 ± 0.1 pb for $\tilde{\chi}_2^0\tilde{\chi}_1^\pm$, $\tilde{\chi}_2^0\tilde{\chi}_1^0$, $\tilde{\chi}_1^0\tilde{\chi}_1^\pm$ and $\tilde{\chi}_1^+\tilde{\chi}_1^-$ production, respectively. The samples used for the $1\ell 1T$ search use the full detector simulation, while those used for the displaced track search use the ATLAS fast simulation as its analysis signature is less dependent to calorimeter responses.

The SM background processes are simulated using a variety of MC generators, with Table 1 providing a summary of the matrix element and parton shower configurations as well as the accuracy of the cross-section

Table 1: A summary of the configurations used to generate the MC samples for the SM background processes. Starting from the second column, the table provides the generators used for the matrix element, the generators used for the parton shower (PS), the order in α_s used to determine the production cross-section, the tune for the underlying event, the PDF set used for the matrix element calculation, and the PDF set used for the parton shower. The symbol V is used to denote the W and Z vector bosons.

| Physics process | Generator | Parton shower | Cross-section | Tune | PDF (generator) | PDF (PS) |
|-------------------------|----------------------------|------------------------------|---------------------|--------------|-------------------|-----------------|
| $V + \text{jets}$ | SHERPA 2.2.11 [80] | SHERPA 2.2.11 | NLO [81–84] | Default [85] | NNPDF3.0NNLO [78] | NNPDF3.0NNLO |
| Diboson (VV) | SHERPA 2.2.1, 2.2.2 | SHERPA 2.2.1, 2.2.2 [86, 87] | NLO | Default | NNPDF3.0NNLO | NNPDF3.0NNLO |
| $t\bar{t}$ | PowHEG Box v2 [88–91] | PYTHIA 8.230 [62] | NNLO+NNLL [92–98] | A14 [63] | NNPDF3.0NLO [78] | NNPDF2.3LO [56] |
| Single-top, s and t | PowHEG Box v2 [89–91, 99] | PYTHIA 8.230 | NLO+NNLL [100, 101] | A14 | NNPDF3.0NLO | NNPDF2.3LO |
| tW | PowHEG Box v2 [89–91, 102] | PYTHIA 8.230 | NLO+NNLL | A14 | NNPDF3.0NLO | NNPDF2.3LO |
| Multijets | PYTHIA 8.230 | PYTHIA 8.230 | LO | A14 | NNPDF2.3LO | NNPDF2.3LO |
| $\gamma + \text{jets}$ | SHERPA 2.2.2 | SHERPA 2.2.2 | NLO | Default | NNPDF3.0NNLO | NNPDF3.0NNLO |

calculation used for each of the background samples. The dominant sources of SM backgrounds for both the displaced track and the $1\ell 1T$ searches arise from vector boson production with subsequent leptonic decays, in association with at least one high- p_T jet. These processes are simulated using SHERPA 2.2.11 with the NNPDF3.0NNLO PDF set [78], where the matrix element calculation includes up to two additional partons at NLO accuracy and up to five additional partons at LO accuracy. Minor backgrounds arise from the production of diboson pairs ($VV = WW, ZZ, WZ$), top quarks ($t\bar{t}$, single- t in the s , t , and tW channels), multijets, and $\gamma + \text{jets}$. The diboson samples are modelled with either SHERPA version 2.2.1 or 2.2.2, depending on the specific process, at NLO accuracy with the NNPDF3.0NNLO PDF set. The $t\bar{t}$, single- t and tW backgrounds are simulated using PowHEG Box v2 for the matrix element and PYTHIA 8.230 for the parton shower, using the NNPDF3.0NLO and NNPDF2.3LO PDF sets, respectively. The diagram removal scheme [79] is used to account for interference effects between the $t\bar{t}$ and tW processes. Multijet samples are modelled at LO using PYTHIA 8.230 and the NNPDF2.3LO PDF set for both the matrix element and the parton shower. Finally, the $\gamma + \text{jets}$ processes are modelled using SHERPA 2.2.2 at NLO accuracy with the NNPDF3.0NNLO PDF set. Backgrounds that are simulated using SHERPA model the decays of b - and c -hadrons internally, while the other samples make use of EVTGEN 1.6.0 or 1.2.0 [65]. Backgrounds such as triboson production and other rare processes involving top quarks or Higgs bosons are found to be negligible in the searches.

5 Event reconstruction

The trajectories of charged particles are reconstructed from the inner detector hits as tracks using clusterisation and combinatorial track finding algorithms [103]. The kinematic variables of the track such as p_T , η and ϕ are defined at the perigee, the point of closest approach of the track to the beam line. Tracks with p_T down to 500 MeV are reconstructed. All events are required to have at least one reconstructed pp interaction vertex with a minimum of two associated tracks. In events with multiple vertices, the primary vertex is defined as the vertex having the highest $\sum p_T^2$ of associated tracks. A set of basic quality criteria [104] is applied to reject events with detector noise or non-collision backgrounds.

Leptons, jets, and tracks are ‘preselected’ using loose identification criteria and must satisfy tighter ‘signal’ identification requirements to be selected for the search regions described in Section 6. Preselected leptons and jets are primarily used to resolve ambiguities between tracks and energy clusters associated with multiple lepton and jet candidates.

Isolation criteria are used in the definition of signal leptons and are based on tracking information, calorimeter energy clusters, or both. Isolation energies are computed as a $\sum p_T$ of nearby activity, excluding the contributions from nearby leptons. Requiring small isolation energies helps to reduce contributions from semileptonic heavy-flavour hadron decays and jets misidentified as prompt leptons. The isolation requirements are based on those described in Refs. [105] and [106]. The isolation variable $p_T^{\text{cone}X}$ is defined as the $\sum p_T$ of all tracks satisfying $\Delta R < X/100$ and $p_T > 1$ GeV. For the $1\ell 1T$ search, this variable is adjusted by subtracting the p_T of the paired lepton or track as described later.

Electrons are required to have $p_T > 4.5$ GeV and $|\eta| < 2.47$. Preselected electrons are further required to satisfy the calorimeter- and tracking-based *Loose* likelihood identification [105] and to have a longitudinal impact parameter z_0 relative to the primary vertex satisfying $|z_0 \sin \theta| < 0.5$ mm. Signal electrons must satisfy the *Medium* identification criterion [105], having typical selection efficiency of over 80% for $p_T > 10$ GeV and 70–80% for $p_T = 4.5$ –10 GeV, and be associated with the primary vertex, with the significance of the transverse impact parameter defined relative to the beam position satisfying $S(d_0) \equiv |d_0|/\sigma(d_0) < 5$, where $\sigma(d_0)$ is the uncertainty of d_0 . For the displaced track search, signal electrons are further refined using the *Loose_VarRad* isolation working point [105], whereas for the $1\ell 1T$ search, the *TightTrackOnly_VarRad* isolation working point [105] is required with an adjustment to subtract the contribution of the signal candidate track. This adjustment is performed to avoid vetoing signal processes in which the two leptons originating from the $\tilde{\chi}_2^0$ are nearby.

Muons are required to satisfy $p_T > 3$ GeV and $|\eta| < 2.5$. Preselected muons are identified using the *Medium* criterion [106], having typical selection efficiency of over 90% for $p_T > 5$ GeV and 50–90% for $p_T = 3$ –5 GeV, and are required to satisfy $|z_0 \sin \theta| < 0.5$ mm. Signal muons must satisfy the promptness requirement of $|d_0|/\sigma(d_0) < 3$. For the displaced track search, signal muons are further refined using the *Pflow_Loose* isolation working point [106], whereas for the $1\ell 1T$ search, the *TightTrackOnly* isolation working point [106] is required with an adjustment to subtract the contribution of the signal candidate track, similar to the electrons.

Jets are reconstructed from particle flow objects [107] using the anti- k_r algorithm [108, 109] with radius parameter $R = 0.4$. Preselected jets are required to have $p_T > 20$ GeV and $|\eta| < 4.5$ after being calibrated according to the procedure in Ref. [110]. For suppressing jets originating from pile-up, jets with $p_T < 60$ GeV and $|\eta| < 2.5$ are required to satisfy the *Tight* working point of the jet vertex tagger [111], using information from the tracks associated with the jet. From the sample of preselected jets, signal jets are further selected when they satisfy $|\eta| < 2.8$, which ensures that the jets are within the acceptance of the high-granularity endcap calorimeters.

Jets originating from the hadronisation of b -quarks, referred to as b -tagged jets, are identified from preselected jets within $|\eta| < 2.5$ using the *DL1r* algorithm [112]. The $p_T > 20$ GeV requirement is maintained to maximise the rejection of the $t\bar{t}$ background in analysis regions that veto events containing b -tagged jets. The b -tagging algorithm working point is chosen so that b -jets from simulated $t\bar{t}$ events are identified with an 85% efficiency, with corresponding rejection factors of approximately 2.9 and 40 for jets containing c -hadrons and jets arising from light-flavour quarks and gluons, respectively [113, 114].

To resolve ambiguities between nearby reconstructed leptons and jets, the following procedures are performed. First, preselected muons that share an inner detector track with a preselected electron candidate are rejected. Next, non b -tagged jets within $\Delta R < 0.2$ of a preselected electron are discarded. Preselected electrons satisfying $\Delta R < \min(0.4, 0.04 + 10 \text{ GeV}/p_T(e))$ relative to a jet are then removed. Non b -tagged jets within $\Delta R < 0.2$ of a preselected muon are then rejected. Finally, preselected muons satisfying $\Delta R < \min(0.4, 0.04 + 10 \text{ GeV}/p_T(\mu))$ with respect to a jet are removed.

The missing transverse momentum $\mathbf{p}_T^{\text{miss}}$ is defined as the negative vector sum of the transverse momenta of all preselected objects (leptons, jets, and photons [105]) and an additional soft term that is constructed from all tracks that are not associated with any lepton or jet but are associated with the primary vertex. A dedicated overlap removal procedure is used to resolve ambiguities between the reconstructed objects. In this way, E_T^{miss} is adjusted for the best calibration of leptons and jets, while maintaining pile-up independence in the soft term [115].

Scale factors are applied to the efficiencies of reconstructed electrons [105], muons [106] and b -tagged jets [116] in the simulated samples to match the reconstruction efficiencies in data. The scale factors for b -tagged jets account for the differences between data and simulated samples in the identification efficiencies for jets including b -hadron decays and for the misidentification rates of jets initiated from charm quarks, light-flavour quarks, or gluons. In addition, dedicated scale factors are also used to reweight simulated samples to properly model the trigger efficiency observed in data.

5.1 Low- p_T lepton-track identification

In the $1\ell 1T$ search, dedicated low- p_T lepton-track identification (ID) methods are used to identify leptons eluding standard identification methods and to gain sensitivity to unexplored low- Δm regions. Tracks with $p_T > 500$ MeV and $|\eta| < 2.5$ are preselected using the *Tight Primary* working point defined in Ref. [117]. In low- p_T regimes with $p_T < 5$ GeV, tracks are dominated by hadrons (mostly charged pions) and fake combinatorial tracks. The target of the low- p_T lepton-track ID is to distinguish lepton-tracks from such background tracks. A low- p_T electron-track ID and a low- p_T muon-track ID are developed separately with dedicated optimisations.

The low- p_T electron-track candidate is required to have $p_T \in [0.5, 5]$ GeV and $|\eta| < 2.5$. Tracks are extrapolated to a matching calorimeter energy cluster based on its position and energy deposit when available, however, the existence of a matched cluster is not always required. The matching for low- p_T electron-tracks is performed without including the effects from multiple scattering, assuming a constant magnetic field in the volume of the inner detector, and using the perigee parameters of the track. A fully connected deep neural network model with two 128-node hidden layers is trained to separate low- p_T electron-tracks from dominant low- p_T hadronic tracks using silicon tracking information, along with optional TRT and electromagnetic calorimeter energy cluster information. Tracking fit errors, hit information in the TRT detector, and energy deposits in the inner layers of the electromagnetic calorimeter show notable differences between electron and hadronic tracks due to the effects of bremsstrahlung. A dedicated identification working point for the $1\ell 1T$ search is dynamically defined by adopting another deep neural network using track p_T , track $|\eta|$, and the score from the previous network as inputs. By setting a threshold on the output score of this network, a working point dependent on each of the inputs is chosen. The latter network is trained with signal higgsino and background W^\pm +jets MC events satisfying the event-selection criteria defined later in Section 6.

The low- p_T muon-track candidate is required to have $p_T \in [1, 5]$ GeV and $|\eta| < 1.6$. In this low- p_T range, muons typically make a full-stop in the calorimeters and do not reach the muon spectrometer. Thus, the low- p_T muon track is identified using information only from the inner detector and calorimeters. As opposed to the case of electron-tracks, muon candidate tracks are always required to have a matching calorimeter energy cluster. A fully connected deep neural network model with six 64-node hidden layers is trained to separate low- p_T muon-tracks from dominant low- p_T hadronic tracks using track p_T , track η , and energy deposits in each calorimeter layer. Low- p_T muons tend to act as minimum ionising particles

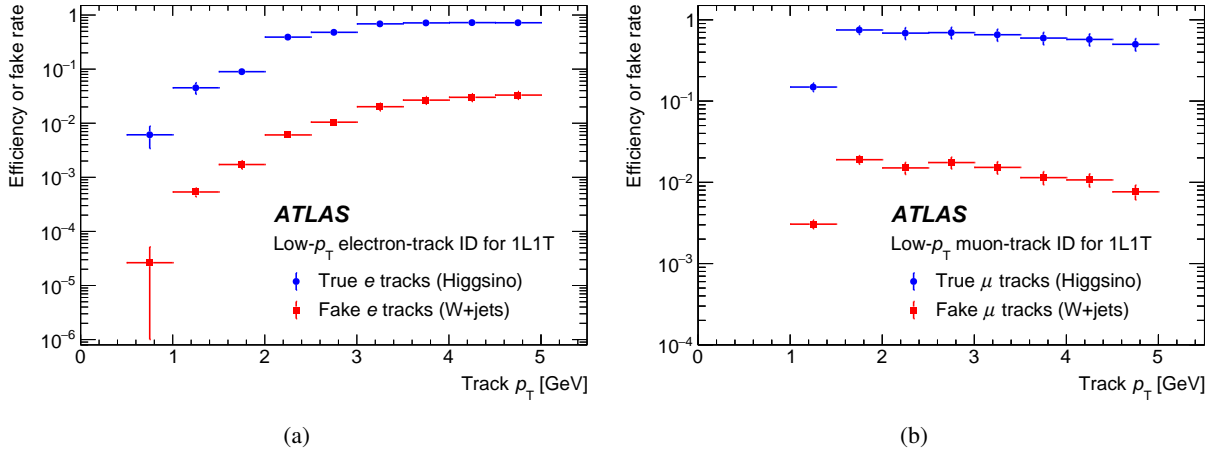


Figure 2: Simulated true-track efficiency and fake-track rate as a function of track p_T for (a) the low- p_T electron-track ID and (b) the low- p_T muon-track ID. The scale factors obtained from dedicated calibration methods are applied with corresponding uncertainties. The total uncertainty including the statistical and systematic uncertainties are shown, where the former uncertainty is found to be negligible. The true track is defined as a track matched to a lepton originating from $\tilde{\chi}_2^0 \rightarrow \tilde{\chi}_1^0 \ell^+ \ell^-$ decay in signal events satisfying the event selections defined later in Section 6. The fake track is defined as a track in $W^\pm + \text{jets}$ events that satisfies the same selection, excluding the track associated with the lepton from the W^\pm decay.

and deposit less energy in the calorimeters compared with low- p_T hadrons, allowing their identification without the use of muon detectors. Similarly to the electron-track case, a dedicated working point for the $1\ell 1T$ search is dynamically defined with another deep neural network using track p_T , track η , and the previous network score, with the training performed with signal higgsino and background $W^\pm + \text{jets}$ MC events that satisfy the $1\ell 1T$ event-selection criteria.

Figure 2 shows the signal and background track efficiencies of the low- p_T lepton-track ID methods as a function of track p_T . Both of the ID selections are optimised to maximise the final sensitivity to signal higgsino models. Both of the lepton-track ID methods have tighter criteria in very low- p_T regimes of $p_T < 1.5$ GeV, where contributions from hadronic and fake tracks become significant. The electron-track ID method has tighter criteria in terms of efficiency to achieve sufficient background suppression in the target region. For the low- p_T electron-track ID, the signal efficiency ranges in 0.6–70%, while the fake rate is kept within 0.003–3%. For the low- p_T muon-track ID, the signal efficiency ranges in 15–75%, while the fake rate is kept within 0.3–2%.

The scale factors and their uncertainties for low- p_T lepton-tracks are obtained using dedicated calibration methods. The low- p_T electron-track ID is calibrated using a ‘tag-and-probe method’ [105] focusing on the distribution of ΔR between the low- p_T electron-track and the photon in $Z \rightarrow e^+ e^- \gamma$ processes, particularly in events where an electron and the photon take away most of the energy, leaving the other electron to have a low p_T . In such event topologies, real low- p_T electrons from $Z \rightarrow e^+ e^- \gamma$ tend to be distributed close to the photon and have small ΔR , whereas fake misidentified electrons are randomly distributed and have broader ΔR distributions. This shape difference in ΔR between the low- p_T electron-track and the photon is used to obtain the identification efficiency in data. The low- p_T muon-track ID is calibrated using a tag-and-probe method using $J/\psi \rightarrow \mu^+ \mu^-$ processes, similar to that used in the calibration of standard muon identification [106]. The invariant mass distribution of the dimuon system is fitted using crystal-ball and quadratic functions. In both cases, the scale factors are evaluated by taking the ratio between the

Table 2: Event-level selections applied to all events used for the displaced track search. The single-lepton trigger is used only for events in control and validation regions. Hereinafter, $\Delta\phi$ variables are defined to be in the range of $[0, \pi)$.

| Variable | Requirement |
|--|--------------------------------------|
| Trigger | E_T^{miss} or single-lepton |
| E_T^{miss} [GeV] | > 275 |
| Number of jets with $p_T > 30$ GeV | $[1, 4]$ |
| Leading jet p_T [GeV] | > 250 |
| Leading jet $ \eta $ | < 2.4 |
| $\min \Delta\phi(E_T^{\text{miss}}, j)$ | > 0.4 |
| Number of preselected leptons ($N_{\text{pre-lep}}$) | $= 0$ (only for SR) |
| Number of tracks | ≥ 1 |

measured efficiency in data and the simulated efficiency in MC. They are only applied to the signal MC samples and the minor SM backgrounds of the $1\ell 1T$ search that are evaluated using MC samples.

6 Event selection

This section describes the event selections for the displaced track and $1\ell 1T$ analysis searches, each focusing on different mass splitting regions, and thus relying on distinct strategies exploiting dedicated neural network models. For both of the searches, signal regions are defined to isolate the signal processes. As later described in Section 7, control regions are defined to normalise the background processes and validation regions adjacent to the signal regions are defined to validate the background estimate.

6.1 Displaced track event selection

The displaced track search targets scenarios where $\Delta m(\tilde{\chi}_1^\pm, \tilde{\chi}_1^0) \approx 0.3\text{--}1.0$ GeV and the SM decay products of the moderately long-lived ($\mathcal{O}(0.1\text{--}1.0$ mm)) $\tilde{\chi}_1^\pm$ and $\tilde{\chi}_1^0$ particles can be reconstructed as low- p_T tracks with significant d_0 . Events are selected using an E_T^{miss} trigger and are first required to satisfy the event-level selections listed in Table 2. The reconstructed E_T^{miss} is required to be larger than 275 GeV, which is well above the 200 GeV threshold where the E_T^{miss} trigger becomes fully efficient. For signal events in which the $\tilde{\chi}_1^0$ -pair significantly contributes to the invisible momentum, the high E_T^{miss} requirement indicates a phase space in which the higgsino system is recoiling against hadronic activity in the form of ISR jets. Thus, all events are required to have at least one central jet with $p_T > 250$ GeV. Up to four jets are allowed in the event, each satisfying $\Delta\phi(E_T^{\text{miss}}, j) > 0.4$. For the signal region (SR), the number of preselected leptons in each event is required to be zero.

To exploit the available information and to maximise the signal sensitivity, a machine learning based approach using neural networks (NN) is adopted for further event selection. In particular, a two-level NN consisting of an event-level NN and a track-level NN is used. Both of the models are fully connected networks implemented in PyTorch [118] and are optimised using binary cross-entropy loss. They each adopt an optimised structure of three hidden layers with 50, 30, and 15 nodes, respectively, and rectified

Table 3: Summary of input variables of (top) event-level NN and (bottom) track-level NN. Events may not contain more than four jets, following the requirement in Table 2.

| | Input variable | Description |
|----------------|---|---|
| Event-level NN | E_T^{miss} | Magnitude of the missing transverse momentum |
| | Leading jet p_T | Kinematics of the leading jet |
| | Leading jet η | |
| | N_{jet}^{30} | Number of jets with $p_T > 30$ GeV |
| | $\min \Delta\phi(E_T^{\text{miss}}, j)$ | Minimum azimuthal angular difference between $\mathbf{p}_T^{\text{miss}}$ and all jets in the event |
| | m_{eff} | Scalar sum of p_T of all jets with $p_T > 30$ GeV and E_T^{miss} |
| | H_T | Scalar sum of p_T of all jets $p_T > 30$ GeV |
| Track-level NN | Track p_T | Kinematics of the track |
| | Track η | |
| | Track d_0 | Transverse impact parameter |
| | Track $S(d_0)$ | Significance of transverse impact parameter $ d_0/\sigma(d_0) $ |
| | Track $z_0 \sin \theta$ | Longitudinal impact parameter |
| | Track p_T^{cone40} | Scalar sum of p_T of tracks within $\Delta R < 0.4$ (excluding itself) |
| | Track p_T^{cone100} | Scalar sum of p_T of tracks within $\Delta R < 1.0$ (excluding itself) |
| | $\Delta\phi(\text{trk}, E_T^{\text{miss}})$ | Azimuthal angular difference between the track and $\mathbf{p}_T^{\text{miss}}$ |
| | Tight Primary | Binary to indicate if the track satisfies the <i>Tight Primary</i> track quality working point |
| | Secondary vertex matching | Binary to indicate if the track is matched to a secondary vertex |
| | Secondary vertex mass | Mass of secondary vertex reconstructed by associated tracks |

linear unit (ReLU) activation. Both of the output scores range from 0 to 1, with higher scores corresponding to more signal-like events or tracks. This two-level NN structure is adopted for its high flexibility in designing and validating the background estimation method later mentioned in Section 7.1.

The lists of input variables for both of the networks are given in Table 3. The event-level NN uses the event topology information based on E_T^{miss} and hadronic jets. The inputs that provide the strongest discrimination power between signal and background processes are E_T^{miss} and the effective mass, m_{eff} , defined as the scalar sum of p_T of all jets with $p_T > 30$ GeV and E_T^{miss} . The track-level NN exploits a variety of track information, such as the kinematics, impact parameters, isolation variables, and angular difference between the track and the missing transverse momentum. In addition, an inclusive secondary vertexing algorithm [119] is used to identify tracks with $p_T > 500$ MeV that are consistent with being produced at vertices that are displaced from the primary vertex, and the invariant mass of the reconstructed secondary vertex, calculated under the assumption that each track is a charged pion, is used to reject tracks associated with the decays of long-lived hadrons such as K_S^0 and Λ^0 . For reconstructed secondary vertices with exactly two associated tracks, at least one of the tracks is required to satisfy $|d_0| > 2.0$ mm. The track d_0 , $S(d_0)$, and isolation variables have the highest importance as they contribute to the separation from low- p_T QCD tracks. The event-level and track-level networks are trained using MC simulated datasets of signal and background events satisfying the selection criteria in Table 2. Details of the NN trainings are summarised in Appendix A.

Events satisfying the selection criteria in Table 2 are assigned an event score by the event-level NN. A track score is also assigned by calculating the output of the track-level NN for each preselected track and selecting the track with the highest track-level NN score in the event. As listed in Table 4, a set of four mutually exclusive SRs are then defined in the event score vs track score 2D plane. The score requirements are optimised to maximise the expected sensitivity to the signals of interest using a significance metric based

Table 4: Definition of the displaced track SRs in the event score vs track score plane. Tighter SRs such as SR-DT-1 have higher sensitivity, while looser SRs such as SR-DT-4 capture additional signal with lower purity that did not fall in the SRs with lower index.

| SR name | Event score | Track score | Additional requirement |
|---------|-------------|-------------|--|
| SR-DT-1 | > 0.712 | > 0.788 | – |
| SR-DT-2 | > 0.645 | > 0.799 | \notin SR-DT-1 |
| SR-DT-3 | > 0.645 | > 0.716 | \notin (SR-DT-1 \cup SR-DT-2) |
| SR-DT-4 | > 0.582 | > 0.705 | \notin (SR-DT-1 \cup SR-DT-2 \cup SR-DT-3) |

Table 5: Kinematic event selections applied to all events used for the $1\ell 1T$ search.

| Variable | Electron channel | Muon channel |
|--|------------------|---------------------|
| Trigger | | E_T^{miss} |
| E_T^{miss} [GeV] | | > 200 |
| Number of jets with $p_T > 20$ GeV | | ≥ 1 |
| Leading jet p_T [GeV] | | > 100 |
| Number of b -tagged jets ($N_{b\text{-jet}}^{20}$) | | $= 0$ |
| Number of signal leptons ($N_{\text{sig-lep}}$) | $= 1$ (electron) | $= 1$ (muon) |
| Lepton p_T [GeV] | [4.5, 10] | [3, 10] |
| Lepton $ z_0 \sin \theta $ [mm] | | < 0.5 |
| Lepton $ d_0/\sigma(d_0) $ | < 5 | < 3 |
| Number of tracks | | ≥ 1 |

on the profile likelihood method [120]. The four SRs cover different regions of kinematic phase space, targeting both of the smaller $\Delta m(\tilde{\chi}_1^\pm, \tilde{\chi}_1^0)$ regions having more displaced tracks and larger $\Delta m(\tilde{\chi}_1^\pm, \tilde{\chi}_1^0)$ regions with higher signal cross-sections but with less tracks with large displacements. They ensure robust coverage across a range of mass splitting scenarios, optimising for the overall sensitivity in different mass points.

6.2 $1\ell 1T$ event selection

All events used for the $1\ell 1T$ search are selected by an E_T^{miss} trigger and are first required to satisfy the kinematic event selections listed in Table 5. The reconstructed E_T^{miss} is required to be larger than 200 GeV to ensure full efficiency of the E_T^{miss} trigger. For higgsino signal events in which the $\tilde{\chi}_1^0$ -pair primarily contributes to the invisible momentum, this high- E_T^{miss} requirement indicates that the higgsino production system is recoiling against hadronic activity in the form of ISR jets. Hence, all events are required to have at least one jet with $p_T > 100$ GeV. Moreover, events with one or more b -tagged jets with $p_T > 20$ GeV are vetoed to suppress background contributions from $t\bar{t}$ production.

Events in the $1\ell 1T$ search are required to have exactly one signal lepton and are further categorised into two channels depending on the lepton flavour. The signal lepton requirement ensures that there is no overlap between the $1\ell 1T$ analysis regions and the SRs of the displaced track search. The p_T of the lepton

Table 6: Track preselections applied to candidates of low- p_T lepton-tracks for the $1\ell 1T$ search.

| Variable | Electron channel | Muon channel |
|-------------------------------------|---------------------------|--------------|
| Track charge | Opposite of lepton charge | |
| Track p_T [GeV] | [0.5, 5] | [1, 5] |
| Track $ \eta $ | < 2.5 | < 1.6 |
| Track $ z_0 \sin \theta $ [mm] | < 0.5 | |
| Track $ d_0 $ [mm] | < 0.5 | |
| Track p_T^{cone30}/p_T | < 0.06 | |
| $m(Z^*)$ [GeV] | < 3 or [3.2, 5] | |
| $\Delta R(\ell, \text{trk})$ | [0.1, 1.4] | |
| $\Delta d_0(\ell, \text{trk})$ [mm] | < 0.25 | < 0.10 |
| $\Delta z_0(\ell, \text{trk})$ [mm] | < 0.30 | < 0.26 |

is required to be below 10 GeV and above the lower bound of lepton identification methods, which are 4.5 GeV and 3 GeV for electrons and muons, respectively. As the decay length of $\tilde{\chi}_2^0$ is $O(0.01\text{--}0.1\text{ mm})$ for the targeted region, the leptons emerging from the $\tilde{\chi}_2^0 \rightarrow \tilde{\chi}_1^0 \ell^+ \ell^-$ decay are expected to be prompt. Thus, requirements on z_0 and d_0 are also imposed for the lepton. Finally, at least one additional track other than the reconstructed lepton is required in each event, which correspond to lepton-track candidates also originating from $\tilde{\chi}_2^0$ for signal higgsino events.

After the kinematic event selections are applied, preselections listed in Table 6 are applied to tracks to identify the candidates for the lepton-track. The charge of the track is required to be the opposite of that of the lepton, as they are expected to originate from Z^* decay. The p_T and $|\eta|$ requirements on the track follow the requirements of the low- p_T lepton-track identification methods described in Section 5. The tracks are also required to be prompt with upper bounds on $|z_0 \sin \theta|$ and $|d_0|$. The upper bound on p_T^{cone30} variable requires the tracks to have little surrounding activity excluding the lepton. The invariant mass $m(Z^*)$ reconstructed from the lepton and the candidate lepton-track is required to be smaller than 5 GeV, excluding 3.0–3.2 GeV to veto J/ψ mass resonances. Contributions from other SM resonances are found to be negligible in the selected range of $m(Z^*)$. As the SUSY system is boosted, the lepton and the lepton-track are expected to be close to each other. Thus, $\Delta R(\ell, \text{trk})$ in $[0.1, 1.4]$ is required; the upper bound is set to 1.4 to veto most background tracks, while the lower bound is set to 0.1 to veto nearby tracks associated with the lepton. Requirements on the impact parameter differences between the lepton and the lepton-track are imposed to further suppress background tracks, as specified in Table 6.

As the event topology of signal higgsino events has large dependence on the mass splitting of the higgsinos $\Delta m(\tilde{\chi}_2^0, \tilde{\chi}_1^0)$, the main event selection of the $1\ell 1T$ search is performed using the machine learning method of a pNN. For very small $\Delta m(\tilde{\chi}_2^0, \tilde{\chi}_1^0)$, the leptons emitted from the $\tilde{\chi}_2^0 \rightarrow \tilde{\chi}_1^0 Z^*$ decay have very low p_T , and the two $\tilde{\chi}_1^0$ tend to become more collimated, leading to higher E_T^{miss} values. In this case, variables such as $\Delta R(\ell, \text{trk})$ and $\Delta\phi(E_T^{\text{miss}}, Z^*)$ have very small values. For larger $\Delta m(\tilde{\chi}_2^0, \tilde{\chi}_1^0)$, the leptons have higher p_T , leading to lower E_T^{miss} , and therefore, larger $\Delta R(\ell, \text{trk})$ and $\Delta\phi(E_T^{\text{miss}}, Z^*)$. The pNN is introduced to consider these dependencies and to classify signal and background events in a dynamic manner. By choosing $\Delta m(\tilde{\chi}_2^0, \tilde{\chi}_1^0)$ as the physics parameter θ (hereinafter referred to as pNN- θ), it is possible to realise $\Delta m(\tilde{\chi}_2^0, \tilde{\chi}_1^0)$ -dependent event selection with a single network model. This also simplifies the training

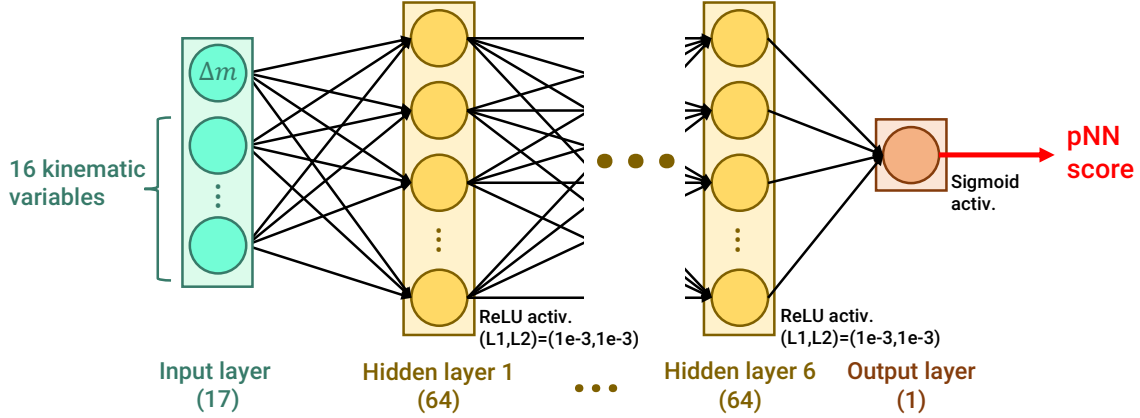


Figure 3: Overall structure of the pNN model used for event selection. The $\Delta m(\tilde{\chi}_2^0, \tilde{\chi}_1^0)$ and 16 kinematic variables are used as inputs, and there are six hidden layers with 64 nodes each. The nodes are fully connected. L1 and L2 regularisations are applied to each layer for increased signal sensitivity. The output pNN score ranges from 0 to 1, with 1 meaning that the input event is signal event-like.

procedure, as the pNN has the ability to smoothly interpolate between different $\Delta m(\tilde{\chi}_2^0, \tilde{\chi}_1^0)$ values used for training, thus giving the possibility to explore various mass splitting scenarios with a limited number of training samples. Hereinafter, regions of the $1\ell 1T$ search for a specific pNN- θ value are labelled with suffixes of ‘-dM{pNN- θ }’.

Figure 3 shows the overall structure of the pNN model developed for the event selection used for both the electron and muon channels. Based on $\Delta m(\tilde{\chi}_2^0, \tilde{\chi}_1^0)$, the pNN- θ , and 16 kinematic variables, the algorithm outputs a signal event-likeness score (hereinafter referred to as pNN score) ranging from 0 to 1. All of the inputs are standardised into a Gaussian distribution. For improved signal sensitivity, L1 and L2 regularisations [121] are applied to each hidden layer to suppress the contributions of background events in high pNN-score regions. The 16 kinematic variables are listed in Table 7. Besides pNN- θ , input variables such as lepton p_T , track p_T , E_T^{miss} , leading jet p_T , $m(Z^*)$, $\Delta R(\ell, \text{trk})$, $H(\ell, \text{trk})/E_T^{\text{miss}}$, $m_T(\ell, E_T^{\text{miss}})$, $\Delta\phi(E_T^{\text{miss}}, Z^*)$, and $\Delta\phi(j_1, Z^*)$ have significant dependencies on $\Delta m(\tilde{\chi}_2^0, \tilde{\chi}_1^0)$, thus having high importance³. The topology differences between signal and background events tend to become more significant for smaller $\Delta m(\tilde{\chi}_2^0, \tilde{\chi}_1^0)$ as the lepton, track, and E_T^{miss} are more likely to be in close proximity for signal processes compared with the dominant W^\pm +jets background processes.

Since the kinematic requirements for leptons and tracks differ for the electron and muon channel, the training of the pNN is done separately for each channel using the same pNN model structure. Higgsino production and W^\pm +jets MC events are used as signal and background training samples, respectively. The pNN is trained with pNN- $\theta = 1, 1.5, 2, 3, 4,$ and 5 GeV and the same values are used to obtain six non-orthogonal search results for each of the lepton flavours. Details of the pNN training are summarised in Appendix B. Figure 4 shows the performance of the pNN for each pNN- θ as a receiver operating characteristic (ROC) curve. The separation of signal and background events is stronger for smaller $\Delta m(\tilde{\chi}_2^0, \tilde{\chi}_1^0)$ values due to the mentioned topology differences.

³ $H(\ell, \text{trk})$ represents the scalar p_T sum of the lepton and the track. $m_T(\ell, E_T^{\text{miss}})$ represents the transverse mass reconstructed from the lepton and the missing transverse momentum and is defined as $\sqrt{2p_T^\ell E_T^{\text{miss}} \{1 - \Delta\phi(\ell, E_T^{\text{miss}})\}}$, where p_T^ℓ is the p_T of the lepton, and $\Delta\phi(\ell, E_T^{\text{miss}})$ is the azimuthal angular difference between the lepton and the missing transverse momentum.

Table 7: Summary of input variables of the pNN. The same set of variables is used for both the electron and muon channels.

| Input variable | Description |
|--|---|
| $\Delta m(\tilde{\chi}_2^0, \tilde{\chi}_1^0)$ | pNN- θ , mass difference between $\tilde{\chi}_2^0$ and $\tilde{\chi}_1^0$ |
| Lepton p_T | Kinematics of the standard lepton |
| Lepton η | |
| Lepton ϕ | |
| Track p_T | |
| Track η | Kinematics of the track |
| Track ϕ | |
| E_T^{miss} | |
| $\phi(E_T^{\text{miss}})$ | |
| Leading jet p_T | Kinematics of the leading jet |
| Leading jet ϕ | |
| $m(Z^*)$ | Mass of Z^* reconstructed from the lepton and the track |
| $\Delta R(\ell, \text{trk})$ | Distance between the lepton and the track |
| $H(\ell, \text{trk})/E_T^{\text{miss}}$ | Ratio of scalar sum of lepton p_T and track p_T to E_T^{miss} |
| $m_T(\ell, E_T^{\text{miss}})$ | Transverse mass reconstructed from the lepton and the missing transverse momentum |
| $\Delta\phi(E_T^{\text{miss}}, Z^*)$ | Azimuthal angular difference between the missing transverse momentum and Z^* |
| $\Delta\phi(j_1, Z^*)$ | Azimuthal angular difference between the leading jet and Z^* |

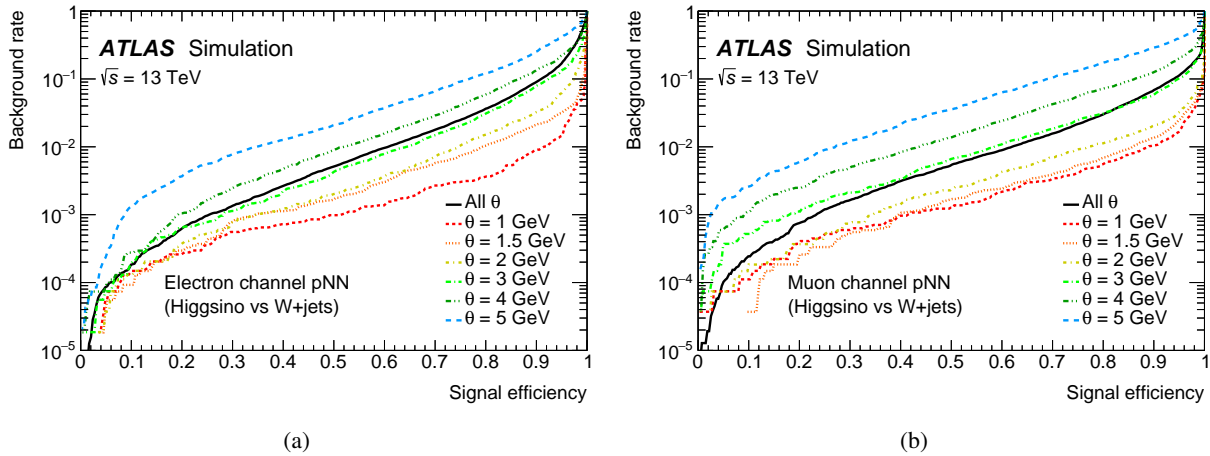


Figure 4: ROC curves of pNN of each pNN- θ for (a) the electron channel and (b) the muon channel. The performance is better for smaller $\Delta m(\tilde{\chi}_2^0, \tilde{\chi}_1^0)$ values for both channels. The steps in the curves are due to the limited statistical precision of the MC samples used.

Table 8: Summary of the selection criteria of the SR.

| Variable | SR-1e1T | SR-1 μ 1T |
|--------------------------------------|---------|---------------|
| $\Delta\phi(E_T^{\text{miss}}, Z^*)$ | | < 1.0 |
| pNN score | | > 0.95 |
| Low- p_T lepton-track ID score | > 0.8 | > 0.6 |

After the application of lepton-track preselection in Table 6, the pNN score is calculated for each candidate track. The track with the highest pNN score is then selected for each event and its score is assigned as the pNN score of the event. Subsequently, selection criteria in Table 8 are applied to select signal-like events with a same-flavour opposite-charge lepton and lepton-track pair and thus to define the SR. As the pNN and low- p_T lepton-track ID are not directly dependent on one another, this significantly reduces the background contribution. The first requirement of high pNN score vetoes background events having non-signal-like event topology. Then by selecting events having a track with high low- p_T lepton-track ID score, significant background suppression is achieved through rejection of hadronic and fake tracks, which are the main background track components in the targeted regime.

7 Background estimation

This section presents the background estimate methods for the displaced track and $1\ell 1T$ analysis searches, each exploiting dedicated semi-data-driven methods to estimate contributions from low- p_T tracks. The control and validation regions used in these methods are found to have negligible contributions from potential signal processes.

For the background estimation and the interpretation of final results, three configurations of fits to the data are used. The first configuration, referred to as the background-only fit, does not include any contributions from the signal models and uses only the control regions to extract the necessary normalisation and reweighting factors. Its results are then extrapolated to the validation and signal regions to compare the post-fit SM predictions with the observed data. The second configuration, referred to as the discovery fit, includes the control regions and one target signal region to derive a p -value representing the compatibility of the observed data with the background-only hypothesis. The third configuration uses both the control and signal regions to determine the compatibility of the observed data to the target signal model. In cases where there is no significant excess in data, this configuration is often referred to as the exclusion fit.

7.1 Displaced track background estimation

SM backgrounds in the SRs for the displaced track search are estimated by using a semi-data-driven approach that combines simulation-based predictions with reweighting corrections derived in dedicated control regions (CRs). Validation regions (VRs) orthogonal to the SRs are used to validate these corrections.

The leading background contributions in the SRs originate from processes that result in high E_T^{miss} from neutrinos, such as $Z(\rightarrow \nu\bar{\nu})+\text{jets}$ and $W^\pm(\rightarrow \tau^\pm\nu_\tau)+\text{jets}$. Subleading contributions come from diboson production and $W^\pm(\rightarrow \ell^\pm\nu_\ell)+\text{jets}$. Other processes such as top quark production and multijet processes are found to have negligible impact in the SRs and are estimated directly from MC simulation.

Table 9: Requirements of the CRs used in the displaced track search. There are no overlapping events between the CRs and the SRs of the displaced track search. $E_T^{\text{miss, no-}\ell}$ denotes E_T^{miss} with the leptons treated as invisible.

| CR name | Trigger | $N_{\text{sig-lep}}$ | $N_{b\text{-jet}}^{20}$ | E_T^{miss} [GeV] | $E_T^{\text{miss, no-}\ell}$ [GeV] |
|-----------------|---------------------|----------------------|-------------------------|---------------------------|------------------------------------|
| CR-DT-1 ℓ | Single-lepton | 1 $e/1\mu$ | = 0 | – | > 200 |
| CR-DT-2 ℓ | Single-lepton | 2 $e/2\mu$ | = 0 | – | > 200 |
| CR-DT-1 $e1\mu$ | Single-lepton | 1 $e+1\mu$ | = 0 | – | > 200 |
| CR-DT-lowMET | E_T^{miss} | = 0 | – | [275, 325] | – |

Each process of the leading and subleading background contributions is normalised by a dedicated normalisation factor obtained by simultaneously fitting kinematic distributions in dedicated CRs listed in Table 9, defined to enhance each of the processes. No requirement is made on the track-level NN score in these CRs. Normalisation factors for $W^\pm(\rightarrow \ell^\pm \nu_\ell)$ +jets and $W^\pm(\rightarrow \tau_{\text{lep}}^\pm \nu_\tau)$ +jets in which the τ -lepton decays leptonically are constrained by fitting the distribution of the transverse mass m_T in CRs requiring exactly one signal lepton, defined as CR-DT-1 ℓ ($\ell = e, \mu$). As m_T tends to be smaller for $W^\pm(\rightarrow \tau_{\text{lep}}^\pm \nu_\tau)$ +jets processes, CR-DT-1 ℓ regions are separated into two bins with m_T in [20, 40) and [40, 120) GeV to simultaneously constrain the corresponding factors. The normalisation factors obtained for $W^\pm(\rightarrow \ell^\pm \nu_\ell)$ +jets and $W^\pm(\rightarrow \tau_{\text{lep}}^\pm \nu_\tau)$ +jets are 1.20 ± 0.01 and 1.2 ± 0.1 , respectively.

Normalisation factors for $Z(\rightarrow \nu\bar{\nu})$ +jets and $Z(\rightarrow \ell^+ \ell^-)$ +jets processes are presumed to be the same and are constrained by fitting the dilepton mass in CRs with two same-flavour leptons, defined as CR-DT-2 ℓ . Diboson processes are inclusively constrained by a similar method in a CR with two different-flavour leptons, defined as CR-DT-1 $e1\mu$. The leptonic CRs CR-DT-1 ℓ , CR-DT-2 ℓ , and CR-DT-1 $e1\mu$ are triggered with single-lepton triggers and require high E_T^{miss} with the leptons treated as invisible particles, denoted by $E_T^{\text{miss, no-}\ell}$, which helps in keeping the event topology similar to the targeted process. The p_T threshold of the single-electron (single-muon) triggers varied between 24 GeV and 26 GeV (20 GeV and 26 GeV) during the 2015–2018 data-taking period. These thresholds ensure that CR-DT-1 ℓ is orthogonal to the SRs of the 1 ℓ 1T search, which require the lepton p_T to be below 5 GeV. The number of b -jets is required to be zero to suppress contributions from top quark processes. The normalisation factors obtained for Z +jets and diboson processes are 1.29 ± 0.01 and 1.4 ± 0.2 , respectively.

Finally, CR-DT-lowMET provides constraints on the normalisation factor for $W^\pm(\rightarrow \tau_{\text{had}}^\pm \nu_\tau)$ +jets processes in which the τ -lepton decays hadronically. In this region, E_T^{miss} is required to be in [275, 325] GeV and the distribution of $\min \Delta\phi(E_T^{\text{miss}}, j)$, defined as the minimum azimuthal separation between the missing transverse momentum and any jet, is used for the fit. The normalisation factor obtained for $W^\pm(\rightarrow \tau_{\text{had}}^\pm \nu_\tau)$ +jets processes is 1.37 ± 0.04 .

In addition to the event-level normalisation, track-level reweighting is applied to correct for any mismodelling in the kinematics of the tracks. The track-level reweighting consists of three factors. The first track reweighting factor is applied to consider the modelling differences between tracks originating from primary vertices and those that do not, dominantly tracks from pile-up. The reweighting factors are process-agnostic and are determined using CR-DT-1 μ , having enough events. CR-DT-1 μ is categorised into two regions by $|z_0 \sin \theta|$: a region with $|z_0 \sin \theta| < 0.1$ mm dominated by tracks associated with the primary collision and a region with $|z_0 \sin \theta| > 0.5$ mm dominated by pile-up tracks. The factors are binned in track p_T and are only applied to tracks with $p_T < 3.2$ GeV, where such mismodelling is prominent. The obtained first reweighting factors range in 1–1.4 with relative uncertainties below 4%. The validity of these factors for

Table 10: Summary of the τ -track criteria applied to obtain the track reweighting factor in CR-DT-lowMET.

| Variable | Requirement |
|--|--|
| Track p_T [GeV] | > 2.5 |
| Track $ \eta $ | < 1.5 |
| Track $ d_0 $ [mm] | < 10 |
| Track $z_0 \sin \theta$ [mm] | < 1.5 |
| Track p_T^{cone40} [GeV] | < 1.0 |
| $\Delta\phi(\text{trk}, E_T^{\text{miss, no-}\ell})$ | ≤ 1.0 |
| Lepton veto | Not matched to a lepton-associated track |

different processes is confirmed in other CRs, such as CR-DT-1e and CR-DT-lowMET.

The second reweighting factor corrects for the mismodelling of the track isolation variable, resulting in fewer isolated tracks in data. Similarly to the first factors, these factors are obtained in CR-DT-1 μ categorised into two regions using the same $|z_0 \sin \theta|$ requirements and are applied to the variables separately. The factors are binned in p_T^{cone40} and their obtained values are in the range of 0.8–1.1 with relative uncertainties below 3%. The validity of these factors has also been confirmed in other CRs to ensure process independency.

The third reweighting factor corrects for the mismodelling of leptonic or hadronic tracks originating from τ -lepton decays under the high- E_T^{miss} preselection with a lower bound of 275 GeV, which is not considered in the first and second factors. A single normalisation factor is obtained in CR-DT-lowMET with additional ‘ τ -track’ criteria as defined in Table 10 to enhance the contributions from the targeted $W^\pm(\rightarrow \tau_{\text{had}}^\pm \nu_\tau)$ +jets processes. The obtained third reweighting factor is 0.64 with a relative uncertainty below 5%. This factor is applied only to simulated tracks originating from τ -leptons.

As shown in Table 11, four VR categories are constructed to validate different aspects of the background estimate method for the displaced track search. Figure 5 illustrates how the different VRs map onto the event-level NN score vs track-level NN score plane. Each of the categories are further divided into three or four regions, depending on their event-level and track-level NN scores. All VRs except VR-DT-Lep use the E_T^{miss} trigger. While some VRs may overlap with CRs by definition, they represent only a small fraction of the event yields in these CRs and therefore still provide a means of validating the background estimate strategy without introducing a significant bias to the fitted normalisation factors.

VR-DT-Evt is defined to have high event-level NN scores, but vetoes events having tracks with high track-level NN scores; it verifies the validity of the event-level NN model and the event-level normalisation factor for each background process. On the other hand, VR-DT-Trk is defined to have a high track-level NN score, but vetoes events with high event-level NN score. It is further required to have moderate E_T^{miss} in the range of 325–500 GeV to ensure a sufficiently low signal contamination and retain orthogonality with CR-DT-lowMET. VR-DT-Trk helps in verifying the validity of track-level NN model and the track-level corrections using reweighting factors.

To validate the estimation method in a region where the event-level and track-level networks both yield high scores, VR-DT-Lep is defined by requiring one signal muon. For this region, a single-muon trigger is used and E_T^{miss} is substituted by $E_T^{\text{miss, no-}\ell}$ to mimic the kinematics in the SRs excluding leptons. All of the event-level and track-level selections for this region are performed with this substitution. Furthermore, VR-DT- τ is defined to validate the modelling of $W^\pm(\rightarrow \tau^\pm \nu_\tau)$ +jets processes in regions with high event-level

NN scores. In VR-DT- τ , tracks are required to satisfy the τ -track criteria used for CR-DT-lowMET but with track $p_T > 8$ GeV to suppress contamination from signal processes.

7.2 $1\ell 1T$ background estimation

SM background processes with a high- p_T jet and a boosted system with neutrinos in the final state could satisfy the leading jet and E_T^{miss} selection of the $1\ell 1T$ search. The identified lepton is usually a real lepton, whereas the tracks identified with the low- p_T lepton-track identification methods have significant contributions from fake leptons. Since these tracks are required to be prompt, most of them are expected to correspond to low- p_T hadrons originating from underlying events. From these object-based considerations, the most dominant SM background process is W^\pm +jets with a leptonic W^\pm decay. In addition to these dominant backgrounds, there are small contributions from events in which the low- p_T lepton-track corresponds to a real lepton. Such backgrounds are contributions from processes that feature two or more leptons in their final states, including Z +jets and diboson. Thus, the SM backgrounds for the $1\ell 1T$ search are categorised into two components: ‘fake lepton-track’ backgrounds from events in which the low- p_T lepton-track corresponds to a fake lepton, and ‘true lepton-track’ backgrounds in which the low- p_T lepton-track corresponds to a real lepton. The dominant fake lepton-track backgrounds are estimated by a data-driven method described below, whereas the small true lepton-track backgrounds are estimated directly using MC simulation.

As MC simulation is not expected to accurately model processes with fake lepton-tracks, a data-driven method is used to estimate the contributions of fake lepton-track backgrounds. The method is performed by defining dedicated control regions, subtracting the true lepton-track contributions from each of the regions, and obtaining the ratio of yields of the fake lepton-track contributions between those regions. For this method, regions are first defined by applying the criteria in Table 5 and Table 6 and imposing requirements on the pNN score and $\Delta\phi(E_T^{\text{miss}}, Z^*)$ as illustrated in Figure 6. The α -region is defined by pNN score > 0.95 and $\Delta\phi(E_T^{\text{miss}}, Z^*) < 1.0$, and the γ -region is defined by pNN score < 0.4 . Both of these are further categorised into ‘pass’ and ‘fail’ regions following Figure 7, based on whether the low- p_T lepton candidate track passes or fails the ID-score requirements in Table 8. The pass region within the α -region therefore corresponds to the SR. Within the γ -region, dominated by SM backgrounds, the pass and fail regions are defined as CR- $1\ell 1T$ -A and CR- $1\ell 1T$ -B, respectively. The ‘transfer factors (TFs)’ are measured by taking the ratio of the number of events belonging to CR- $1\ell 1T$ -A and that of CR- $1\ell 1T$ -B, separately for each of the track p_T bins in [0.5, 1.0], [1.0, 1.5], [1.5, 2.0], [2.0, 3.0], and [3.0, 5.0] GeV for the electron channel and [1.0, 1.5], [1.5, 2.0], [2.0, 3.0], and [3.0, 5.0] GeV for the muon channel. The measured TFs are then applied to the number of events in the fail region within the α -region, defined as CR- $1\ell 1T$ -C. This p_T -binned method allows to consider the effects of indirect correlations between the low- p_T lepton-track ID and the event selection pNN through the track kinematics and helps in increasing the accuracy of estimating the pNN-score distribution in the SR. The TF values range in $\mathcal{O}(10^{-4}-10^{-2})$, typically having larger values in higher track p_T bins.

Three VRs are defined to validate the background estimation method of the $1\ell 1T$ search. VR- $1\ell 1T$ -highLarge(hL) is defined as the low- p_T lepton-track ID pass region within the β -region in Figure 6 with pNN score higher than 0.4 and $\Delta\phi(E_T^{\text{miss}}, Z^*)$ larger than 1.4, to test the validity of applying the TFs measured in low pNN-score regions to high pNN-score regions. The TFs used to estimate the background in the SR are applied to the fail region within β -region, labelled as CR- $1\ell 1T$ -hL, to estimate the yield in VR- $1\ell 1T$ -hL.

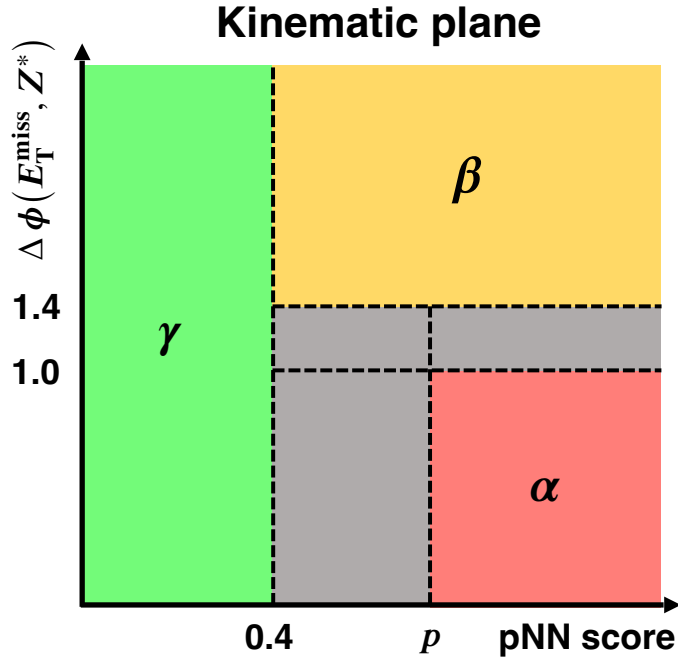


Figure 6: Kinematic plane diagram used for region definitions of the $1\ell 1T$ search. In terms of kinematic variables, the SRs, CRs, and VRs are defined by imposing requirements on the pNN score and $\Delta\phi(E_T^{\text{miss}}, Z^*)$. The value p is either 0.95 for the SRs and their corresponding CRs or 0.4 for the VRs and their corresponding CRs.

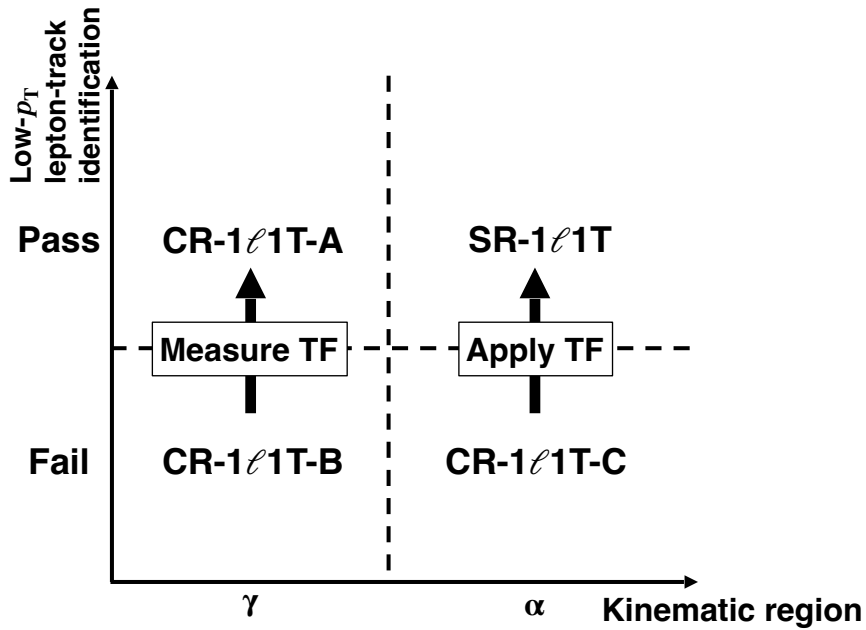


Figure 7: Schematic diagram of the background estimation method. CR-1 ℓ 1T-A and CR-1 ℓ 1T-B are used to measure the transfer factors (pass-to-fail ratio) of the low- p_T lepton-track identification. The transfer factors are binned by the track p_T to correctly estimate the pNN-score shape in the SR. The measured transfer factors are then applied to CR-1 ℓ 1T-C to estimate the background in SR-1 ℓ 1T.

Table 12: List of CRs and VRs used in the $1\ell 1T$ search. OS/SS stands for opposite/same sign, and SF/DF stands for same/different flavour, of the lepton and the lepton-track. The pNN-score thresholds for α -regions for SS-SF and OS-DF are lowered to 0.4 to increase event yields. For DF regions, there are additional requirements on the low- p_T lepton-track ID scores to avoid possible region overlaps with the SR in the other channel.

| Region name | Sign | Flavour | pNN score | $\Delta\phi(E_T^{\text{miss}}, Z^*)$ | Low- p_T lepton-track ID | Description |
|----------------------|------|---------|-----------|--------------------------------------|----------------------------|---|
| CR- $1\ell 1T$ -A | OS | SF | < 0.4 | – | Pass | TF measurement numerator |
| CR- $1\ell 1T$ -B | OS | SF | < 0.4 | – | Fail | TF measurement denominator |
| CR- $1\ell 1T$ -C | OS | SF | > 0.95 | < 1.0 | Fail | TF application CR for SR |
| CR- $1\ell 1T$ -hL | OS | SF | > 0.4 | > 1.4 | Fail | TF application CR for VR- $1\ell 1T$ -hL |
| CR- $1\ell 1T$ -SS-A | SS | SF | < 0.4 | – | Pass | TF-SS measurement numerator |
| CR- $1\ell 1T$ -SS-B | SS | SF | < 0.4 | – | Fail | TF-SS measurement denominator |
| CR- $1\ell 1T$ -SS-C | SS | SF | > 0.4 | < 1.0 | Fail | TF-SS application CR for VR-SS |
| CR- $1\ell 1T$ -DF-A | OS | DF | < 0.4 | – | Pass | TF-DF measurement numerator |
| CR- $1\ell 1T$ -DF-B | OS | DF | < 0.4 | – | Fail | TF-DF measurement denominator |
| CR- $1\ell 1T$ -DF-C | OS | DF | > 0.4 | < 1.0 | Fail | TF-DF application CR for VR-DF |
| VR- $1\ell 1T$ -hL | OS | SF | > 0.4 | > 1.4 | Pass | VR within OS-SF with large $\Delta\phi(E_T^{\text{miss}}, Z^*)$ |
| VR- $1\ell 1T$ -SS | SS | SF | > 0.4 | < 1.0 | Pass | VR with SS-SF |
| VR- $1\ell 1T$ -DF | OS | DF | > 0.4 | < 1.0 | Pass | VR with OS-DF |

VR- $1\ell 1T$ -DF and VR- $1\ell 1T$ -SS are used to validate the overall estimation method. VR- $1\ell 1T$ -DF is defined by inverting the flavour requirement of the standardly identified lepton (e.g. a muon and a low- p_T electron track are required for VR- $1\ell 1T$ -DF). To avoid possible overlaps with the SRs, the track is explicitly required to fail the ‘other’ low- p_T lepton-track criterion indicated in Table 8 (e.g. the track in VR- $1\ell 1T$ -DF is required to have low- p_T muon-track ID score below 0.6). VR- $1\ell 1T$ -SS is defined by requiring the same charge between the lepton and the low- p_T lepton-track. Except for the loosened pNN-score requirement of > 0.4 to ensure sufficient statistics, kinematic requirements are the same as those for the SR. For these two VRs, the yields are obtained with dedicated CRs and TFs, similar to the method illustrated in Figure 7. All of the CRs and VRs used in the $1\ell 1T$ search are listed in Table 12.

8 Systematic uncertainties

Systematic uncertainties are evaluated for all signal samples and background processes. The uncertainties are common to both the displaced track and $1\ell 1T$ searches unless noted.

Figure 8 shows the relative systematic uncertainties in the predicted SM background yields in the SRs derived from background-only fits to the CRs. Experimental uncertainties include the uncertainties related to the reconstruction and selection of objects relevant to the analysis. As both the displaced track and $1\ell 1T$ searches target boosted topologies with a high- p_T leading jet and high E_T^{miss} , uncertainties in these objects are found to be dominant experimental uncertainties. Jet uncertainties, mainly involving jet energy scale (JES) and jet energy resolution (JER), are evaluated as a function of jet p_T and η . These uncertainties are determined from data and MC studies such as the measurement of jet- p_T balance in dijet and Z/γ +jets processes [110]. Uncertainties related to b -jet identification and vertex tagging are also considered. Uncertainties in the modelling of E_T^{miss} in the MC simulation are estimated by propagating the energy and momentum scale of the objects entering the calculation of E_T^{miss} and the variations of the resolution and scale of the soft-term. Lepton systematic uncertainties include those of the reconstruction,

identification and isolation efficiencies, and those of the momentum/energy resolution and scale [106, 122]. Other experimental uncertainties include those of pile-up modelling, tracking efficiency, and track impact parameter resolutions. For the background MC samples of the $1\ell 1T$ search, the experimental uncertainties only affect the subdominant true lepton-track component, hence to avoid fit instabilities, a single conservative 50% envelope uncertainty is assigned to cover all of the experimental uncertainties. Moreover, the $1\ell 1T$ search considers the uncertainties in low- p_T lepton-track identification performance, such as those originating from the calibration.

For the displaced track search, uncertainties in the semi-data driven background estimation are considered. Uncertainties in the event-level normalisation factors for each background processes and track-level reweighting factors, originating from the data and MC statistics in the CRs, are taken into account by performing a simultaneous fit with all uncertainties included. The relative uncertainty values of these factors are typically below 10%.

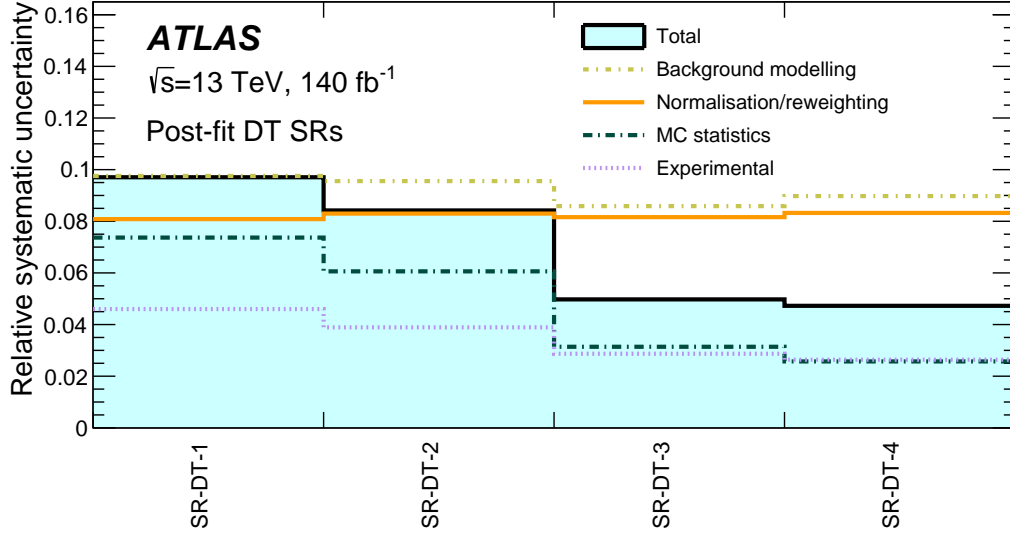
For the $1\ell 1T$ search, the uncertainties in the transfer factors and those originating from the data statistics in the corresponding CRs are considered by a simultaneous fit. Moreover, non-closure uncertainties are applied to the fake lepton-track component to consider uncertainties originating from the data-driven estimation method itself, such as the choice of variables used to define the CRs. The non-closure uncertainties are evaluated using the agreement in all VRs of the $1\ell 1T$ search and by taking their envelopes. Non-closure uncertainties of 15% and 40% are assigned to the fake lepton-track components of the $1e 1T$ and $1\mu 1T$ channels, respectively.

Theory modelling uncertainties are also considered for MC samples of dominant background processes. For the displaced track search, these uncertainties are considered for all background processes, whereas for the $1\ell 1T$ search, the theory uncertainties are considered only for V +jets and diboson samples, as the overall contribution of the true lepton-track background is about 10–20% compared with the total background.

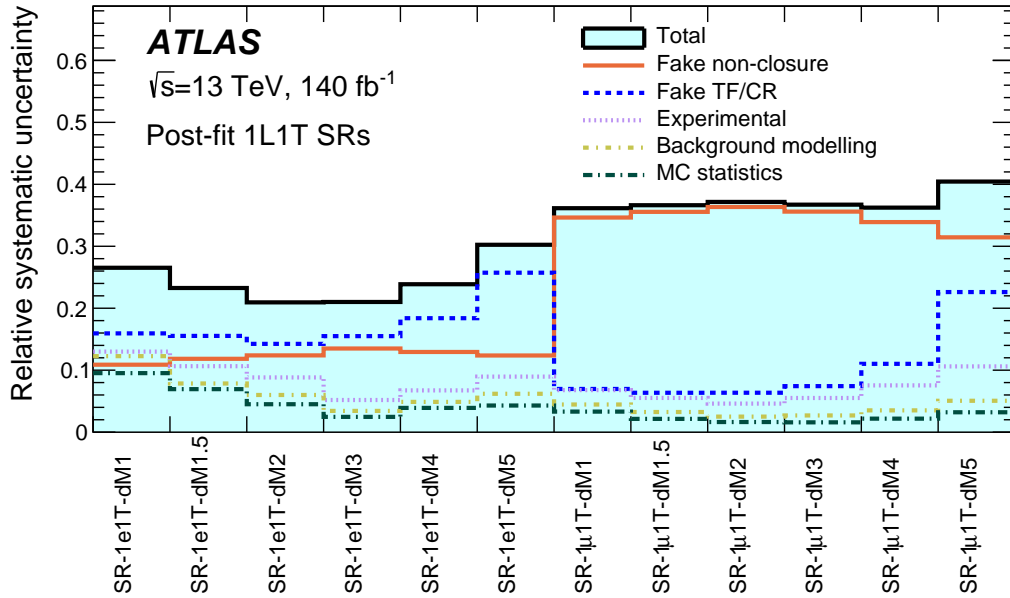
Common to both of the searches, the uncertainties originating from the choice of QCD renormalisation and factorisation scales are evaluated by varying the corresponding MC generator parameters up and down by a factor of two around their nominal values. The uncertainties associated with the choice of PDF set [56, 78] and that in the strong coupling constant α_s are also considered. Furthermore for the displaced track search, uncertainties in the resummation and matching scale between matrix elements and parton showers are considered for V +jets samples by varying up and down the corresponding parameters in SHERPA.

For signal samples, uncertainties in multi-parton interactions and parton showers are considered on top of the theory uncertainties mentioned above. These uncertainties are evaluated from the change of yields with different tune variations using a few of the samples. Five types of variations are considered according to the A14 tune of PYTHIA [63]: one for underlying event effects, one for jet structure effects, and three for different aspects of extra jet production. The sum in quadrature of the five variations is used as the overall uncertainty. A maximum of 6.4% is assigned for the displaced track search and flat 15% is assigned for the $1\ell 1T$ search.

As shown in Figure 8, the systematic uncertainty of the displaced track search is dominated by uncertainties in the normalisation and track reweighting factors, and the background modelling uncertainties. The impact of a given category of uncertainties is estimated by taking the results from the nominal background-only likelihood fit to the CRs, fixing the parameters associated with the other uncertainties to their best-fit values, and propagating the variations of the remaining floating parameters to the background prediction in the SRs using the covariance matrix from the nominal fit [123]. The profile likelihood method used for the fits is described in more detail in Section 9. Since the individual uncertainties in different categories can be correlated, the uncertainties from each category do not necessarily sum in quadrature to the total systematic



(a)



(b)

Figure 8: The relative systematic uncertainties (post-fit) in the fitted SM background event yields in the SRs obtained from a background-only fit to the CRs for (a) the displaced track search and (b) the $1\ell 1T$ search. ‘Normalisation/reweighting’ category for the displaced track includes all uncertainties relevant to the normalisation and reweighting factors used in the background estimation. ‘Fake non-closure’ category for the $1\ell 1T$ search denotes the non-closure uncertainty assigned to the fake lepton-track background component. ‘Fake TF/CR’ category for the $1\ell 1T$ search includes all uncertainties related to the transfer factors and statistical uncertainties in the CRs for the data-driven estimate of the fake lepton-track component. The uncertainties related to the reconstruction and identification of jets, E_T^{miss} , leptons, and lepton-tracks are included in the ‘Experimental’ category. ‘Background modelling’ category includes all theory uncertainties in the background processes. The ‘MC Statistics’ uncertainty originates from the limited size of the MC samples. The individual uncertainties can be correlated and therefore do not necessarily sum in quadrature to the total uncertainty.

uncertainty using this decomposition method, and can even be larger than the total in the case of the displaced track SRs. For the $1\ell 1T$ search, the non-closure uncertainty in the fake lepton-track contribution is the most significant, especially for $1\mu 1T$. For $1e 1T$, uncertainties in the transfer factors and CR statistical uncertainties become more dominant, due to limited data.

9 Results

Data in the control regions, validation regions, and signal regions are compared with SM predictions using a profile likelihood method [124]. The systematic uncertainties are treated as nuisance parameters with Gaussian-distributed constraints in the likelihood. The correlations between the uncertainties are considered in this method. Following the comparisons in the control and validation regions in Section 9.1, results in the signal regions are shown in Section 9.2. Section 9.3 and Section 9.4 show the results of model-independent and model-dependent interpretations, respectively.

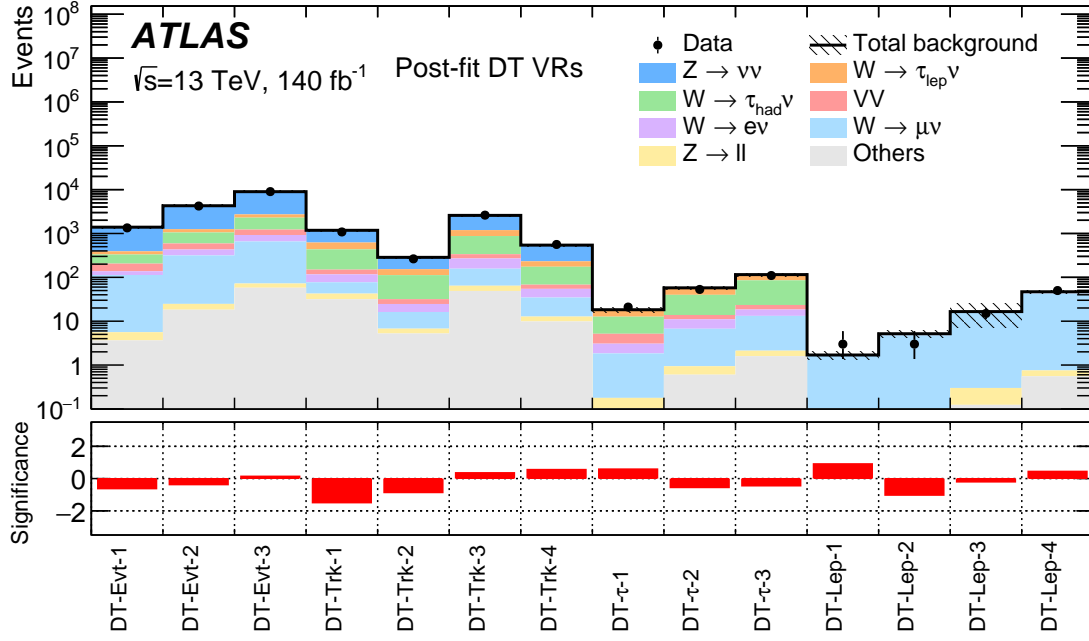
9.1 Control and validation regions

Background-only fits of the CRs are performed using only the CRs to constrain the fit parameters. For the displaced track search, a simultaneous fit is performed using all CRs to constrain all event normalisation and track reweighting factors. For the $1\ell 1T$ search, data in CR- $1\ell 1T$ -A, CR- $1\ell 1T$ -B, and CR- $1\ell 1T$ -C are fitted simultaneously to constrain the TFs and to obtain the background contribution in the SRs. The same procedure is performed to estimate the SM background yields in the VRs, using the dedicated CRs mentioned in Section 7.2.

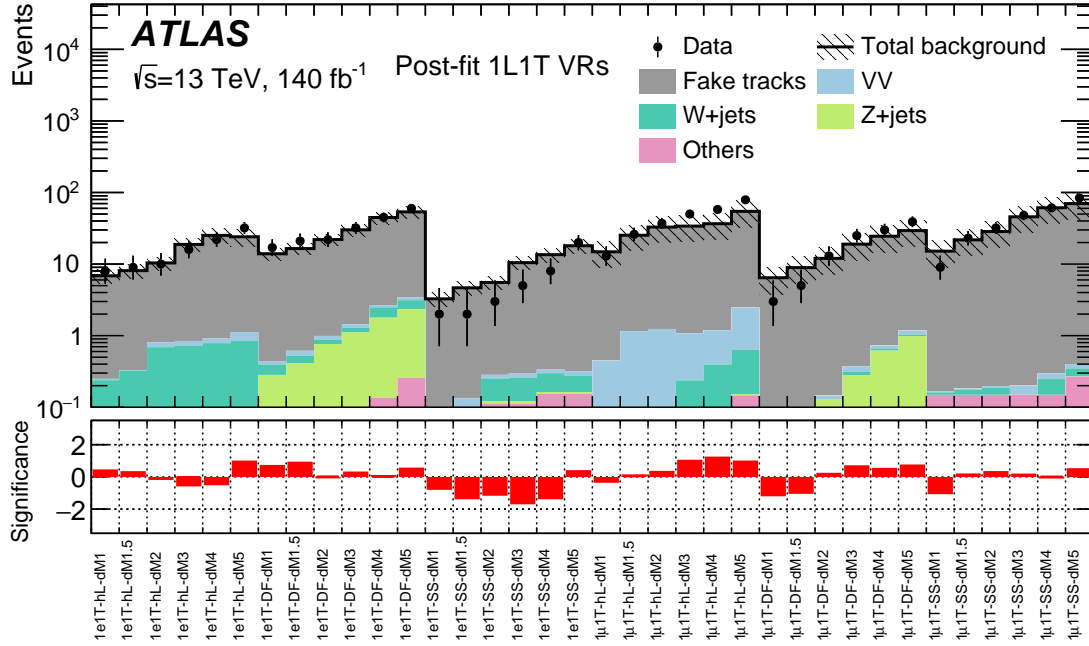
The SM background prediction obtained from the background-only fit is first compared with data in the VRs to verify the validity and accuracy of the background estimation method. Figure 9 shows a comparison between the data and estimated background event yields in the VRs. Good agreement is observed in all regions for both the displaced track and the $1\ell 1T$ searches, with deviations below 2σ . Non-closure uncertainties in the fake lepton-track components mentioned in Section 8 are applied to the $1\ell 1T$ search. Figures 10 and 11 show examples of kinematic distributions in the VRs after a background-only fit using the CRs. Good agreement between data and predicted background is observed in both the shape and the normalisation of the variables.

9.2 Event yields in signal regions

The data and the SM background prediction obtained from the background-only fit are then compared in the SRs. Such comparisons are shown in Figure 12 and Table 13. Deviations in all regions are within 2σ . The largest deviations for the displaced track and $1\ell 1T$ searches are found to be -1.3σ in SR-DT-4 and 1.5σ in SR- $1\mu 1T$ -dM5, respectively. Figures 13 and 14 show examples of kinematic distributions in the SRs after a background-only fit using the CRs. Good agreement between data and predicted background is observed in both the shape and the normalisation of the variables. For the $1\ell 1T$ search, the $m(Z^*)$ distribution in Figure 14 demonstrates that the pNN is successfully learning to select events based on the reconstructed Z^* mass.



(a)



(b)

Figure 9: Comparison of the observed and expected event yields in all VRs of (a) the displaced track search and (b) the $1\ell 1T$ search. The bottom panel in each plot shows the significance of the difference between the observed and the predicted yields, following the profile likelihood method of Ref. [125] in the case where the observed yield exceeds the prediction and using the same expression with an overall minus sign when the observed yield is below the prediction. (a) All slices are shown for each of the four VR categories: VR-DT-Evt, VR-DT-Trk, VR-DT- τ , and VR-DT-Lep. (b) On the left of the plot are VRs for $1e1T$ and on the right are VRs for $1\mu 1T$. All six pNN- $\theta = 1, 1.5, 2, 3, 4,$ and 5 GeV slices are shown for each of the three VRs: VR-hL, VR-DF, and VR-SS. The category ‘Others’ contains background processes including top quarks, multijets and γ +jets. Uncertainties in the estimated background include both the statistical and systematic uncertainties.

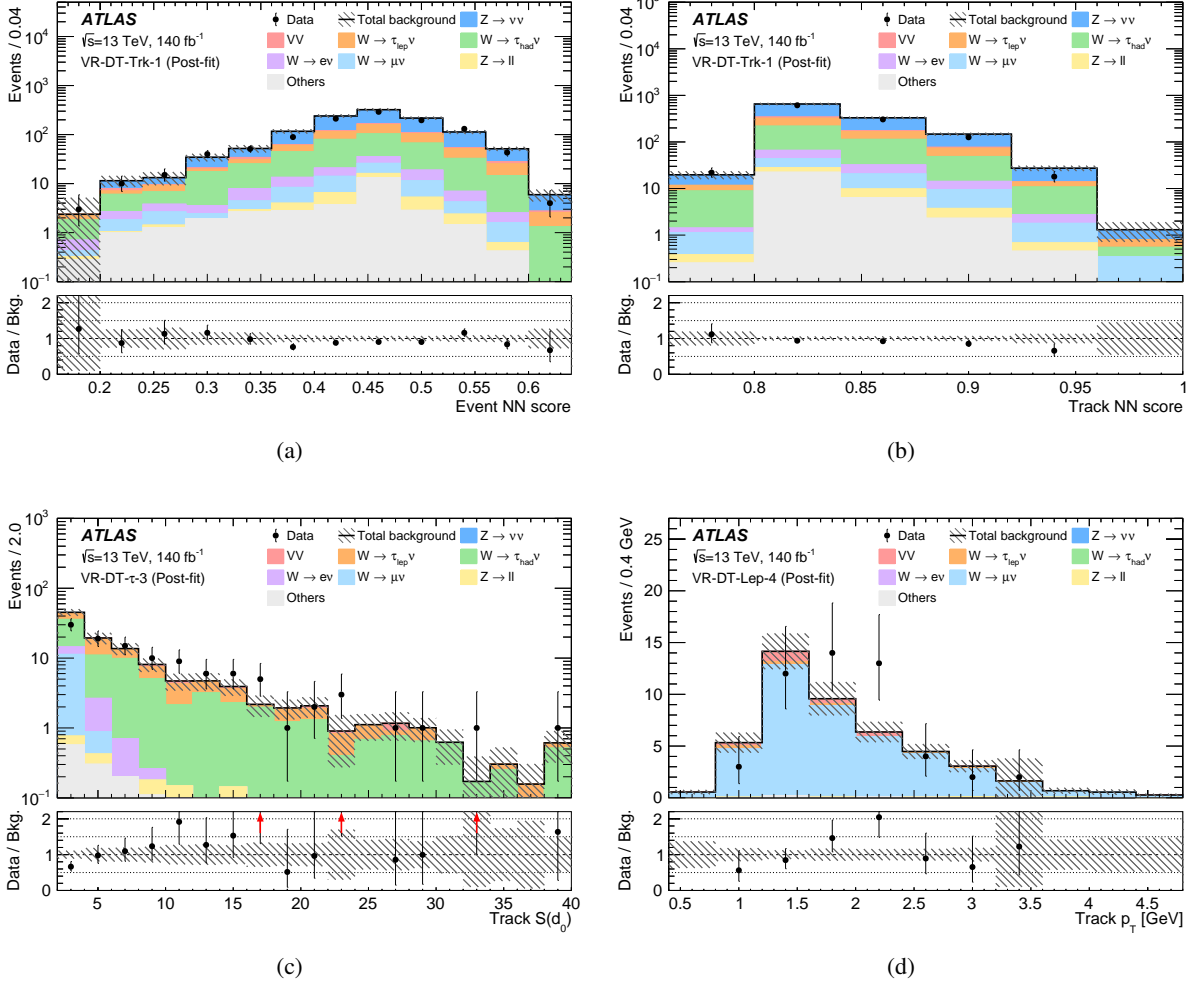


Figure 10: Examples of kinematic distributions in the VRs of the displaced track search after the background-only fit using the CRs. (a) and (b) show distributions of event-level and track-level NN scores in VR-DT-Trk-1, respectively. (c) shows the distribution of transverse impact parameter significance, $S(d_0)$, of the track in VR-DT- τ -3. (d) shows the distribution of track p_T in VR-DT-Lep-4. The category ‘Others’ contains background processes including top quarks, multijets and γ +jets. The uncertainty bands on the expected background include all statistical and systematic uncertainties. Upper arrows in the lower panel indicate data points outside the vertical range shown.

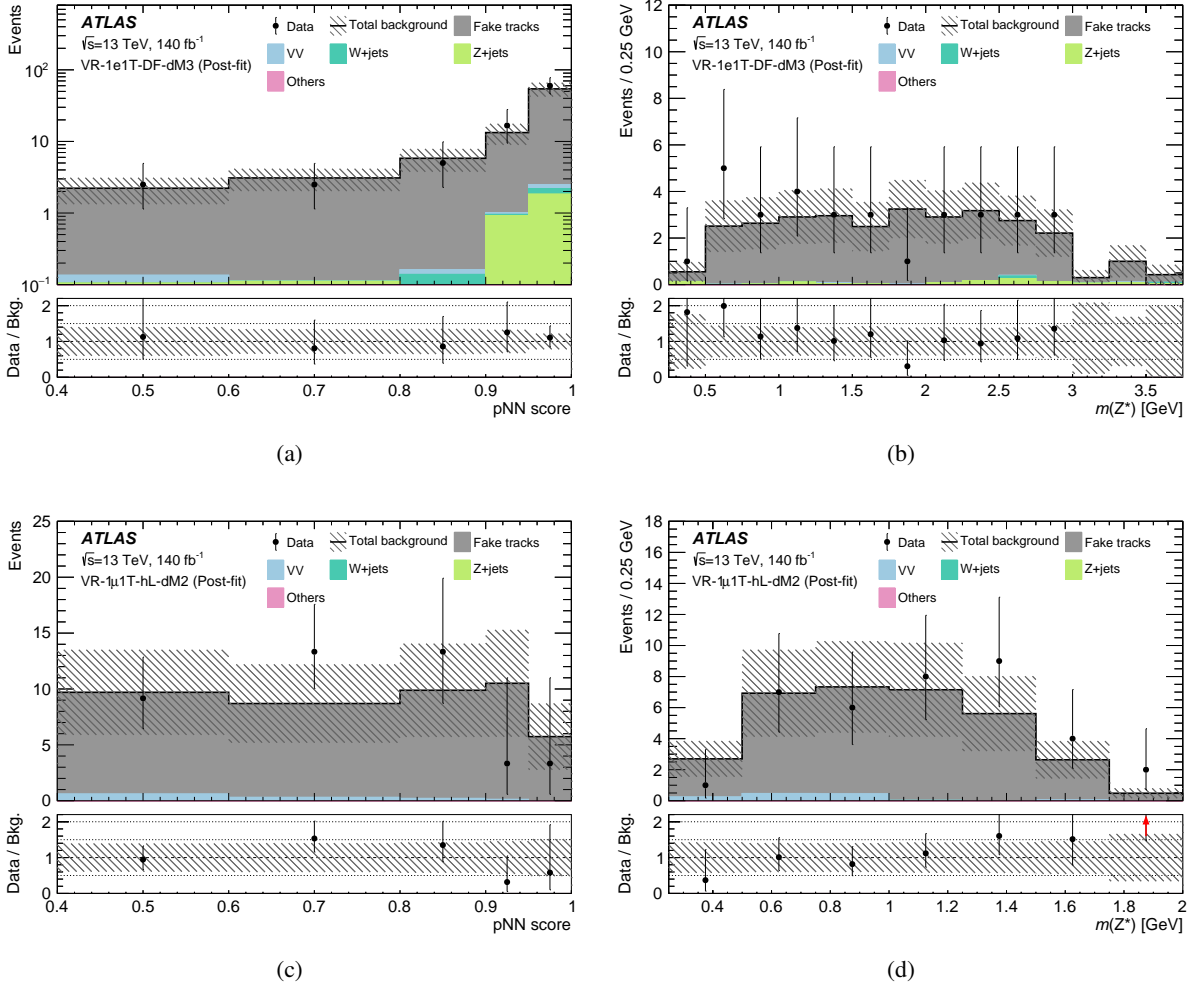


Figure 11: Examples of kinematic distributions in the VRs of the $1l1T$ search after the background-only fit using the CRs. (a) and (b) show distributions of pNN score and $m(Z^*)$ in VR-1e1T-DF-dM3, respectively. (c) and (d) show distributions of pNN score and $m(Z^*)$ in VR-1 μ 1T-hL-dM2. The category ‘Others’ contains background processes including top quarks, multijets and γ +jets. The uncertainty bands on the expected background include all statistical and systematic uncertainties. Upper arrows in the lower panel indicate data points outside the vertical range shown.

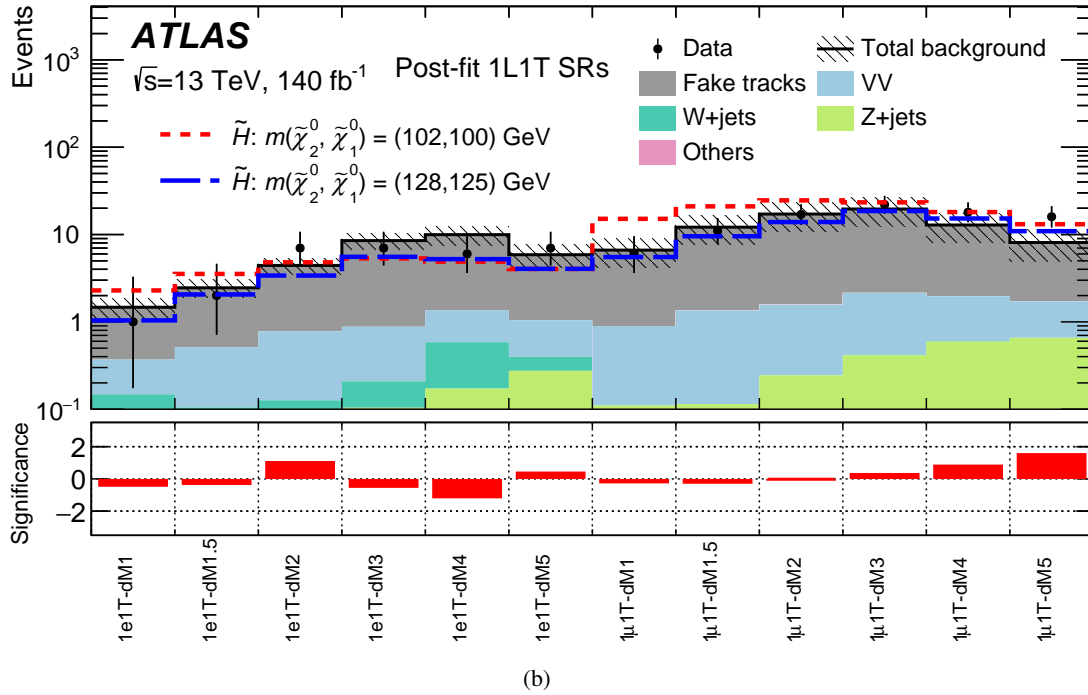
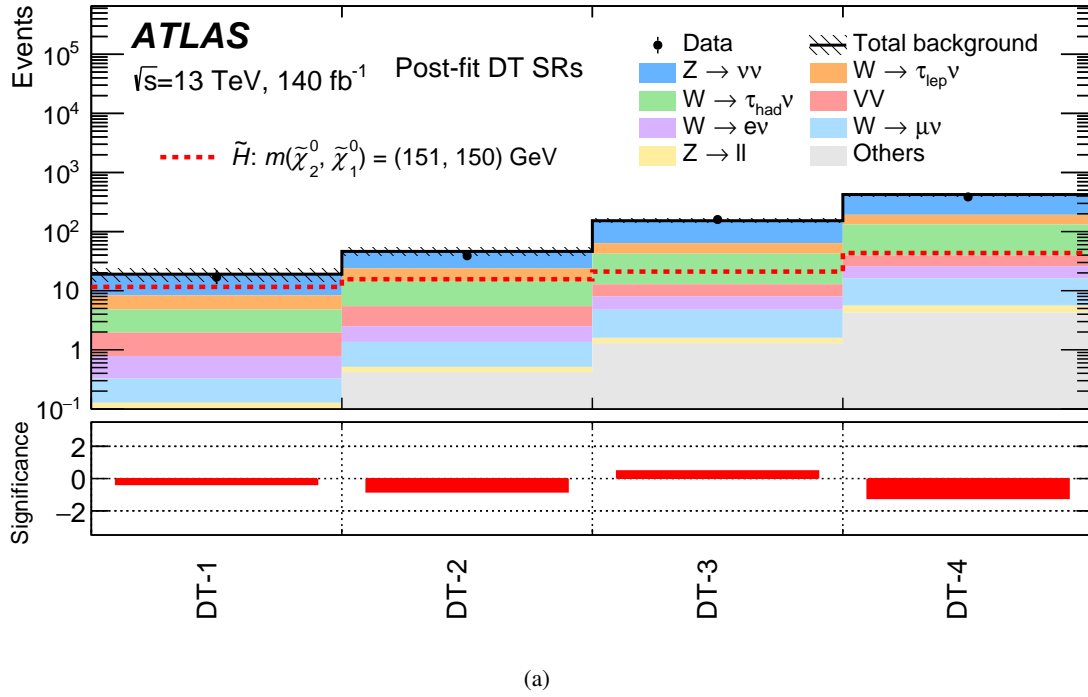


Figure 12: Comparison of the observed and expected event yields in all SRs of (a) the displaced track search and (b) the $1\ell 1T$ search. The bottom panel in each plot shows the significance of the difference between the observed and the predicted yields, following the profile likelihood method of Ref. [125] in the case where the observed yield exceeds the prediction and using the same expression with an overall minus sign when the observed yield is below the prediction. (a) All four SRs are shown for the displaced track search. (b) On the left of the plot are the SRs for $1e1T$ and on the right are the SRs for $1\mu 1T$. All six $p_{NN-\theta} = 1, 1.5, 2, 3, 4,$ and 5 GeV slices are shown. The category ‘Others’ contains background processes including top quarks, multijets and γ +jets. Uncertainties in the estimated background include both statistical and systematic uncertainties. Predicted yields for some signal mass points are overlaid for reference.

Table 13: Observed yields and predicted event yields in the SRs from a background-only fit using the CRs for (top) the displaced track search and (bottom) the $1\ell 1T$ search. The category ‘Others’ contains background processes including top quarks, multijets and γ +jets. Uncertainties in the predicted background yields include statistical and systematic uncertainties.

| SR name | SR-DT-1 | SR-DT-2 | SR-DT-3 | SR-DT-4 |
|--|-----------------|-----------------|-----------------|----------------|
| Observed | 17 | 39 | 160 | 386 |
| Fitted SM events | 19.0 ± 1.9 | 46.2 ± 3.9 | 152.9 ± 7.6 | 424 ± 20 |
| $Z \rightarrow \nu\bar{\nu}$ | 10.5 ± 1.5 | 21.9 ± 3.2 | 87 ± 10 | 226 ± 29 |
| $W^\pm \rightarrow \tau_{\text{had}}^\pm \nu_\tau$ | 3.0 ± 0.7 | 9.6 ± 3.0 | 31.6 ± 6.0 | 99 ± 23 |
| $W^\pm \rightarrow \tau_{\text{lep}}^\pm \nu_\tau$ | 3.6 ± 1.1 | 9.5 ± 2.0 | 21.4 ± 5.6 | 60 ± 12 |
| VV | 1.2 ± 0.4 | 2.9 ± 0.5 | 4.8 ± 1.0 | 13.4 ± 2.5 |
| $W^\pm \rightarrow e^\pm \nu_e$ | 0.5 ± 0.2 | 1.1 ± 0.5 | 3.2 ± 1.7 | 9.8 ± 4.1 |
| $W^\pm \rightarrow \mu^\pm \nu_\mu$ | 0.20 ± 0.05 | 0.84 ± 0.08 | 3.2 ± 0.3 | 10.5 ± 1.0 |
| $Z \rightarrow \ell^+ \ell^-$ | 0.04 ± 0.02 | 0.1 ± 0.1 | 0.30 ± 0.10 | 1.3 ± 0.4 |
| Others | 0.1 ± 0.1 | 0.4 ± 0.2 | 1.3 ± 0.4 | 4.3 ± 1.5 |

| | SR pNN- θ [GeV] | 1 | 1.5 | 2 | 3 | 4 | 5 |
|---------------|------------------------|------------------------|------------------------|------------------------|------------------------|------------------------|------------------------|
| | Observed | 1 | 2 | 7 | 7 | 6 | 7 |
| SR- $1e1T$ | Fitted SM events | 1.5 ± 0.4 | 2.5 ± 0.6 | 4.4 ± 0.9 | 8.5 ± 1.8 | 10.0 ± 2.4 | 5.8 ± 1.8 |
| | Fake tracks | 1.1 ± 0.4 | 1.9 ± 0.6 | 3.7 ± 1.1 | 7.6 ± 2.2 | 8.6 ± 2.5 | 4.8 ± 1.8 |
| | VV | 0.22 ± 0.17 | 0.41 ± 0.29 | 0.66 ± 0.43 | 0.67 ± 0.43 | 0.78 ± 0.53 | 0.64 ± 0.44 |
| | W^\pm +jets | $0.10^{+0.13}_{-0.10}$ | $0.10^{+0.13}_{-0.10}$ | $0.10^{+0.13}_{-0.10}$ | $0.10^{+0.13}_{-0.10}$ | $0.41^{+0.43}_{-0.41}$ | $0.12^{+0.14}_{-0.12}$ |
| | Z +jets | $0.04^{+0.09}_{-0.04}$ | < 0.01 | $0.02^{+0.09}_{-0.02}$ | $0.10^{+0.16}_{-0.10}$ | $0.17^{+0.20}_{-0.17}$ | $0.27^{+0.28}_{-0.27}$ |
| | Others | < 0.01 | < 0.01 | < 0.01 | < 0.01 | < 0.01 | < 0.01 |
| | | Observed | 6 | 11 | 17 | 22 | 18 |
| SR- $1\mu 1T$ | Fitted SM events | 6.6 ± 2.2 | 12.2 ± 4.5 | 17.2 ± 6.4 | 19.6 ± 7.2 | 12.9 ± 4.7 | 8.1 ± 3.3 |
| | Fake tracks | 5.7 ± 2.5 | 10.8 ± 4.6 | 15.6 ± 6.6 | 17.5 ± 7.5 | 10.9 ± 4.9 | 6.4 ± 3.5 |
| | VV | 0.79 ± 0.52 | 1.2 ± 0.8 | 1.3 ± 0.8 | 1.7 ± 1.0 | 1.4 ± 0.8 | 1.1 ± 0.7 |
| | W^\pm +jets | < 0.01 | < 0.01 | < 0.01 | < 0.01 | < 0.01 | < 0.01 |
| | Z +jets | 0.11 ± 0.09 | 0.11 ± 0.09 | 0.24 ± 0.18 | 0.41 ± 0.28 | 0.59 ± 0.36 | 0.66 ± 0.41 |
| | Others | < 0.01 | < 0.01 | < 0.01 | < 0.01 | < 0.01 | < 0.01 |

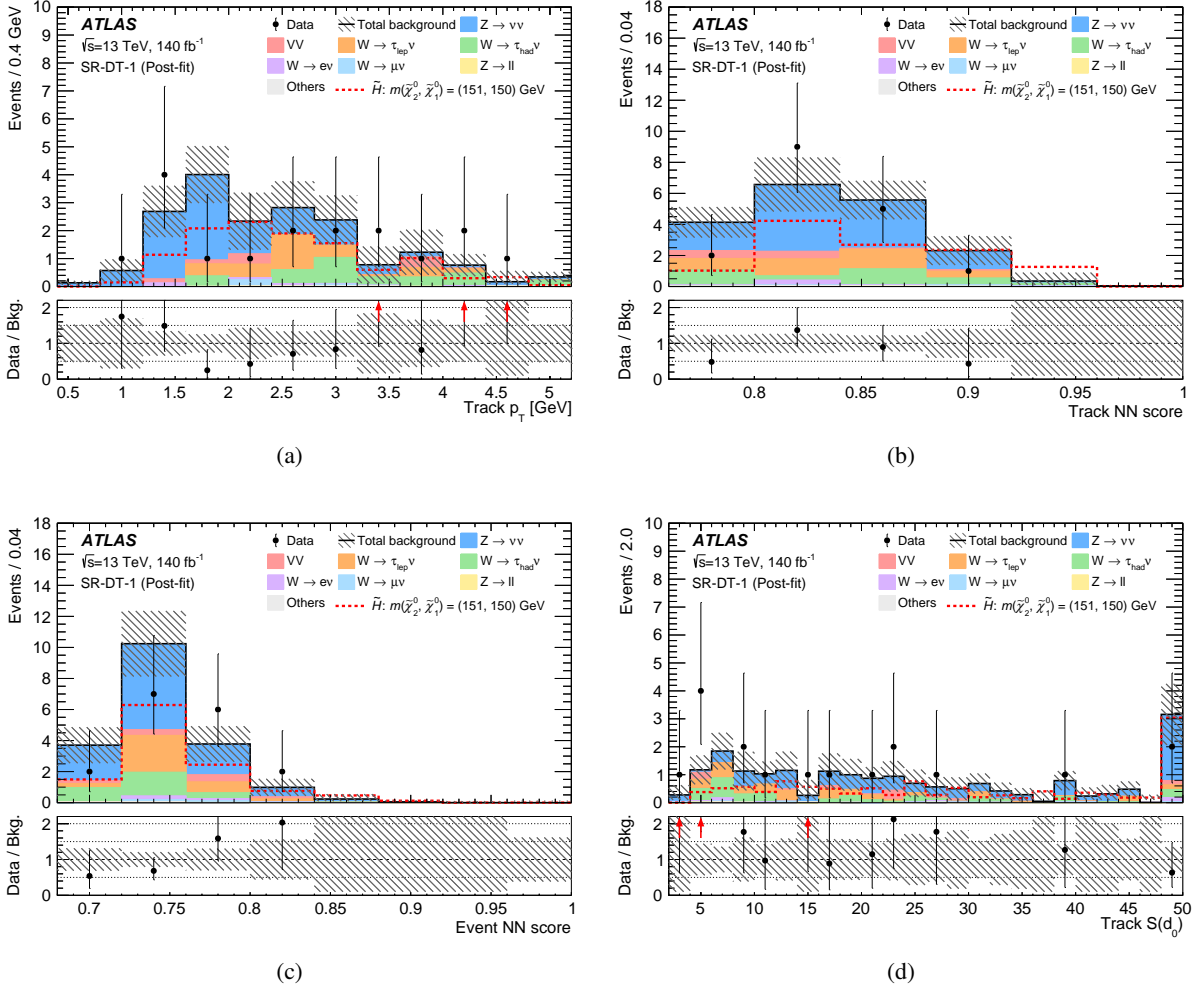


Figure 13: Examples of kinematic distributions in the SRs of the displaced track search after the background-only fit using the CRs. Overflow events are included in the last bin of the track $S(d_0)$ distribution. The category ‘Others’ contains background processes including top quarks, multijets and γ +jets. The uncertainty bands on the expected background include all statistical and systematic uncertainties. Upper arrows in the lower panel indicate data points outside the vertical range shown. Predicted yields for a signal mass point of $m(\tilde{\chi}_2^0, \tilde{\chi}_1^\pm, \tilde{\chi}_1^0) = (151, 150.5, 150)$ GeV is overlaid for reference.

9.3 Model-independent interpretation

For the $1l1T$ search, SR- $1l1T$ -dM1, SR- $1l1T$ -dM3, and SR- $1l1T$ -dM5 are used to test the excesses of events in the SRs and to set upper limits on the visible cross-sections of physics beyond the SM. For this purpose, each SR is constructed by combining the corresponding electron and muon channel SRs into a single bin. A discovery fit configuration is applied, where a generic signal model with an unconstrained normalisation parameter is included to estimate the contributions from any phenomena beyond the SM. The probability under the SM-only hypothesis is quantified by calculating the p -value and the corresponding significance for each SR. For the final state targeted by the displaced track search, analogous results are reported in Ref. [27], where the SRs are defined by a fixed set of kinematic requirements without the use of machine learning classifiers, thus enabling more straightforward reinterpretations of the results in the

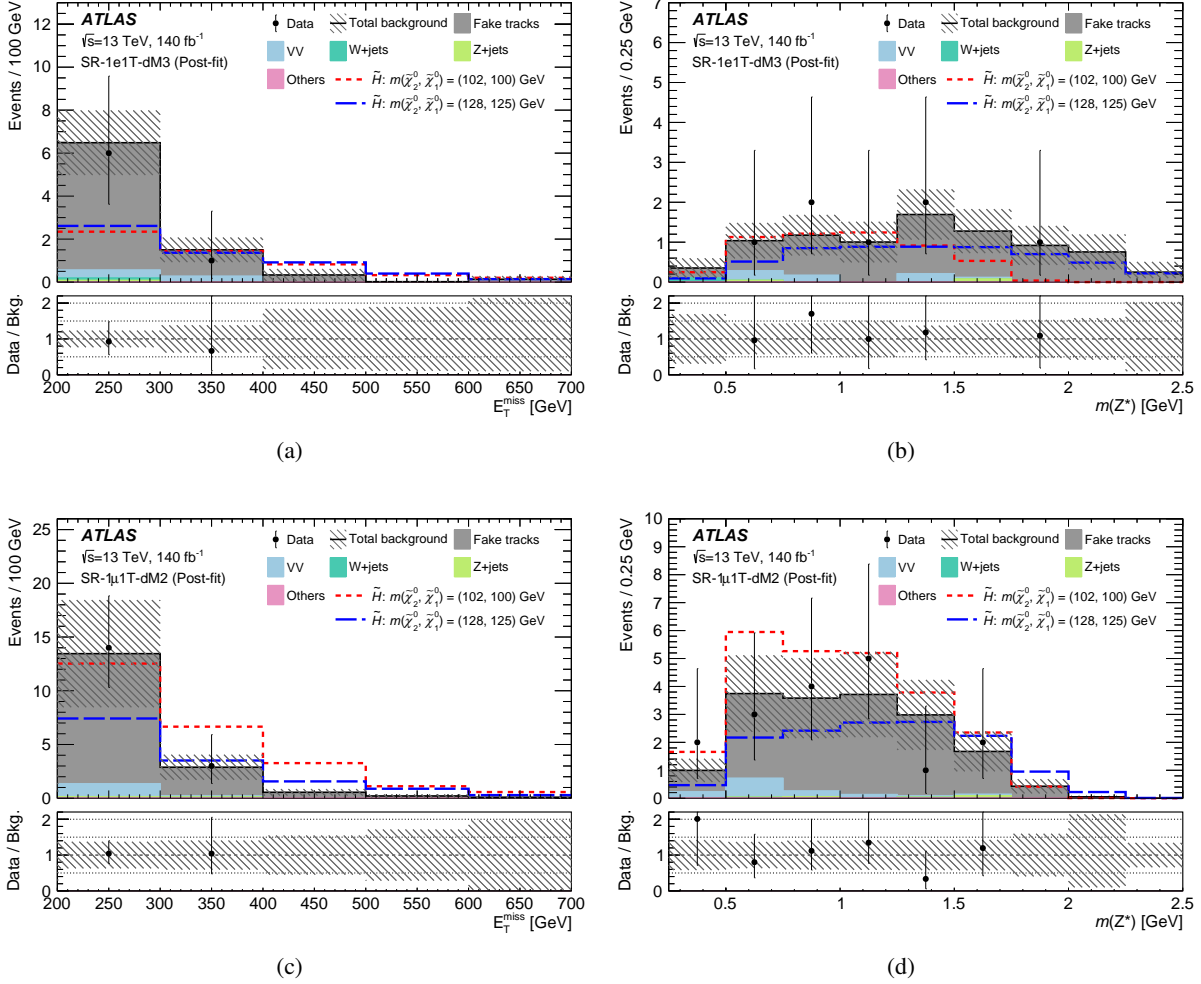


Figure 14: Examples of kinematic distributions in the SRs of the $1\ell 1T$ search after the background-only fit using the CRs. (a) and (b) show distributions of E_T^{miss} and $m(Z^*)$ in SR-1e1T-dM3, respectively. (c) and (d) show distributions for E_T^{miss} and $m(Z^*)$ in SR-1 μ 1T-dM2, respectively. The category ‘Others’ contains background processes including top quarks, multijets and γ +jets. The uncertainty bands on the expected background include all statistical and systematic uncertainties. Predicted yields for signal mass points of $m(\tilde{\chi}_2^0, \tilde{\chi}_1^0) = (102, 100)$ and $(128, 125)$ GeV are overlaid for reference.

Table 14: Results of the model-independent interpretation of the $1\ell 1T$ search. For each SR indicated in the first column, the observed N_{obs} number of events and predicted N_{exp} number of SM events are shown in the second and third columns. The following columns show the observed 95% CL upper limits on the visible cross-section, $\langle\epsilon\sigma\rangle_{\text{obs}}^{95}$, and on the observed and expected number of signal events corresponding to physics beyond the SM, denoted by S_{obs}^{95} and S_{exp}^{95} , respectively. The $\pm 1\sigma$ variations are also shown for S_{exp}^{95} . The final columns show the p -value for the SM-only hypothesis $p(S = 0)$ and the corresponding Gaussian-equivalent statistical significance σ , where p -values are capped at 0.5. For cases in which the data yield is smaller than expected, the p -value and the significance are not shown.

| SR name | N_{obs} | N_{exp} | $\langle\epsilon\sigma\rangle_{\text{obs}}^{95}$ [fb] | S_{obs}^{95} | S_{exp}^{95} | $p(S = 0)$ | σ |
|---------------------|------------------|------------------|---|-----------------------|-----------------------|------------|----------|
| SR- $1\ell 1T$ -dM1 | 7 | 8.1 ± 2.4 | 0.05 | 7.4 | $8.1^{+3.7}_{-2.2}$ | – | – |
| SR- $1\ell 1T$ -dM3 | 29 | 28.1 ± 7.4 | 0.13 | 18.5 | $18.1^{+6.5}_{-4.7}$ | 0.47 | 0.07 |
| SR- $1\ell 1T$ -dM5 | 23 | 13.9 ± 3.7 | 0.14 | 20.1 | $12.7^{+5.3}_{-3.5}$ | 0.07 | 1.48 |

context of some generic beyond the SM physics process.

Table 14 shows the results of the model-independent interpretation for the $1\ell 1T$ search. Data and predicted SM yields agree well in SR- $1\ell 1T$ -dM1 and SR- $1\ell 1T$ -dM3, resulting in 95% confidence level (CL) upper limits of 0.05 fb and 0.13 fb on the visible cross-section of physics beyond the SM. Consistent with the deviation observed in SR- $1\mu 1T$ -dM5, a deviation of 1.5σ is observed between data and the SM predictions in SR- $1\ell 1T$ -dM5, resulting in a looser upper limit of 0.14 fb.

9.4 Model-dependent interpretation

Exclusion fits are performed to set limits on the higgsino model under study. For the displaced track search and for each pNN- θ of the $1\ell 1T$ search, all CRs and SRs are fitted simultaneously with a parameter of interest corresponding to the signal strength, which scales the signal yields in all regions. The CL_s prescription [126] is used to perform hypothesis tests on the target higgsino model. Exclusion limits at 95% CL are presented in a two-dimensional plane with the horizontal axis given by the mass of $\tilde{\chi}_1^\pm$ and the vertical axis given by the mass difference between $\tilde{\chi}_1^\pm$ and $\tilde{\chi}_1^0$, where the simplified higgsino model assumes $\Delta m(\tilde{\chi}_2^0, \tilde{\chi}_1^0) = 2\Delta m(\tilde{\chi}_1^\pm, \tilde{\chi}_1^0)$.

Figure 15 shows the exclusion contours for the displaced track and $1\ell 1T$ searches overlaid on other search results. For the displaced track search, as slight deficits are observed in SR-DT-1, 2, and 4, the observed limit extends beyond the expected, reaching up to about $m(\tilde{\chi}_1^\pm) = 200$ GeV for $\Delta m(\tilde{\chi}_1^\pm, \tilde{\chi}_1^0) = 0.6$ GeV. Excluded $\Delta m(\tilde{\chi}_1^\pm, \tilde{\chi}_1^0)$ ranges from 0.3 to 1.2 GeV.

The exclusion contours of the $1\ell 1T$ search are drawn by taking an envelope of the six contours obtained from the six pNN- θ configurations. This procedure is performed by selecting the pNN- θ with the best expected CL_s for each mass of the signal samples. The expected sensitivity of the $1\ell 1T$ search originates largely from $1\mu 1T$, as the muon-identification efficiency is higher compared with that of electrons in the very low- p_T regime. The effects of slight deficit in data observed in SR- $1e 1T$ -dM4 and slight excess observed in SR- $1\mu 1T$ -dM5 cancel out to yield an observed limit close to the expected limit. The observed limit extends up to $m(\tilde{\chi}_1^\pm) = 130$ GeV at $\Delta m(\tilde{\chi}_1^\pm, \tilde{\chi}_1^0) = 2$ GeV.

The two searches complementarily explore simplified higgsino models in $\Delta m(\tilde{\chi}_1^\pm, \tilde{\chi}_1^0) = 0.3\text{--}3$ GeV, surpassing existing limits set by the LEP experiment [33] and ATLAS searches [27, 29, 127].

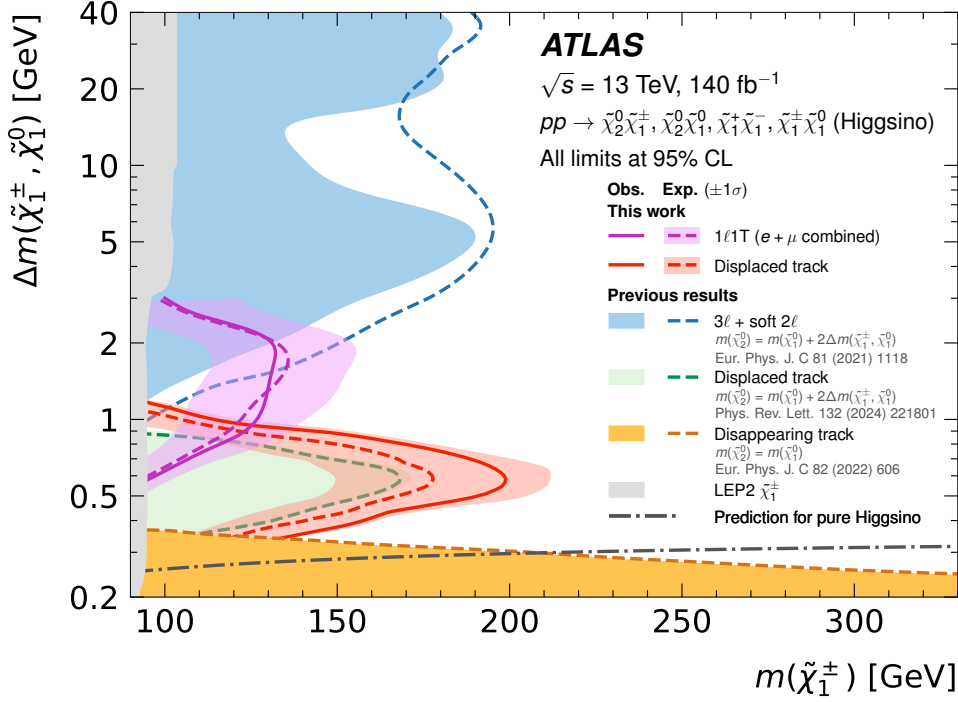


Figure 15: Observed (solid line) and expected (dashed line) limits at 95% CL for simplified higgsino models for $1\ell 1T$ (purple) and displaced track (red) searches. The limits are drawn in the $\Delta m(\tilde{\chi}_1^\pm, \tilde{\chi}_1^0)$ vs $m(\tilde{\chi}_1^\pm)$ plane, with the assumption of $\Delta m(\tilde{\chi}_2^0, \tilde{\chi}_1^0) = 2\Delta m(\tilde{\chi}_1^\pm, \tilde{\chi}_1^0)$. The grey region denotes the mass exclusion limits from the LEP experiment [33]. The blue, light green, and yellow regions indicate the limits from ATLAS soft lepton [29, 30], displaced track [27], and disappearing track [23] searches.

10 Conclusion

Two searches for the direct production of higgsinos with compressed mass spectra are presented, based on 140 fb^{-1} of $\sqrt{s} = 13 \text{ TeV}$ pp collision data collected by the ATLAS experiment at the LHC. Events are required to contain missing transverse momentum, a high- p_T jet, and at least one soft charged particle consistent with the decay of a higgsino-like $\tilde{\chi}_2^0$ or $\tilde{\chi}_1^\pm$ into a nearly mass-degenerate higgsino-like $\tilde{\chi}_1^0$. For models with $\Delta m(\tilde{\chi}_1^\pm, \tilde{\chi}_1^0) \lesssim 1 \text{ GeV}$, the charginos are expected to have non-negligible lifetimes and low- p_T , displaced tracks from their potential decays are identified to reduce contributions from SM background processes. For models with larger mass splittings where the higgsino decays are expected to be prompt, events are selected that feature two low- p_T electrons or muons with opposite charge, where one of the leptons is identified using novel soft-lepton taggers. Both of the searches use neural networks to provide discrimination between signal and SM background processes.

In each search, the data are found to be consistent with the SM predictions and the results are used to set lower limits on the higgsino masses at 95% CL in a simplified model where $\Delta m(\tilde{\chi}_2^0, \tilde{\chi}_1^0) = 2\Delta m(\tilde{\chi}_1^\pm, \tilde{\chi}_1^0)$. The $1\ell 1T$ search is able to set limits in a region where $0.8 \text{ GeV} \lesssim \Delta m(\tilde{\chi}_1^\pm, \tilde{\chi}_1^0) \lesssim 2.0 \text{ GeV}$, extending the limits established by the LEP experiments up to a maximum of $m(\tilde{\chi}_1^\pm) = 132 \text{ GeV}$ for $\Delta m(\tilde{\chi}_1^\pm, \tilde{\chi}_1^0) = 1.8 \text{ GeV}$. Additionally, upper limits on the visible cross-section are set at 95% CL for generic beyond the SM physics processes in the $1\ell 1T$ SRs that are optimized for 1, 3, and 5 GeV mass splittings. The displaced track

search is able to extend the limits on $m(\tilde{\chi}_1^\pm)$ previously set by the ATLAS experiment in this final state by approximately 30 GeV, with a maximum exclusion set at $m(\tilde{\chi}_1^\pm) = 199$ GeV for $\Delta m(\tilde{\chi}_1^\pm, \tilde{\chi}_1^0) = 0.6$ GeV. Taken together, the searches presented here exclude $\tilde{\chi}_1^\pm$ masses below 126 GeV at 95% CL over the targeted range of $\Delta m(\tilde{\chi}_1^\pm, \tilde{\chi}_1^0)$ within the simplified higgsino model. The limits set by the LEP experiments are now superseded by ATLAS in all ranges of $\Delta m(\tilde{\chi}_1^\pm, \tilde{\chi}_1^0)$ by these searches, providing additional scrutiny on the existence of light higgsinos with compressed mass splittings.

Acknowledgements

We thank CERN for the very successful operation of the LHC and its injectors, as well as the support staff at CERN and at our institutions worldwide without whom ATLAS could not be operated efficiently.

The crucial computing support from all WLCG partners is acknowledged gratefully, in particular from CERN, the ATLAS Tier-1 facilities at TRIUMF/SFU (Canada), NDGF (Denmark, Norway, Sweden), CC-IN2P3 (France), KIT/GridKA (Germany), INFN-CNAF (Italy), NL-T1 (Netherlands), PIC (Spain), RAL (UK) and BNL (USA), the Tier-2 facilities worldwide and large non-WLCG resource providers. Major contributors of computing resources are listed in Ref. [128].

We gratefully acknowledge the support of ANPCyT, Argentina; YerPhI, Armenia; ARC, Australia; BMWFW and FWF, Austria; ANAS, Azerbaijan; CNPq and FAPESP, Brazil; NSERC, NRC and CFI, Canada; CERN; ANID, Chile; CAS, MOST and NSFC, China; Minciencias, Colombia; MEYS CR, Czech Republic; DNRF and DNSRC, Denmark; IN2P3-CNRS and CEA-DRF/IRFU, France; SRNSFG, Georgia; BMFTR, HGF and MPG, Germany; GSRI, Greece; RGC and Hong Kong SAR, China; ICHEP and Academy of Sciences and Humanities, Israel; INFN, Italy; MEXT and JSPS, Japan; CNRST, Morocco; NWO, Netherlands; RCN, Norway; MNiSW, Poland; FCT, Portugal; MNE/IFA, Romania; MSTDI, Serbia; MSSR, Slovakia; ARIS and MVZI, Slovenia; DSI/NRF, South Africa; MICIU/AEI, Spain; SRC and Wallenberg Foundation, Sweden; SERI, SNSF and Cantons of Bern and Geneva, Switzerland; NSTC, Taipei; TENMAK, Türkiye; STFC/UKRI, United Kingdom; DOE and NSF, United States of America.

Individual groups and members have received support from BCKDF, CANARIE, CRC and DRAC, Canada; CERN-CZ, FORTE and PRIMUS, Czech Republic; COST, ERC, ERDF, Horizon 2020, ICSC-NextGenerationEU and Marie Skłodowska-Curie Actions, European Union; Investissements d’Avenir Labex, Investissements d’Avenir Idex and ANR, France; DFG and AvH Foundation, Germany; Herakleitos, Thales and Aristeia programmes co-financed by EU-ESF and the Greek NSRF, Greece; BSF-NSF and MINERVA, Israel; NCN and NAWA, Poland; La Caixa Banking Foundation, CERCA Programme Generalitat de Catalunya and PROMETEO and GenT Programmes Generalitat Valenciana, Spain; Göran Gustafssons Stiftelse, Sweden; The Royal Society and Leverhulme Trust, United Kingdom.

In addition, individual members wish to acknowledge support from CERN: European Organization for Nuclear Research (CERN DOCT); Chile: Agencia Nacional de Investigación y Desarrollo (FONDECYT 1230812, FONDECYT 1240864, Fondecyt 3240661, Fondecyt Regular 1240721); China: Chinese Ministry of Science and Technology (MOST-2023YFA1605700, MOST-2023YFA1609300), National Natural Science Foundation of China (NSFC - 12175119, NSFC 12275265); Czech Republic: Czech Science Foundation (GACR - 24-11373S), Ministry of Education Youth and Sports (ERC-CZ-LL2327, FORTE CZ.02.01.01/00/22_008/0004632), PRIMUS Research Programme (PRIMUS/21/SCI/017); EU: H2020 European Research Council (ERC - 101002463); European Union: European Research Council (BARD No. 101116429, ERC - 948254, ERC 101089007), European Regional Development Fund (SMASH COFUND

101081355, SLO ERDF), Horizon 2020 Framework Programme (MUCCA - CHIST-ERA-19-XAI-00), European Union, Future Artificial Intelligence Research (FAIR-NextGenerationEU PE00000013), Italian Center for High Performance Computing, Big Data and Quantum Computing (ICSC, NextGenerationEU); France: Agence Nationale de la Recherche (ANR-21-CE31-0022, ANR-22-EDIR-0002, ANR-24-CE31-0504-01); Germany: Baden-Württemberg Stiftung (BW Stiftung-Postdoc Eliteprogramme), Deutsche Forschungsgemeinschaft (DFG - 469666862, DFG - CR 312/5-2); China: Research Grants Council (GRF); Italy: Istituto Nazionale di Fisica Nucleare (ICSC, NextGenerationEU), Ministero dell'Università e della Ricerca (NextGenEU 153D23001490006 M4C2.1.1, NextGenEU I53D23000820006 M4C2.1.1, NextGenEU I53D23001490006 M4C2.1.1, SOE2024_0000023); Japan: Japan Society for the Promotion of Science (JSPS KAKENHI JP22H01227, JSPS KAKENHI JP22H04944, JSPS KAKENHI JP22KK0227, JSPS KAKENHI JP24K23939, JSPS KAKENHI JP25H00650, JSPS KAKENHI JP25H01291, JSPS KAKENHI JP25K01023); Norway: Research Council of Norway (RCN-314472); Poland: Ministry of Science and Higher Education (IDUB AGH, POB8, D4 no 9722), Polish National Science Centre (NCN 2021/42/E/ST2/00350, NCN OPUS 2023/51/B/ST2/02507, NCN OPUS nr 2022/47/B/ST2/03059, NCN UMO-2019/34/E/ST2/00393, UMO-2022/47/O/ST2/00148, UMO-2023/49/B/ST2/04085, UMO-2023/51/B/ST2/00920, UMO-2024/53/N/ST2/00869); Portugal: Foundation for Science and Technology (FCT); Spain: Generalitat Valenciana (ASFAE/2022/008), Ministry of Science and Innovation (MCIN & NextGenEU PCI2022-135018-2, MICIN & FEDER PID2021-125273NB, RYC2019-028510-I, RYC2020-030254-I, RYC2021-031273-I, RYC2022-038164-I), Ministerio de Ciencia, Innovación y Universidades/Agencia Estatal de Investigación (PID2022-142604OB-C22); Sweden: Carl Trygger Foundation (Carl Trygger Foundation CTS 22:2312), Swedish Research Council (Swedish Research Council 2023-04654, VR 2021-03651, VR 2022-03845, VR 2022-04683, VR 2023-03403, VR 2024-05451), Knut and Alice Wallenberg Foundation (KAW 2018.0458, KAW 2022.0358, KAW 2023.0366); Switzerland: Swiss National Science Foundation (SNSF - PCEFP2_194658); United Kingdom: Leverhulme Trust (Leverhulme Trust RPG-2020-004), Royal Society (NIF-R1-231091); United States of America: U.S. Department of Energy (ECA DE-AC02-76SF00515), Neubauer Family Foundation.

Appendix

A NN trainings for the displaced track search

The event-level and track-level networks for the displaced track search presented in Section 6.1 are trained using signal and background MC events satisfying the selection criteria in Table 2. The simulated signal and background events are split into five batches, of which 60%, 20%, and 20% are allocated to training, validation, and testing sets, respectively. The training is performed using a five-fold cross-validation configuration with early stopping to minimise overfitting. A total of approximately 2.0×10^5 and 1.0×10^5 events are used for signal and background samples, respectively. The training configurations of the event-level and track-level NNs are summarised in Table 15.

B pNN training for the $1\ell 1T$ search

As mentioned in Section 6.2, higgsino production and W^\pm +jets MC events are used to train the pNN for the $1\ell 1T$ search. To ensure enough statistics, higgsino production MC events are used inclusively in terms of mass points and production channels. The pNN- θ of background training samples are assigned randomly so that their distribution matches that of the signal training samples. All training samples are required to satisfy the event and track preselections described in Table 5 and Table 6. For the electron channel, about 2.2×10^4 signal events and 6.3×10^5 background events are used for the training and its validation, where 20% are assigned as validation samples. For the muon channel, about 5.1×10^4 signal events and 3.8×10^5 background events are used for the training and its validation, where 20% are assigned as validation samples. The training configurations of the pNN are also summarised in Table 15, common to both electron and muon channels.

Table 15: Summary of the training configurations of the event-level and track-level NNs for the displaced track (DT) search and the event selection pNN for the $1\ell 1T$ search.

| Hyperparameter | Event-level (DT) | Track-level (DT) | pNN ($1\ell 1T$) |
|--------------------------------|------------------|----------------------|--------------------|
| Number of learnable parameters | 2411 | 2611 | 21957 |
| EarlyStopping | | Enabled | |
| Initial learning rate | | 0.01 | 0.0001 |
| Loss type | | Binary cross-entropy | |
| Optimiser | | Adam [129] | |

References

- [1] Y. Gol'fand and E. Likhtman, *Extension of the Algebra of Poincare Group Generators and Violation of P Invariance*, [JETP Lett. **13** \(1971\) 323](#), [*Pisma Zh. Eksp. Teor. Fiz.* **13** (1971) 452].
- [2] D. V. Volkov and V. P. Akulov, *Is the neutrino a goldstone particle?*, [Phys. Lett. B **46** \(1973\) 109](#).
- [3] J. Wess and B. Zumino, *Supergauge transformations in four dimensions*, [Nucl. Phys. B **70** \(1974\) 39](#).
- [4] J. Wess and B. Zumino, *Supergauge invariant extension of quantum electrodynamics*, [Nucl. Phys. B **78** \(1974\) 1](#).
- [5] S. Ferrara and B. Zumino, *Supergauge invariant Yang-Mills theories*, [Nucl. Phys. B **79** \(1974\) 413](#).
- [6] A. Salam and J. Strathdee, *Super-symmetry and non-Abelian gauges*, [Phys. Lett. B **51** \(1974\) 353](#).
- [7] G. R. Farrar and P. Fayet, *Phenomenology of the production, decay, and detection of new hadronic states associated with supersymmetry*, [Phys. Lett. B **76** \(1978\) 575](#).
- [8] H. Goldberg, *Constraint on the Photino Mass from Cosmology*, [Phys. Rev. Lett. **50** \(1983\) 1419](#), Erratum: [Phys. Rev. Lett. **103** \(2009\) 099905](#).
- [9] J. Ellis, J. Hagelin, D. V. Nanopoulos, K. A. Olive and M. Srednicki, *Supersymmetric relics from the big bang*, [Nucl. Phys. B **238** \(1984\) 453](#).
- [10] N. Sakai, *Naturalness in supersymmetric GUTS*, [Z. Phys. C **11** \(1981\) 153](#).
- [11] S. Dimopoulos, S. Raby and F. Wilczek, *Supersymmetry and the scale of unification*, [Phys. Rev. D **24** \(1981\) 1681](#).
- [12] L. E. Ibáñez and G. G. Ross, *Low-energy predictions in supersymmetric grand unified theories*, [Phys. Lett. B **105** \(1981\) 439](#).
- [13] S. Dimopoulos and H. Georgi, *Softly broken supersymmetry and SU(5)*, [Nucl. Phys. B **193** \(1981\) 150](#).
- [14] R. Barbieri and G. F. Giudice, *Upper bounds on supersymmetric particle masses*, [Nucl. Phys. B **306** \(1988\) 63](#).
- [15] B. de Carlos and J. A. Casas, *One-loop analysis of the electroweak breaking in supersymmetric models and the fine-tuning problem*, [Phys. Lett. B **309** \(1993\) 320](#), arXiv: [hep-ph/9303291](#).
- [16] P. Fayet, *Supersymmetry and weak, electromagnetic and strong interactions*, [Phys. Lett. B **64** \(1976\) 159](#).
- [17] P. Fayet, *Spontaneously broken supersymmetric theories of weak, electromagnetic and strong interactions*, [Phys. Lett. B **69** \(1977\) 489](#).
- [18] R. Barbieri and D. Pappadopulo, *S-particles at their naturalness limits*, [JHEP **10** \(2009\) 061](#), arXiv: [0906.4546 \[hep-ph\]](#).
- [19] H. Baer, V. Barger and P. Huang, *Hidden SUSY at the LHC: the light higgsino-world scenario and the role of a lepton collider*, [JHEP **11** \(2011\) 031](#), arXiv: [1107.5581 \[hep-ph\]](#).
- [20] M. Papucci, J. T. Ruderman and A. Weiler, *Natural SUSY endures*, [JHEP **09** \(2012\) 035](#), arXiv: [1110.6926 \[hep-ph\]](#).

- [21] H. Baer, V. Barger, P. Huang, A. Mustafayev and X. Tata, *Radiative Natural Supersymmetry with a 125 GeV Higgs Boson*, *Phys. Rev. Lett.* **109** (2012) 161802, arXiv: [1207.3343 \[hep-ph\]](#).
- [22] ATLAS Collaboration, *Search for long-lived charginos based on a disappearing-track signature in pp collisions at $\sqrt{s} = 13$ TeV with the ATLAS detector*, *JHEP* **06** (2018) 022, arXiv: [1712.02118 \[hep-ex\]](#).
- [23] ATLAS Collaboration, *Search for long-lived charginos based on a disappearing-track signature using 136fb^{-1} of pp collisions at $\sqrt{s} = 13$ TeV with the ATLAS detector*, *Eur. Phys. J. C* **82** (2022) 606, arXiv: [2201.02472 \[hep-ex\]](#).
- [24] CMS Collaboration, *Search for disappearing tracks as a signature of new long-lived particles in proton–proton collisions at $\sqrt{s} = 13$ TeV*, *JHEP* **08** (2018) 016, arXiv: [1804.07321 \[hep-ex\]](#).
- [25] CMS Collaboration, *Search for disappearing tracks in proton–proton collisions at $\sqrt{s} = 13$ TeV*, *Phys. Lett. B* **806** (2020) 135502, arXiv: [2004.05153 \[hep-ex\]](#).
- [26] H. Fukuda, N. Nagata, H. Oide, H. Otono and S. Shirai, *Cornering Higgsinos Using Soft Displaced Tracks*, *Phys. Rev. Lett.* **124** (2020) 101801, arXiv: [1910.08065 \[hep-ex\]](#).
- [27] ATLAS Collaboration, *Search for Nearly Mass-Degenerate Higgsinos Using Low-Momentum Mildly Displaced Tracks in pp Collisions at $\sqrt{s} = 13$ TeV with the ATLAS Detector*, *Phys. Rev. Lett.* **132** (2024) 221801, arXiv: [2401.14046 \[hep-ex\]](#).
- [28] ATLAS Collaboration, *Search for electroweak production of supersymmetric states in scenarios with compressed mass spectra at $\sqrt{s} = 13$ TeV with the ATLAS detector*, *Phys. Rev. D* **97** (2018) 052010, arXiv: [1712.08119 \[hep-ex\]](#).
- [29] ATLAS Collaboration, *Searches for electroweak production of supersymmetric particles with compressed mass spectra in $\sqrt{s} = 13$ TeV pp collisions with the ATLAS detector*, *Phys. Rev. D* **101** (2020) 052005, arXiv: [1911.12606 \[hep-ex\]](#).
- [30] ATLAS Collaboration, *Search for chargino–neutralino pair production in final states with three leptons and missing transverse momentum in $\sqrt{s} = 13$ TeV pp collisions with the ATLAS detector*, *Eur. Phys. J. C* **81** (2021) 1118, arXiv: [2106.01676 \[hep-ex\]](#).
- [31] CMS Collaboration, *Search for electroweak production of charginos and neutralinos in proton–proton collisions at $\sqrt{s} = 13$ TeV*, *JHEP* **04** (2022) 147, arXiv: [2106.14246 \[hep-ex\]](#).
- [32] CMS Collaboration, *Search for Higgsinos in final states with low-momentum lepton-track pairs at 13 TeV*, 2025, arXiv: [2511.16394 \[hep-ex\]](#).
- [33] ALEPH, DELPHI, L3, OPAL Experiments, *Combined LEP Chargino Results, up to 208 GeV for low DM*, LEPSUSYWG/02-04.1, 2002, URL: http://lepsusy.web.cern.ch/lepsusy/www/inoslowdmsummer02/charginolowdm_pub.html.
- [34] A. Djouadi et al., *The Minimal Supersymmetric Standard Model: Group Summary Report*, 1998, arXiv: [hep-ph/9901246](#).
- [35] C. F. Berger, J. S. Gainer, J. L. Hewett and T. G. Rizzo, *Supersymmetry without prejudice*, *JHEP* **02** (2009) 023, arXiv: [0812.0980 \[hep-ph\]](#).

- [36] ATLAS Collaboration, *ATLAS Run 2 searches for electroweak production of supersymmetric particles interpreted within the $p\text{MSSM}$* , *JHEP* **05** (2024) 106, arXiv: [2402.01392 \[hep-ex\]](#).
- [37] ATLAS Collaboration, *The ATLAS Experiment at the CERN Large Hadron Collider*, *JINST* **3** (2008) S08003.
- [38] J. Alwall, M.-P. Le, M. Lisanti and J. G. Wacker, *Searching for directly decaying gluinos at the Tevatron*, *Phys. Lett. B* **666** (2008) 34, arXiv: [0803.0019 \[hep-ph\]](#).
- [39] J. Alwall, P. C. Schuster and N. Toro, *Simplified models for a first characterization of new physics at the LHC*, *Phys. Rev. D* **79** (2009) 075020, arXiv: [0810.3921 \[hep-ph\]](#).
- [40] D. Alves et al., *Simplified models for LHC new physics searches*, *J. Phys. G* **39** (2012) 105005, arXiv: [1105.2838 \[hep-ph\]](#).
- [41] R. S. Pasechnik, V. A. Beylin, V. I. Kuksa and G. M. Vereshkov, *Neutralino-nucleon interaction in the Split SUSY scenario of the Dark Matter*, *IJMPA* **24** (2009) 6051, arXiv: [0903.4201 \[hep-ph\]](#).
- [42] P. Baldi, K. Cranmer, T. Faucett, P. Sadowski and D. Whiteson, *Parameterized neural networks for high-energy physics*, *Eur. Phys. J. C* **76** (2016) 235, arXiv: [1601.07913 \[hep-ex\]](#).
- [43] ATLAS Collaboration, *Study of the material of the ATLAS inner detector for Run 2 of the LHC*, *JINST* **12** (2017) P12009, arXiv: [1707.02826 \[hep-ex\]](#).
- [44] ATLAS Collaboration, *ATLAS Insertable B-Layer: Technical Design Report*, ATLAS-TDR-19; CERN-LHCC-2010-013, 2010, URL: <https://cds.cern.ch/record/1291633>, Addendum: ATLAS-TDR-19-ADD-1; CERN-LHCC-2012-009, 2012, URL: <https://cds.cern.ch/record/1451888>.
- [45] B. Abbott et al., *Production and integration of the ATLAS Insertable B-Layer*, *JINST* **13** (2018) T05008, arXiv: [1803.00844 \[physics.ins-det\]](#).
- [46] ATLAS Collaboration, *Impact Parameter resolutions in di-jet events*, ATL-IDTR-2018-008, 2018, URL: <https://atlas.web.cern.ch/Atlas/GROUPS/PHYSICS/PLOTS/IDTR-2018-008/>.
- [47] G. Avoni et al., *The new LUCID-2 detector for luminosity measurement and monitoring in ATLAS*, *JINST* **13** (2018) P07017.
- [48] ATLAS Collaboration, *Performance of the ATLAS trigger system in 2015*, *Eur. Phys. J. C* **77** (2017) 317, arXiv: [1611.09661 \[hep-ex\]](#).
- [49] ATLAS Collaboration, *Software and computing for Run 3 of the ATLAS experiment at the LHC*, *Eur. Phys. J. C* **85** (2025) 234, arXiv: [2404.06335 \[hep-ex\]](#).
- [50] ATLAS Collaboration, *Luminosity determination in pp collisions at $\sqrt{s} = 13$ TeV using the ATLAS detector at the LHC*, *Eur. Phys. J. C* **83** (2023) 982, arXiv: [2212.09379 \[hep-ex\]](#).
- [51] ATLAS Collaboration, *ATLAS data quality operations and performance for 2015–2018 data-taking*, *JINST* **15** (2020) P04003, arXiv: [1911.04632 \[physics.ins-det\]](#).
- [52] ATLAS Collaboration, *Performance of the missing transverse momentum triggers for the ATLAS detector during Run-2 data taking*, *JHEP* **08** (2020) 080, arXiv: [2005.09554 \[hep-ex\]](#).

- [53] ATLAS Collaboration, *Performance of electron and photon triggers in ATLAS during LHC Run 2*, *Eur. Phys. J. C* **80** (2020) 47, arXiv: [1909.00761 \[hep-ex\]](#).
- [54] ATLAS Collaboration, *Performance of the ATLAS muon triggers in Run 2*, *JINST* **15** (2020) P09015, arXiv: [2004.13447 \[physics.ins-det\]](#).
- [55] T. Sjöstrand, S. Mrenna and P. Skands, *A brief introduction to PYTHIA 8.1*, *Comput. Phys. Commun.* **178** (2008) 852, arXiv: [0710.3820 \[hep-ph\]](#).
- [56] NNPDF Collaboration, R. D. Ball et al., *Parton distributions with LHC data*, *Nucl. Phys. B* **867** (2013) 244, arXiv: [1207.1303 \[hep-ph\]](#).
- [57] ATLAS Collaboration, *The Pythia 8 A3 tune description of ATLAS minimum bias and inelastic measurements incorporating the Donnachie–Landshoff diffractive model*, ATL-PHYS-PUB-2016-017, 2016, URL: <https://cds.cern.ch/record/2206965>.
- [58] ATLAS Collaboration, *The ATLAS Simulation Infrastructure*, *Eur. Phys. J. C* **70** (2010) 823, arXiv: [1005.4568 \[physics.ins-det\]](#).
- [59] S. Agostinelli et al., *GEANT4 – a simulation toolkit*, *Nucl. Instrum. Meth. A* **506** (2003) 250.
- [60] J. Alwall et al., *The automated computation of tree-level and next-to-leading order differential cross sections, and their matching to parton shower simulations*, *JHEP* **07** (2014) 079, arXiv: [1405.0301 \[hep-ph\]](#).
- [61] C. Bierlich et al., *A comprehensive guide to the physics and usage of PYTHIA 8.3*, *SciPost Phys. Codebases* (2022) 8, arXiv: [2203.11601 \[hep-ph\]](#).
- [62] T. Sjöstrand et al., *An introduction to PYTHIA 8.2*, *Comput. Phys. Commun.* **191** (2015) 159, arXiv: [1410.3012 \[hep-ph\]](#).
- [63] ATLAS Collaboration, *ATLAS Pythia 8 tunes to 7 TeV data*, ATL-PHYS-PUB-2014-021, 2014, URL: <https://cds.cern.ch/record/1966419>.
- [64] L. Lönnblad and S. Prestel, *Matching tree-level matrix elements with interleaved showers*, *JHEP* **03** (2012) 019, arXiv: [1109.4829 \[hep-ph\]](#).
- [65] D. J. Lange, *The EvtGen particle decay simulation package*, *Nucl. Instrum. Meth. A* **462** (2001) 152.
- [66] P. Artoisenet, R. Frederix, O. Mattelaer and R. Rietkerk, *Automatic spin-entangled decays of heavy resonances in Monte Carlo simulations*, *JHEP* **03** (2013) 015, arXiv: [1212.3460 \[hep-ph\]](#).
- [67] A. Djouadi, M. M. Mühlleitner and M. Spira, *Decays of Supersymmetric Particles: the Program SUSY-HIT (SUSpect-SdecaY-Hdecay-InTerface)*, *Acta Phys. Polon. B* **38** (2007) 635, arXiv: [hep-ph/0609292](#).
- [68] W. Beenakker et al., *Production of Charginos, Neutralinos, and Stopped Squarks at Hadron Colliders*, *Phys. Rev. Lett.* **83** (1999) 3780, arXiv: [hep-ph/9906298](#),
Erratum: *Phys. Rev. Lett.* **100** (2008) 029901.
- [69] J. Debove, B. Fuks and M. Klasen, *Threshold resummation for gaugino pair production at hadron colliders*, *Nucl. Phys. B* **842** (2011) 51, arXiv: [1005.2909 \[hep-ph\]](#).
- [70] B. Fuks, M. Klasen, D. R. Lamprea and M. Rothering, *Gaugino production in proton-proton collisions at a center-of-mass energy of 8 TeV*, *JHEP* **10** (2012) 081, arXiv: [1207.2159 \[hep-ph\]](#).

- [71] B. Fuks, M. Klasen, D. R. Lamprea and M. Rothering, *Precision predictions for electroweak superpartner production at hadron colliders with RESUMMINO*, *Eur. Phys. J. C* **73** (2013) 2480, arXiv: [1304.0790 \[hep-ph\]](#).
- [72] J. Fiaschi and M. Klasen, *Neutralino-chargino pair production at NLO+NLL with resummation-improved parton density functions for LHC Run II*, *Phys. Rev. D* **98** (2018) 055014, arXiv: [1805.11322 \[hep-ph\]](#).
- [73] G. Bozzi, B. Fuks and M. Klasen, *Threshold resummation for slepton-pair production at hadron colliders*, *Nucl. Phys. B* **777** (2007) 157, arXiv: [hep-ph/0701202](#).
- [74] B. Fuks, M. Klasen, D. R. Lamprea and M. Rothering, *Revisiting slepton pair production at the Large Hadron Collider*, *JHEP* **01** (2014) 168, arXiv: [1310.2621 \[hep-ph\]](#).
- [75] J. Fiaschi and M. Klasen, *Slepton pair production at the LHC in NLO+NLL with resummation-improved parton densities*, *JHEP* **03** (2018) 094, arXiv: [1801.10357 \[hep-ph\]](#).
- [76] J. Pumplin et al., *New Generation of Parton Distributions with Uncertainties from Global QCD Analysis*, *JHEP* **07** (2002) 012, arXiv: [hep-ph/0201195](#).
- [77] A. D. Martin, W. J. Stirling, R. S. Thorne and G. Watt, *Parton distributions for the LHC*, *Eur. Phys. J. C* **63** (2009) 189, arXiv: [0901.0002 \[hep-ph\]](#).
- [78] NNPDF Collaboration, R. D. Ball et al., *Parton distributions for the LHC run II*, *JHEP* **04** (2015) 040, arXiv: [1410.8849 \[hep-ph\]](#).
- [79] S. Frixione, E. Laenen, P. Motylinski, C. White and B. R. Webber, *Single-top hadroproduction in association with a W boson*, *JHEP* **07** (2008) 029, arXiv: [0805.3067 \[hep-ph\]](#).
- [80] E. Bothmann et al., *Event generation with Sherpa 2.2*, *SciPost Phys.* **7** (2019) 034, arXiv: [1905.09127 \[hep-ph\]](#).
- [81] S. Höche, F. Krauss, M. Schönherr and F. Siegert, *A critical appraisal of NLO+PS matching methods*, *JHEP* **09** (2012) 049, arXiv: [1111.1220 \[hep-ph\]](#).
- [82] S. Höche, F. Krauss, M. Schönherr and F. Siegert, *QCD matrix elements + parton showers. The NLO case*, *JHEP* **04** (2013) 027, arXiv: [1207.5030 \[hep-ph\]](#).
- [83] S. Catani, F. Krauss, B. R. Webber and R. Kuhn, *QCD Matrix Elements + Parton Showers*, *JHEP* **11** (2001) 063, arXiv: [hep-ph/0109231](#).
- [84] S. Höche, F. Krauss, S. Schumann and F. Siegert, *QCD matrix elements and truncated showers*, *JHEP* **05** (2009) 053, arXiv: [0903.1219 \[hep-ph\]](#).
- [85] ATLAS Collaboration, *Multi-Boson Simulation for 13 TeV ATLAS Analyses*, ATL-PHYS-PUB-2017-005, 2017, URL: <https://cds.cern.ch/record/2261933>.
- [86] T. Gleisberg and S. Höche, *Comix, a new matrix element generator*, *JHEP* **12** (2008) 039, arXiv: [0808.3674 \[hep-ph\]](#).

- [87] S. Schumann and F. Krauss,
A parton shower algorithm based on Catani–Seymour dipole factorisation, *JHEP* **03** (2008) 038, arXiv: [0709.1027 \[hep-ph\]](#).
- [88] S. Frixione, G. Ridolfi and P. Nason,
A positive-weight next-to-leading-order Monte Carlo for heavy flavour hadroproduction, *JHEP* **09** (2007) 126, arXiv: [0707.3088 \[hep-ph\]](#).
- [89] P. Nason, *A new method for combining NLO QCD with shower Monte Carlo algorithms*, *JHEP* **11** (2004) 040, arXiv: [hep-ph/0409146](#).
- [90] S. Frixione, P. Nason and C. Oleari,
Matching NLO QCD computations with parton shower simulations: the POWHEG method, *JHEP* **11** (2007) 070, arXiv: [0709.2092 \[hep-ph\]](#).
- [91] S. Alioli, P. Nason, C. Oleari and E. Re, *A general framework for implementing NLO calculations in shower Monte Carlo programs: the POWHEG BOX*, *JHEP* **06** (2010) 043, arXiv: [1002.2581 \[hep-ph\]](#).
- [92] M. Beneke, P. Falgari, S. Klein and C. Schwinn,
Hadronic top-quark pair production with NNLL threshold resummation, *Nucl. Phys. B* **855** (2012) 695, arXiv: [1109.1536 \[hep-ph\]](#).
- [93] M. Cacciari, M. Czakon, M. Mangano, A. Mitov and P. Nason, *Top-pair production at hadron colliders with next-to-next-to-leading logarithmic soft-gluon resummation*, *Phys. Lett. B* **710** (2012) 612, arXiv: [1111.5869 \[hep-ph\]](#).
- [94] P. Bärnreuther, M. Czakon and A. Mitov, *Percent-Level-Precision Physics at the Tevatron: Next-to-Next-to-Leading Order QCD Corrections to $q\bar{q} \rightarrow t\bar{t} + X$* , *Phys. Rev. Lett.* **109** (2012) 132001, arXiv: [1204.5201 \[hep-ph\]](#).
- [95] M. Czakon and A. Mitov, *NNLO corrections to top-pair production at hadron colliders: the all-fermionic scattering channels*, *JHEP* **12** (2012) 054, arXiv: [1207.0236 \[hep-ph\]](#).
- [96] M. Czakon and A. Mitov,
NNLO corrections to top pair production at hadron colliders: the quark-gluon reaction, *JHEP* **01** (2013) 080, arXiv: [1210.6832 \[hep-ph\]](#).
- [97] M. Czakon, P. Fiedler and A. Mitov,
Total Top-Quark Pair-Production Cross Section at Hadron Colliders Through $\mathcal{O}(\alpha_S^4)$, *Phys. Rev. Lett.* **110** (2013) 252004, arXiv: [1303.6254 \[hep-ph\]](#).
- [98] M. Czakon and A. Mitov,
Top++: A program for the calculation of the top-pair cross-section at hadron colliders, *Comput. Phys. Commun.* **185** (2014) 2930, arXiv: [1112.5675 \[hep-ph\]](#).
- [99] S. Alioli, P. Nason, C. Oleari and E. Re,
NLO single-top production matched with shower in POWHEG: s- and t-channel contributions, *JHEP* **09** (2009) 111, arXiv: [0907.4076 \[hep-ph\]](#), Erratum: *JHEP* **02** (2010) 011.
- [100] N. Kidonakis,
Two-loop soft anomalous dimensions for single top quark associated production with a W^- or H^- , *Phys. Rev. D* **82** (2010) 054018, arXiv: [1005.4451 \[hep-ph\]](#).
- [101] N. Kidonakis, ‘Top Quark Production’, *Proceedings, Helmholtz International Summer School on Physics of Heavy Quarks and Hadrons (HQ2013)* (JINR, Dubna, Russia, 15th–28th July 2013) 139, arXiv: [1311.0283 \[hep-ph\]](#).

- [102] E. Re, *Single-top Wt -channel production matched with parton showers using the POWHEG method*, *Eur. Phys. J. C* **71** (2011) 1547, arXiv: [1009.2450 \[hep-ph\]](#).
- [103] ATLAS Collaboration, *Performance of the ATLAS track reconstruction algorithms in dense environments in LHC Run 2*, *Eur. Phys. J. C* **77** (2017) 673, arXiv: [1704.07983 \[hep-ex\]](#).
- [104] ATLAS Collaboration, *Characterisation and mitigation of beam-induced backgrounds observed in the ATLAS detector during the 2011 proton–proton run*, *JINST* **8** (2013) P07004, arXiv: [1303.0223 \[hep-ex\]](#).
- [105] ATLAS Collaboration, *Electron and photon efficiencies in LHC Run 2 with the ATLAS experiment*, *JHEP* **05** (2024) 162, arXiv: [2308.13362 \[hep-ex\]](#).
- [106] ATLAS Collaboration, *Muon reconstruction and identification efficiency in ATLAS using the full Run 2 pp collision data set at $\sqrt{s} = 13$ TeV*, *Eur. Phys. J. C* **81** (2021) 578, arXiv: [2012.00578 \[hep-ex\]](#).
- [107] ATLAS Collaboration, *Jet reconstruction and performance using particle flow with the ATLAS Detector*, *Eur. Phys. J. C* **77** (2017) 466, arXiv: [1703.10485 \[hep-ex\]](#).
- [108] M. Cacciari, G. P. Salam and G. Soyez, *The anti- k_t jet clustering algorithm*, *JHEP* **04** (2008) 063, arXiv: [0802.1189 \[hep-ph\]](#).
- [109] M. Cacciari, G. P. Salam and G. Soyez, *FastJet user manual*, *Eur. Phys. J. C* **72** (2012) 1896, arXiv: [1111.6097 \[hep-ph\]](#).
- [110] ATLAS Collaboration, *Jet energy scale and resolution measured in proton–proton collisions at $\sqrt{s} = 13$ TeV with the ATLAS detector*, *Eur. Phys. J. C* **81** (2021) 689, arXiv: [2007.02645 \[hep-ex\]](#).
- [111] ATLAS Collaboration, *Performance of pile-up mitigation techniques for jets in pp collisions at $\sqrt{s} = 8$ TeV using the ATLAS detector*, *Eur. Phys. J. C* **76** (2016) 581, arXiv: [1510.03823 \[hep-ex\]](#).
- [112] ATLAS Collaboration, *ATLAS flavour-tagging algorithms for the LHC Run 2 pp collision dataset*, *Eur. Phys. J. C* **83** (2023) 681, arXiv: [2211.16345 \[physics.data-an\]](#).
- [113] ATLAS Collaboration, *Measurement of the c -jet mistagging efficiency in $t\bar{t}$ events using pp collision data at $\sqrt{s} = 13$ TeV collected with the ATLAS detector*, *Eur. Phys. J. C* **82** (2022) 95, arXiv: [2109.10627 \[hep-ex\]](#).
- [114] ATLAS Collaboration, *Calibration of the light-flavour jet mistagging efficiency of the b -tagging algorithms with Z +jets events using 139fb^{-1} of ATLAS proton–proton collision data at $\sqrt{s} = 13$ TeV*, *Eur. Phys. J. C* **83** (2023) 728, arXiv: [2301.06319 \[hep-ex\]](#).
- [115] ATLAS Collaboration, *The performance of missing transverse momentum reconstruction and its significance with the ATLAS detector using 140fb^{-1} of $\sqrt{s} = 13$ TeV pp collisions*, *Eur. Phys. J. C* **85** (2025) 606, arXiv: [2402.05858 \[hep-ex\]](#).
- [116] ATLAS Collaboration, *ATLAS b -jet identification performance and efficiency measurement with $t\bar{t}$ events in pp collisions at $\sqrt{s} = 13$ TeV*, *Eur. Phys. J. C* **79** (2019) 970, arXiv: [1907.05120 \[hep-ex\]](#).

- [117] ATLAS Collaboration, *Early Inner Detector Tracking Performance in the 2015 Data at $\sqrt{s} = 13$ TeV*, ATL-PHYS-PUB-2015-051, 2015, URL: <https://cds.cern.ch/record/2110140>.
- [118] A. Paszke et al., ‘PyTorch: An Imperative Style, High-Performance Deep Learning Library’, *Advances in Neural Information Processing Systems*, ed. by H. Wallach et al., vol. 32, Curran Associates, Inc., 2019, arXiv: [1912.01703](https://arxiv.org/abs/1912.01703) [cs.LG].
- [119] ATLAS Collaboration, *Performance of vertex reconstruction algorithms for detection of new long-lived particle decays within the ATLAS inner detector*, ATL-PHYS-PUB-2019-013, 2019, URL: <https://cds.cern.ch/record/2669425>.
- [120] ATLAS Collaboration, *Formulae for Estimating Significance*, ATL-PHYS-PUB-2020-025, 2020, URL: <https://cds.cern.ch/record/2736148>.
- [121] A. Ng, *Feature selection, L1 vs. L2 regularization, and rotational invariance*, *Proceedings of the Twenty-First International Conference on Machine Learning (2004)*.
- [122] ATLAS Collaboration, *Electron and photon performance measurements with the ATLAS detector using the 2015–2017 LHC proton–proton collision data*, *JINST* **14** (2019) P12006, arXiv: [1908.00005](https://arxiv.org/abs/1908.00005) [hep-ex].
- [123] M. Baak et al., *HistFitter software framework for statistical data analysis*, *Eur. Phys. J. C* **75** (2015) 153, arXiv: [1410.1280](https://arxiv.org/abs/1410.1280) [hep-ex].
- [124] G. Cowan, K. Cranmer, E. Gross and O. Vitells, *Asymptotic formulae for likelihood-based tests of new physics*, *Eur. Phys. J. C* **71** (2011) 1554, arXiv: [1007.1727](https://arxiv.org/abs/1007.1727) [physics.data-an], Erratum: *Eur. Phys. J. C* **73** (2013) 2501.
- [125] R. D. Cousins, J. T. Linnemann and J. Tucker, *Evaluation of three methods for calculating statistical significance when incorporating a systematic uncertainty into a test of the background-only hypothesis for a Poisson process*, *Nucl. Instrum. Meth. A* **595** (2008) 480, arXiv: [physics/0702156](https://arxiv.org/abs/physics/0702156) [physics.data-an].
- [126] A. L. Read, *Presentation of search results: the CL_s technique*, *J. Phys. G* **28** (2002) 2693.
- [127] ATLAS Collaboration, *Search for squarks and gluinos in final states with same-sign leptons and jets using 139fb^{-1} of data collected with the ATLAS detector*, *JHEP* **06** (2020) 046, arXiv: [1909.08457](https://arxiv.org/abs/1909.08457) [hep-ex].
- [128] ATLAS Collaboration, *ATLAS Computing Acknowledgements*, ATL-SOFT-PUB-2025-001, 2025, URL: <https://cds.cern.ch/record/2922210>.
- [129] D. P. Kingma and J. Ba, ‘Adam: A Method for Stochastic Optimization’, 2014, arXiv: [1412.6980](https://arxiv.org/abs/1412.6980) [cs.LG].

The ATLAS Collaboration

G. Aad [ID¹⁰⁴](#), E. Aakvaag [ID¹⁷](#), B. Abbott [ID¹²³](#), S. Abdelhameed [ID^{119a}](#), K. Abeling [ID⁵⁵](#), N.J. Abicht [ID⁴⁹](#), S.H. Abidi [ID³⁰](#), M. Aboelela [ID⁴⁵](#), A. Aboulhorma [ID^{36e}](#), H. Abramowicz [ID¹⁵⁷](#), Y. Abulaiti [ID¹²⁰](#), B.S. Acharya [ID^{69a,69b,m}](#), A. Ackermann [ID^{63a}](#), C. Adam Bourdarios [ID⁴](#), L. Adamczyk [ID^{87a}](#), S.V. Addepalli [ID¹⁴⁹](#), M.J. Addison [ID¹⁰³](#), J. Adelman [ID¹¹⁸](#), A. Adiguzel [ID^{22c}](#), T. Adye [ID¹³⁷](#), A.A. Affolder [ID¹³⁹](#), Y. Afik [ID⁴⁰](#), M.N. Agaras [ID¹³](#), A. Aggarwal [ID¹⁰²](#), C. Agheorghiesei [ID^{28c}](#), F. Ahmadov [ID^{39,ad}](#), S. Ahuja [ID⁹⁷](#), X. Ai [ID^{143b}](#), G. Aielli [ID^{76a,76b}](#), A. Aikot [ID¹⁶⁹](#), M. Ait Tamlihat [ID^{36e}](#), B. Aitbenchikh [ID^{36a}](#), M. Akbiyik [ID¹⁰²](#), T.P.A. Åkesson [ID¹⁰⁰](#), A.V. Akimov [ID¹⁵¹](#), D. Akiyama [ID¹⁷⁴](#), N.N. Akolkar [ID²⁵](#), S. Aktas [ID¹⁷²](#), G.L. Alberghi [ID^{24b}](#), J. Albert [ID¹⁷¹](#), U. Alberti [ID²⁰](#), P. Albicocco [ID⁵³](#), G.L. Albouy [ID⁶⁰](#), S. Alderweireldt [ID⁵²](#), Z.L. Alegria [ID¹²⁴](#), M. Aleksa [ID³⁷](#), I.N. Aleksandrov [ID³⁹](#), C. Alexa [ID^{28b}](#), T. Alexopoulos [ID¹⁰](#), F. Alfonsi [ID^{24b}](#), M. Algren [ID⁵⁶](#), M. Alhroob [ID¹⁷³](#), B. Ali [ID¹³⁵](#), H.M.J. Ali [ID^{93,w}](#), S. Ali [ID³²](#), S.W. Alibocus [ID⁹⁴](#), M. Aliev [ID^{34c}](#), G. Alimonti [ID^{71a}](#), W. Alkakhki [ID⁵⁵](#), C. Allaire [ID⁶⁶](#), B.M.M. Allbrooke [ID¹⁵²](#), J.S. Allen [ID¹⁰³](#), J.F. Allen [ID⁵²](#), P.P. Allport [ID²¹](#), A. Aloisio [ID^{72a,72b}](#), F. Alonso [ID⁹²](#), C. Alpigiani [ID¹⁴²](#), Z.M.K. Alsolami [ID⁹³](#), A. Alvarez Fernandez [ID¹⁰²](#), M. Alves Cardoso [ID⁵⁶](#), M.G. Alviggi [ID^{72a,72b}](#), M. Aly [ID¹⁰³](#), Y. Amaral Coutinho [ID^{83b}](#), A. Ambler [ID¹⁰⁶](#), C. Amelung [ID³⁷](#), M. Amerl [ID¹⁰³](#), C.G. Ames [ID¹¹¹](#), T. Amezza [ID¹³⁰](#), D. Amidei [ID¹⁰⁸](#), B. Amini [ID⁵⁴](#), K. Amirie [ID¹⁶¹](#), A. Amirkhanov [ID³⁹](#), S.P. Amor Dos Santos [ID^{133a}](#), K.R. Amos [ID¹⁶⁹](#), D. Amperiadou [ID¹⁵⁸](#), S. An [ID⁸⁴](#), C. Anastopoulos [ID¹⁴⁵](#), T. Andeen [ID¹¹](#), J.K. Anders [ID⁹⁴](#), A.C. Anderson [ID⁵⁹](#), A. Andreatza [ID^{71a,71b}](#), S. Angelidakis [ID⁹](#), A. Angerami [ID⁴²](#), A.V. Anisenkov [ID³⁹](#), A. Annovi [ID^{74a}](#), C. Antel [ID³⁷](#), E. Antipov [ID¹⁵¹](#), M. Antonelli [ID⁵³](#), F. Anulli [ID^{75a}](#), M. Aoki [ID⁸⁴](#), T. Aoki [ID¹⁵⁹](#), M.A. Aparo [ID¹⁵²](#), L. Aperio Bella [ID⁴⁸](#), M. Apicella [ID³¹](#), C. Appelt [ID¹⁵⁷](#), A. Apyan [ID²⁷](#), M. Arampatzi [ID¹⁰](#), S.J. Arbiol Val [ID⁸⁸](#), C. Arcangeletti [ID⁵³](#), A.T.H. Arce [ID⁵¹](#), J-F. Arguin [ID¹¹⁰](#), S. Argyropoulos [ID¹⁵⁸](#), J.-H. Arling [ID⁴⁸](#), O. Arnaez [ID⁴](#), H. Arnold [ID¹⁵¹](#), G. Artoni [ID^{75a,75b}](#), H. Asada [ID¹¹³](#), K. Asai [ID¹²¹](#), S. Asatryan [ID¹⁷⁹](#), N.A. Asbah [ID³⁷](#), R.A. Ashby Pickering [ID¹⁷³](#), A.M. Aslam [ID⁹⁷](#), K. Assamagan [ID³⁰](#), R. Astalos [ID^{29a}](#), K.S.V. Astrand [ID¹⁰⁰](#), S. Atashi [ID¹⁶⁵](#), R.J. Atkin [ID^{34a}](#), H. Atmani [ID^{36f}](#), P.A. Atlasiddha [ID¹³¹](#), K. Augsten [ID¹³⁵](#), A.D. Auriol [ID⁴¹](#), V.A. Austrup [ID¹⁰³](#), G. Avolio [ID³⁷](#), K. Axiotis [ID⁵⁶](#), A. Azzam [ID¹³](#), D. Babal [ID^{29b}](#), H. Bachacou [ID¹³⁸](#), K. Bachas [ID^{158,q}](#), A. Bachi [ID³⁵](#), E. Bachmann [ID⁵⁰](#), M.J. Backes [ID^{63a}](#), A. Badea [ID⁴⁰](#), T.M. Baer [ID¹⁰⁸](#), P. Bagnaia [ID^{75a,75b}](#), M. Bahmani [ID¹⁹](#), D. Bahner [ID⁵⁴](#), K. Bai [ID¹²⁶](#), J.T. Baines [ID¹³⁷](#), L. Baines [ID⁹⁶](#), O.K. Baker [ID¹⁷⁸](#), E. Bakos [ID¹⁶](#), D. Bakshi Gupta [ID⁸](#), L.E. Balabram Filho [ID^{83b}](#), V. Balakrishnan [ID¹²³](#), R. Balasubramanian [ID⁴](#), E.M. Baldin [ID³⁸](#), P. Balek [ID^{87a}](#), E. Ballabene [ID^{24b,24a}](#), F. Balli [ID¹³⁸](#), L.M. Baltes [ID^{63a}](#), W.K. Balunas [ID³³](#), J. Balz [ID¹⁰²](#), I. Bamwidhi [ID^{119b}](#), E. Banas [ID⁸⁸](#), M. Bandieramonte [ID¹³²](#), A. Bandyopadhyay [ID²⁵](#), S. Bansal [ID²⁵](#), L. Barak [ID¹⁵⁷](#), M. Barakat [ID⁴⁸](#), E.L. Barberio [ID¹⁰⁷](#), D. Barberis [ID^{18b}](#), M. Barbero [ID¹⁰⁴](#), M.Z. Barel [ID¹¹⁷](#), T. Barillari [ID¹¹²](#), M-S. Barisits [ID³⁷](#), T. Barklow [ID¹⁴⁹](#), P. Baron [ID¹³⁶](#), D.A. Baron Moreno [ID¹⁰³](#), A. Baroncelli [ID⁶²](#), A.J. Barr [ID¹²⁹](#), J.D. Barr [ID⁹⁸](#), F. Barreiro [ID¹⁰¹](#), J. Barreiro Guimarães da Costa [ID¹⁴](#), M.G. Barros Teixeira [ID^{133a}](#), S. Barsov [ID³⁸](#), F. Bartels [ID^{63a}](#), R. Bartoldus [ID¹⁴⁹](#), A.E. Barton [ID⁹³](#), P. Bartos [ID^{29a}](#), A. Basan [ID¹⁰²](#), M. Baselga [ID⁴⁹](#), S. Bashiri [ID⁸⁸](#), A. Bassalat [ID^{66,b}](#), M.J. Basso [ID^{162a}](#), S. Bataju [ID⁴⁵](#), R. Bate [ID¹⁷⁰](#), R.L. Bates [ID⁵⁹](#), S. Batlamous [ID¹⁰¹](#), M. Battaglia [ID¹³⁹](#), D. Battulga [ID¹⁹](#), M. Bauge [ID^{75a,75b}](#), M. Bauer [ID⁷⁹](#), P. Bauer [ID²⁵](#), L.T. Bayer [ID⁴⁸](#), L.T. Bazzano Hurrell [ID³¹](#), J.B. Beacham [ID¹¹²](#), T. Beau [ID¹³⁰](#), J.Y. Beaucamp [ID⁹²](#), P.H. Beauchemin [ID¹⁶⁴](#), P. Bechtel [ID²⁵](#), H.P. Beck [ID^{20,p}](#), K. Becker [ID¹⁷³](#), A.J. Beddall [ID⁸²](#), V.A. Bednyakov [ID³⁹](#), C.P. Bee [ID¹⁵¹](#), L.J. Beemster [ID¹⁶](#), M. Begalli [ID^{83d}](#), M. Begel [ID³⁰](#), J.K. Behr [ID⁴⁸](#), J.F. Beirer [ID³⁷](#), F. Beisiegel [ID²⁵](#), M. Belfkir [ID^{119b}](#), G. Bella [ID¹⁵⁷](#), L. Bellagamba [ID^{24b}](#), A. Bellerive [ID³⁵](#), C.D. Bellgraph [ID⁶⁸](#), P. Bellos [ID²¹](#), K. Beloborodov [ID³⁸](#), I. Benaoumeur [ID²¹](#), D. Benckekroun [ID^{36a}](#), F. Bendebba [ID^{36a}](#), Y. Benhammou [ID¹⁵⁷](#),

K.C. Benkendorfer ⁶¹, L. Beresford ⁴⁸, M. Beretta ⁵³, E. Bergeaas Kuutmann ¹⁶⁷, N. Berger ⁴,
 B. Bergmann ¹³⁵, J. Beringer ^{18a}, G. Bernardi ⁵, C. Bernius ¹⁴⁹, F.U. Bernlochner ²⁵,
 F. Bernon ³⁷, A. Berrocal Guardia ¹³, T. Berry ⁹⁷, P. Berta ¹³⁶, A. Berthold ⁵⁰, A. Berti ^{133a},
 R. Bertrand ¹⁰⁴, S. Bethke ¹¹², A. Betti ^{75a,75b}, A.J. Bevan ⁹⁶, L. Bezio ⁵⁶, N.K. Bhalla ⁵⁴,
 S. Bharthuar ¹¹², S. Bhatta ¹⁵¹, P. Bhattarai ¹⁴⁹, Z.M. Bhatti ¹²⁰, K.D. Bhide ⁵⁴,
 V.S. Bhopatkar ¹²⁴, R.M. Bianchi ¹³², G. Bianco ^{24b,24a}, O. Biebel ¹¹¹, M. Biglietti ^{77a},
 C.S. Billingsley ⁴⁵, Y. Bimgdi ^{36f}, M. Bindi ⁵⁵, A. Bingham ¹⁷⁷, A. Bingul ^{22b}, C. Bini ^{75a,75b},
 G.A. Bird ³³, M. Birman ¹⁷⁵, M. Biroš ¹³⁶, S. Biryukov ¹⁵², T. Bisanz ⁴⁹, E. Bisceglie ^{24b,24a},
 J.P. Biswal ¹³⁷, D. Biswas ¹⁴⁷, I. Bloch ⁴⁸, A. Blue ⁵⁹, U. Blumenschein ⁹⁶,
 V.S. Bobrovnikov ³⁹, L. Boccardo ^{57b,57a}, M. Boehler ⁵⁴, B. Boehm ¹⁷², D. Bogavac ¹³,
 A.G. Bogdanchikov ³⁸, L.S. Boggia ¹³⁰, V. Boisvert ⁹⁷, P. Bokan ³⁷, T. Bold ^{87a}, M. Bomben ⁵,
 M. Bona ⁹⁶, M. Boonekamp ¹³⁸, A.G. Borbély ⁵⁹, I.S. Bordulev ³⁸, G. Borissov ⁹³,
 D. Bortoletto ¹²⁹, D. Boscherini ^{24b}, M. Bosman ¹³, K. Bouaouda ^{36a}, N. Bouchhar ¹⁶⁹,
 L. Boudet ⁴, J. Boudreau ¹³², E.V. Bouhova-Thacker ⁹³, D. Boumediene ⁴¹, R. Bouquet ^{57b,57a},
 A. Boveia ¹²², J. Boyd ³⁷, D. Boye ³⁰, I.R. Boyko ³⁹, L. Bozianu ⁵⁶, J. Bracinik ²¹,
 N. Brahimy ⁴, G. Brandt ¹⁷⁷, O. Brandt ³³, B. Brau ¹⁰⁵, J.E. Brau ¹²⁶, R. Brenner ¹⁷⁵,
 L. Brenner ¹¹⁷, R. Brenner ¹⁶⁷, S. Bressler ¹⁷⁵, G. Brianti ^{78a,78b}, D. Britton ⁵⁹, D. Britzger ¹¹²,
 I. Brock ²⁵, R. Brock ¹⁰⁹, G. Brooijmans ⁴², A.J. Brooks ⁶⁸, E.M. Brooks ^{162b}, E. Brost ³⁰,
 L.M. Brown ^{171,162a}, L.E. Bruce ⁶¹, T.L. Bruckler ¹²⁹, P.A. Bruckman de Renstrom ⁸⁸,
 B. Brüers ⁴⁸, A. Bruni ^{24b}, G. Bruni ^{24b}, D. Brunner ^{47a,47b}, M. Bruschi ^{24b}, N. Bruscinò ^{75a,75b},
 T. Buanes ¹⁷, Q. Buat ¹⁴², D. Buchin ¹¹², A.G. Buckley ⁵⁹, O. Bulekov ⁸², B.A. Bullard ¹⁴⁹,
 S. Burdin ⁹⁴, C.D. Burgard ⁴⁹, A.M. Burger ⁹¹, B. Burghgrave ⁸, O. Burlayenko ⁵⁴,
 J. Burleson ¹⁶⁸, J.C. Burzynski ¹⁴⁸, E.L. Busch ⁴², V. Büscher ¹⁰², P.J. Bussey ⁵⁹, J.M. Butler ²⁶,
 C.M. Buttar ⁵⁹, J.M. Butterworth ⁹⁸, W. Buttinger ¹³⁷, C.J. Buxo Vazquez ¹⁰⁹, A.R. Buzykaev ³⁹,
 S. Cabrera Urbán ¹⁶⁹, L. Cadamuro ⁶⁶, H. Cai ³⁷, Y. Cai ^{24b,114c,24a}, Y. Cai ^{114a},
 V.M.M. Cairo ³⁷, O. Cakir ^{3a}, N. Calace ³⁷, P. Calafiura ^{18a}, G. Calderini ¹³⁰, P. Calfayan ³⁵,
 L. Calic ¹⁰⁰, G. Callea ⁵⁹, L.P. Caloba ^{83b}, D. Calvet ⁴¹, S. Calvet ⁴¹, R. Camacho Toro ¹³⁰,
 S. Camarda ³⁷, D. Camarero Munoz ²⁷, P. Camarri ^{76a,76b}, C. Camincher ¹⁷¹, M. Campanelli ⁹⁸,
 A. Camplani ⁴³, V. Canale ^{72a,72b}, A.C. Canbay ^{3a}, E. Canonero ⁹⁷, J. Cantero ¹⁶⁹, Y. Cao ¹⁶⁸,
 F. Capocasa ²⁷, M. Capua ^{44b,44a}, A. Carbone ^{71a,71b}, R. Cardarelli ^{76a}, J.C.J. Cardenas ⁸,
 M.P. Cardiff ²⁷, G. Carducci ^{44b,44a}, T. Carli ³⁷, G. Carlino ^{72a}, J.I. Carlotto ¹³,
 B.T. Carlson ^{132,r}, E.M. Carlson ¹⁷¹, J. Carmignani ⁹⁴, L. Carminati ^{71a,71b}, A. Carnelli ⁴,
 M. Carnesale ³⁷, S. Caron ¹¹⁶, E. Carquin ^{140g}, I.B. Carr ¹⁰⁷, S. Carrá ^{73a,73b}, G. Carratta ^{24b,24a},
 C. Carrion Martinez ¹⁶⁹, A.M. Carroll ¹²⁶, M.P. Casado ^{13,h}, P. Casolaro ^{72a,72b}, M. Caspar ⁴⁸,
 W.R. Castiglioni ⁴⁰, F.L. Castillo ⁴, L. Castillo Garcia ¹³, V. Castillo Gimenez ¹⁶⁹,
 N.F. Castro ^{133a,133e}, A. Catinaccio ³⁷, J.R. Catmore ¹²⁸, T. Cavaliere ⁴, V. Cavaliere ³⁰,
 L.J. Caviedes Betancourt ^{23b}, E. Celebi ⁸², S. Cella ³⁷, V. Cepaitis ⁵⁶, K. Cerny ¹²⁵,
 A.S. Cerqueira ^{83a}, A. Cerri ^{74a,am}, L. Cerrito ^{76a,76b}, F. Cerutti ^{18a}, B. Cervato ^{71a,71b},
 A. Cervelli ^{24b}, G. Cesarini ⁵³, S.A. Cetin ⁸², P.M. Chabrilat ¹³⁰, R. Chakkappai ⁶⁶,
 S. Chakraborty ¹⁷³, A. Chambers ⁶¹, J. Chan ^{18a}, W.Y. Chan ¹⁵⁹, J.D. Chapman ³³,
 E. Chapon ¹³⁸, B. Chargeishvili ^{155b}, D.G. Charlton ²¹, C. Chauhan ¹³⁶, Y. Che ^{114a},
 S. Chekanov ⁶, S.V. Chekulaev ^{162a}, G.A. Chelkov ^{39,a}, B. Chen ¹⁵⁷, B. Chen ¹⁷¹, H. Chen ^{114a},
 H. Chen ³⁰, J. Chen ^{144a}, J. Chen ¹⁴⁸, M. Chen ¹²⁹, S. Chen ⁸⁹, S.J. Chen ^{114a}, X. Chen ^{144a},
 X. Chen ^{15,ah}, Z. Chen ⁶², C.L. Cheng ¹⁷⁶, H.C. Cheng ^{64a}, S. Cheong ¹⁴⁹, A. Cheplakov ³⁹,
 E. Cherepanova ¹¹⁷, R. Cherkaoui El Moursli ^{36e}, E. Cheu ⁷, K. Cheung ⁶⁵, L. Chevalier ¹³⁸,
 V. Chiarella ⁵³, G. Chiarelli ^{74a}, G. Chiodini ^{70a}, A.S. Chisholm ²¹, A. Chitan ^{28b},
 M. Chitishvili ¹⁶⁹, M.V. Chizhov ^{39,s}, K. Choi ¹¹, Y. Chou ¹⁴², E.Y.S. Chow ¹¹⁶, K.L. Chu ¹⁷⁵,

M.C. Chu ^{64a}, X. Chu ^{14,114c}, Z. Chubinidze ⁵³, J. Chudoba ¹³⁴, J.J. Chwastowski ⁸⁸,
D. Cieri ¹¹², K.M. Ciesla ^{87a}, V. Cindro ⁹⁵, A. Ciocio ^{18a}, F. Cirotto ^{72a,72b}, Z.H. Citron ¹⁷⁵,
M. Citterio ^{71a}, D.A. Ciubotaru ^{28b}, A. Clark ⁵⁶, P.J. Clark ⁵², N. Clarke Hall ⁹⁸, C. Clarry ¹⁶¹,
S.E. Clawson ⁴⁸, C. Clement ^{47a,47b}, Y. Coadou ¹⁰⁴, M. Cobal ^{69a,69c}, A. Coccaro ^{57b},
R.F. Coelho Barrue ^{133a}, R. Coelho Lopes De Sa ¹⁰⁵, S. Coelli ^{71a}, L.S. Colangeli ¹⁶¹, B. Cole ⁴²,
P. Collado Soto ¹⁰¹, J. Collot ⁶⁰, R. Coluccia ^{70a,70b}, P. Conde Muiño ^{133a,133g}, M.P. Connell ^{34c},
S.H. Connell ^{34c}, E.I. Conroy ¹²⁹, M. Contreras Cossio ¹¹, F. Conventi ^{72a,aj},
A.M. Cooper-Sarkar ¹²⁹, L. Corazzina ^{75a,75b}, F.A. Corchia ^{24b,24a}, A. Cordeiro Oudot Choi ¹⁴²,
L.D. Corpe ⁴¹, M. Corradi ^{75a,75b}, F. Corriveau ^{106,ab}, A. Cortes-Gonzalez ¹⁵⁹, M.J. Costa ¹⁶⁹,
F. Costanza ⁴, D. Costanzo ¹⁴⁵, B.M. Cote ¹²², J. Couthures ⁴, G. Cowan ⁹⁷, K. Cranmer ¹⁷⁶,
L. Cremer ⁴⁹, D. Cremonini ^{24b,24a}, S. Crépe-Renaudin ⁶⁰, F. Crescioli ¹³⁰, T. Cresta ^{73a,73b},
M. Cristinziani ¹⁴⁷, M. Cristoforetti ^{78a,78b}, V. Croft ¹¹⁷, G. Crosetti ^{44b,44a}, A. Cueto ¹⁰¹,
H. Cui ⁹⁸, Z. Cui ⁷, B.M. Cunnett ¹⁵², W.R. Cunningham ⁵⁹, F. Curcio ¹⁶⁹, J.R. Curran ⁵²,
M.J. Da Cunha Sargedas De Sousa ^{57b,57a}, J.V. Da Fonseca Pinto ^{83b}, C. Da Via ¹⁰³,
W. Dabrowski ^{87a}, T. Dado ³⁷, S. Dahbi ¹⁵⁴, T. Dai ¹⁰⁸, D. Dal Santo ²⁰, C. Dallapiccola ¹⁰⁵,
M. Dam ⁴³, G. D'amen ³⁰, V. D'Amico ¹¹¹, J. Damp ¹⁰², J.R. Dandoy ³⁵, M. D'Andrea ^{57b,57a},
D. Dannheim ³⁷, G. D'anniballe ^{74a,74b}, M. Danninger ¹⁴⁸, V. Dao ¹⁵¹, G. Darbo ^{57b},
S.J. Das ³⁰, F. Dattola ⁴⁸, S. D'Auria ^{71a,71b}, A. D'Avanzo ^{72a,72b}, T. Davidek ¹³⁶,
J. Davidson ¹⁷³, I. Dawson ⁹⁶, K. De ⁸, C. De Almeida Rossi ¹⁶¹, R. De Asmundis ^{72a},
N. De Biase ⁴⁸, S. De Castro ^{24b,24a}, N. De Groot ¹¹⁶, P. de Jong ¹¹⁷, H. De la Torre ¹¹⁸,
A. De Maria ^{114a}, A. De Salvo ^{75a}, U. De Sanctis ^{76a,76b}, F. De Santis ^{70a,70b}, A. De Santo ¹⁵²,
J.B. De Vivie De Regie ⁶⁰, J. Debevc ⁹⁵, D.V. Dedovich ³⁹, J. Degens ⁹⁴, A.M. Deiana ⁴⁵,
J. Del Peso ¹⁰¹, L. Delagrangé ¹³⁰, F. Deliot ¹³⁸, C.M. Delitzsch ⁴⁹, M. Della Pietra ^{72a,72b},
D. Della Volpe ⁵⁶, A. Dell'Acqua ³⁷, L. Dell'Asta ^{71a,71b}, M. Delmastro ⁴, C.C. Delogu ¹⁰²,
P.A. Delsart ⁶⁰, S. Demers ¹⁷⁸, M. Demichev ³⁹, S.P. Denisov ³⁸, H. Denizli ^{22a,1},
L. D'Eramo ⁴¹, D. Derendarz ⁸⁸, F. Derue ¹³⁰, P. Dervan ^{94,*}, A.M. Desai ¹, K. Desch ²⁵,
F.A. Di Bello ^{57b,57a}, A. Di Ciaccio ^{76a,76b}, L. Di Ciaccio ⁴, A. Di Domenico ^{75a,75b},
C. Di Donato ^{72a,72b}, A. Di Girolamo ³⁷, G. Di Gregorio ³⁷, A. Di Luca ^{78a,78b},
B. Di Micco ^{77a,77b}, R. Di Nardo ^{77a,77b}, K.F. Di Petrillo ⁴⁰, M. Diamantopoulou ³⁵, F.A. Dias ¹¹⁷,
M.A. Diaz ^{140a,140b}, A.R. Didenko ³⁹, M. Didenko ¹⁶⁹, S.D. Diefenbacher ^{18a}, E.B. Diehl ¹⁰⁸,
S. Díez Cornell ⁴⁸, C. Díez Pardos ¹⁴⁷, C. Dimitriadi ¹⁵⁰, A. Dimitrievska ²¹, A. Dimri ¹⁵¹,
Y. Ding ⁶², J. Dingfelder ²⁵, T. Dingley ¹²⁹, I-M. Dinu ^{28b}, S.J. Dittmeier ^{63b}, F. Dittus ³⁷,
M. Divisek ¹³⁶, B. Dixit ⁹⁴, F. Djama ¹⁰⁴, T. Djobava ^{155b}, C. Doglioni ^{103,100},
A. Dohnalova ^{29a}, Z. Dolezal ¹³⁶, K. Domijan ^{87a}, K.M. Dona ⁴⁰, M. Donadelli ^{83d},
B. Dong ¹⁰⁹, J. Donini ⁴¹, A. D'Onofrio ^{72a,72b}, M. D'Onofrio ⁹⁴, J. Dopke ¹³⁷, A. Doria ^{72a},
N. Dos Santos Fernandes ^{133a}, I.A. Dos Santos Luz ^{83e}, P. Dougan ¹⁰³, M.T. Dova ⁹²,
A.T. Doyle ⁵⁹, M.P. Drescher ⁵⁵, E. Dreyer ¹⁷⁵, I. Drivas-koulouris ¹⁰, M. Drnevich ¹²⁰,
D. Du ⁶², T.A. du Pree ¹¹⁷, Z. Duan ^{114a}, M. Dubau ⁴, F. Dubinin ³⁹, M. Dubovsky ^{29a},
E. Duchovni ¹⁷⁵, G. Duckeck ¹¹¹, P.K. Duckett ⁹⁸, O.A. Ducu ^{28b}, D. Duda ⁵², A. Dudarev ³⁷,
M.M. Dudek ⁸⁸, E.R. Duden ²⁷, M. D'uffizi ¹⁰³, L. Dufflot ⁶⁶, M. Dührssen ³⁷, I. Duminica ^{28g},
A.E. Dumitriu ^{28b}, M. Dunford ^{63a}, K. Dunne ^{47a,47b}, A. Duperrin ¹⁰⁴, H. Duran Yildiz ^{3a},
A. Durglishvili ^{155b}, G.I. Dyckes ^{18a}, M. Dyndal ^{87a}, B.S. Dziedzic ³⁷, Z.O. Earnshaw ¹⁵²,
G.H. Eberwein ¹²⁹, B. Eckerova ^{29a}, S. Eggebrecht ⁵⁵, E. Egidio Purcino De Souza ^{83e},
G. Eigen ¹⁷, K. Einsweiler ^{18a}, T. Ekelof ¹⁶⁷, P.A. Ekman ¹⁰⁰, S. El Farkh ^{36b}, Y. El Ghazali ⁶²,
H. El Jarrari ³⁷, A. El Moussaouy ^{36a}, D. Elitez ³⁷, M. Ellert ¹⁶⁷, F. Ellinghaus ¹⁷⁷,
T.A. Elliot ⁹⁷, N. Ellis ³⁷, J. Elmsheuser ³⁰, M. Elsayy ^{119a}, M. Elsing ³⁷, D. Emeliyanov ¹³⁷,
Y. Enari ⁸⁴, I. Ene ^{18a}, S. Epari ¹¹⁰, D. Ernani Martins Neto ⁸⁸, F. Ernst ³⁷, M. Errenst ¹⁷⁷,

M. Escalier ⁶⁶, C. Escobar ¹⁶⁹, E. Etzion ¹⁵⁷, G. Evans ^{133a,133b}, H. Evans ⁶⁸, L.S. Evans ⁴⁸,
A. Ezhilov ³⁸, S. Ezzarqtouni ^{36a}, F. Fabbri ^{24b,24a}, L. Fabbri ^{24b,24a}, G. Facini ⁹⁸, V. Fadeyev ¹³⁹,
R.M. Fakhruddinov ³⁸, D. Fakoudis ¹⁰², S. Falciano ^{75a}, L.F. Falda Ulhoa Coelho ^{133a},
F. Fallavollita ¹¹², G. Falsetti ^{44b,44a}, J. Faltova ¹³⁶, C. Fan ¹⁶⁸, K.Y. Fan ^{64b}, Y. Fan ¹⁴,
Y. Fang ^{14,114c}, M. Fantì ^{71a,71b}, M. Faraj ^{69a,69b}, Z. Farazpay ⁹⁹, A. Farbin ⁸, A. Farilla ^{77a},
K. Farman ¹⁵⁴, T. Farooque ¹⁰⁹, J.N. Farr ¹⁷⁸, S.M. Farrington ^{137,52}, F. Fassi ^{36e},
D. Fassouliotis ⁹, L. Fayard ⁶⁶, P. Federic ¹³⁶, P. Federicova ¹³⁴, O.L. Fedin ^{38,a}, M. Feickert ¹⁷⁶,
L. Feligioni ¹⁰⁴, D.E. Fellers ^{18a}, C. Feng ^{143a}, Y. Feng ¹⁴, Z. Feng ¹¹⁷, M.J. Fenton ¹⁶⁵,
L. Ferencz ⁴⁸, B. Fernandez Barbadillo ⁹³, P. Fernandez Martinez ⁶⁷, M.J.V. Fernoux ¹⁰⁴,
J. Ferrando ⁹³, A. Ferrari ¹⁶⁷, P. Ferrari ^{117,116}, R. Ferrari ^{73a}, D. Ferrere ⁵⁶, C. Ferretti ¹⁰⁸,
M.P. Fewell ¹, D. Fiacco ^{75a,75b}, F. Fiedler ¹⁰², P. Fiedler ¹³⁵, S. Filimonov ³⁹, M.S. Filip ^{28b,t},
A. Filipčić ⁹⁵, E.K. Filmer ^{162a}, F. Filthaut ¹¹⁶, M.C.N. Fiolhais ^{133a,133c,c}, L. Fiorini ¹⁶⁹,
W.C. Fisher ¹⁰⁹, T. Fitschen ¹⁰³, P.M. Fitzhugh ¹³⁸, I. Fleck ¹⁴⁷, P. Fleischmann ¹⁰⁸, T. Flick ¹⁷⁷,
M. Flores ^{34d,ag}, L.R. Flores Castillo ^{64a}, L. Flores Sanz De Acedo ³⁷, F.M. Follega ^{78a,78b},
N. Fomin ³³, J.H. Foo ¹⁶¹, A. Formica ¹³⁸, A.C. Forti ¹⁰³, E. Fortin ³⁷, A.W. Fortman ^{18a},
L. Foster ^{18a}, L. Fountas ^{9,i}, D. Fournier ⁶⁶, H. Fox ⁹³, P. Francavilla ^{74a,74b}, S. Francescato ⁶¹,
S. Franchellucci ⁵⁶, M. Franchini ^{24b,24a}, S. Franchino ^{63a}, D. Francis ³⁷, L. Franco ¹¹⁶,
L. Franconi ⁴⁸, M. Franklin ⁶¹, G. Frattari ²⁷, Y.Y. Frid ¹⁵⁷, J. Friend ⁵⁹, N. Fritzsche ³⁷,
A. Froch ⁵⁶, D. Froidevaux ³⁷, J.A. Frost ¹²⁹, Y. Fu ¹⁰⁹, S. Fuenzalida Garrido ^{140g},
M. Fujimoto ¹⁰⁴, K.Y. Fung ^{64a}, E. Furtado De Simas Filho ^{83e}, M. Furukawa ¹⁵⁹, J. Fuster ¹⁶⁹,
A. Gaa ⁵⁵, A. Gabrielli ^{24b,24a}, A. Gabrielli ¹⁶¹, P. Gadow ³⁷, G. Gagliardi ^{57b,57a},
L.G. Gagnon ^{18a}, S. Gaid ^{85b}, S. Galantzan ¹⁵⁷, J. Gallagher ¹, E.J. Gallas ¹²⁹, A.L. Gallen ¹⁶⁷,
B.J. Gallop ¹³⁷, K.K. Gan ¹²², S. Ganguly ¹⁵⁹, Y. Gao ⁵², A. Garabaglu ¹⁴²,
F.M. Garay Walls ^{140a,140b}, C. García ¹⁶⁹, A. Garcia Alonso ¹¹⁷, A.G. Garcia Caffaro ¹⁷⁸,
J.E. García Navarro ¹⁶⁹, M.A. Garcia Ruiz ^{23b}, M. Garcia-Sciveres ^{18a}, G.L. Gardner ¹³¹,
R.W. Gardner ⁴⁰, N. Garelli ¹⁶⁴, R.B. Garg ¹⁴⁹, J.M. Gargan ⁵², C.A. Garner ¹⁶¹, C.M. Garvey ^{34a},
V.K. Gassmann ¹⁶⁴, G. Gaudio ^{73a}, V. Gautam ¹³, P. Gauzzi ^{75a,75b}, J. Gavranovic ⁹⁵,
I.L. Gavrilenko ^{133a}, A. Gavrilyuk ³⁸, C. Gay ¹⁷⁰, G. Gaycken ¹²⁶, E.N. Gazis ¹⁰, A. Gekow ¹²²,
C. Gemme ^{57b}, M.H. Genest ⁶⁰, A.D. Gentry ¹¹⁵, S. George ⁹⁷, T. Geralis ⁴⁶, A.A. Gerwin ¹²³,
P. Gessinger-Befurt ³⁷, M.E. Geyik ¹⁷⁷, M. Ghani ¹⁷³, K. Ghorbanian ⁹⁶, A. Ghosal ¹⁴⁷,
A. Ghosh ¹⁶⁵, A. Ghosh ⁷, B. Giacobbe ^{24b}, S. Giagu ^{75a,75b}, T. Giani ¹¹⁷, A. Giannini ⁶²,
S.M. Gibson ⁹⁷, M. Gignac ¹³⁹, D.T. Gil ^{87b}, A.K. Gilbert ^{87a}, B.J. Gilbert ⁴², D. Gillberg ³⁵,
G. Gilles ¹¹⁷, D.M. Gingrich ^{2,ai}, M.P. Giordani ^{69a,69c}, P.F. Giraud ¹³⁸, G. Giugliarelli ^{69a,69c},
D. Giugni ^{71a}, F. Giuli ^{76a,76b}, I. Gkialas ^{9,i}, L.K. Gladilin ³⁸, C. Glasman ¹⁰¹, M. Glazewska ²⁰,
R.M. Gleason ¹⁶⁵, G. Glemža ⁴⁸, M. Glisic ¹²⁶, I. Gnesi ^{44b}, Y. Go ³⁰, M. Goblirsch-Kolb ³⁷,
B. Gocke ⁴⁹, D. Godin ¹¹⁰, B. Gokturk ^{22a}, S. Goldfarb ¹⁰⁷, T. Golling ⁵⁶, M.G.D. Gololo ^{34c},
D. Golubkov ³⁸, J.P. Gombas ¹⁰⁹, A. Gomes ^{133a,133b}, G. Gomes Da Silva ¹⁴⁷,
A.J. Gomez Delegido ³⁷, R. Gonçalves ^{133a}, L. Gonella ²¹, A. Gongadze ^{155c}, F. Gonnella ²¹,
J.L. Gonski ¹⁴⁹, R.Y. González Andana ⁵², S. González de la Hoz ¹⁶⁹, M.V. Gonzalez Rodrigues ⁴⁸,
R. Gonzalez Suarez ¹⁶⁷, S. Gonzalez-Sevilla ⁵⁶, L. Goossens ³⁷, B. Gorini ³⁷, E. Gorini ^{70a,70b},
A. Gorišek ⁹⁵, T.C. Gosart ¹³¹, A.T. Goshaw ⁵¹, M.I. Gostkin ³⁹, S. Goswami ¹²⁴,
C.A. Gottardo ³⁷, S.A. Gotz ¹¹¹, M. Gouighri ^{36b}, A.G. Goussiou ¹⁴², N. Govender ^{34c},
R.P. Grabarczyk ¹²⁹, I. Grabowska-Bold ^{87a}, K. Graham ³⁵, E. Gramstad ¹²⁸,
S. Grancagnolo ^{70a,70b}, C.M. Grant ¹, P.M. Gravila ^{28f}, F.G. Gravili ^{70a,70b}, H.M. Gray ^{18a},
M. Greco ¹¹², M.J. Green ¹, C. Grefe ²⁵, A.S. Grefsrud ¹⁷, I.M. Gregor ⁴⁸, K.T. Greif ¹⁶⁵,
P. Grenier ¹⁴⁹, S.G. Grewe ¹¹², A.A. Grillo ¹³⁹, K. Grimm ³², S. Grinstein ^{13,x}, J.-F. Grivaz ⁶⁶,
E. Gross ¹⁷⁵, J. Grosse-Knetter ⁵⁵, L. Guan ¹⁰⁸, G. Guerrieri ³⁷, R. Guevara ¹²⁸, R. Gugel ¹⁰²,

J.A.M. Guhit ¹⁰⁸, A. Guida ¹⁹, E. Guilloton ¹⁷³, S. Guindon ³⁷, F. Guo ^{14,114c}, J. Guo ^{144a},
 L. Guo ⁴⁸, L. Guo ^{114b,v}, Y. Guo ¹⁰⁸, A. Gupta ⁴⁹, R. Gupta ¹³², S. Gupta ²⁷, S. Gurbuz ²⁵,
 S.S. Gurdasani ⁴⁸, G. Gustavino ^{75a,75b}, P. Gutierrez ¹²³, L.F. Gutierrez Zagazeta ¹³¹,
 M. Gutsche ⁵⁰, C. Gutschow ⁹⁸, C. Gwenlan ¹²⁹, C.B. Gwilliam ⁹⁴, E.S. Haaland ¹²⁸,
 A. Haas ¹²⁰, M. Habedank ⁵⁹, C. Haber ^{18a}, H.K. Hadavand ⁸, A. Haddad ⁴¹, A. Hadeef ⁵⁰,
 A.I. Hagan ⁹³, J.J. Hahn ¹⁴⁷, E.H. Haines ⁹⁸, M. Haleem ¹⁷², J. Haley ¹²⁴, G.D. Hallowell ¹⁰⁴,
 K. Hamano ¹⁷¹, H. Hamdaoui ¹⁶⁷, M. Hamer ²⁵, S.E.D. Hammoud ⁶⁶, E.J. Hampshire ⁹⁷,
 J. Han ^{143a}, L. Han ^{114a}, L. Han ⁶², S. Han ¹⁴, K. Hanagaki ⁸⁴, M. Hance ¹³⁹, D.A. Hangal ⁴²,
 H. Hanif ¹⁴⁸, M.D. Hank ¹³¹, J.B. Hansen ⁴³, P.H. Hansen ⁴³, D. Harada ⁵⁶, T. Harenberg ¹⁷⁷,
 S. Harkusha ¹⁷⁹, M.L. Harris ¹⁰⁵, Y.T. Harris ²⁵, J. Harrison ¹³, N.M. Harrison ¹²²,
 P.F. Harrison ¹⁷³, M.L.E. Hart ⁹⁸, N.M. Hartman ¹¹², N.M. Hartmann ¹¹¹, R.Z. Hasan ^{97,137},
 Y. Hasegawa ¹⁴⁶, F. Haslbeck ¹²⁹, S. Hassan ¹⁷, R. Hauser ¹⁰⁹, M. Haviernik ¹³⁶,
 C.M. Hawkes ²¹, R.J. Hawkings ³⁷, Y. Hayashi ¹⁵⁹, D. Hayden ¹⁰⁹, C. Hayes ¹⁰⁸,
 R.L. Hayes ¹¹⁷, C.P. Hays ¹²⁹, J.M. Hays ⁹⁶, H.S. Hayward ⁹⁴, M. He ^{14,114c}, Y. He ⁴⁸,
 Y. He ⁹⁸, N.B. Heatley ⁹⁶, V. Hedberg ¹⁰⁰, C. Heidegger ⁵⁴, K.K. Heidegger ⁵⁴, J. Heilman ³⁵,
 S. Heim ⁴⁸, T. Heim ^{18a}, J.G. Heinlein ¹³¹, J.J. Heinrich ¹²⁶, L. Heinrich ¹¹², J. Hejbal ¹³⁴,
 M. Helbig ⁵⁰, A. Held ¹⁷⁶, S. Hellesund ¹⁷, C.M. Helling ¹⁷⁰, S. Hellman ^{47a,47b},
 A.M. Henriques Correia ³⁷, H. Herde ¹⁰⁰, Y. Hernández Jiménez ¹⁵¹, L.M. Herrmann ²⁵,
 T. Herrmann ⁵⁰, G. Herten ⁵⁴, R. Hertenberger ¹¹¹, L. Hervas ³⁷, M.E. Hespings ¹⁰²,
 N.P. Hessey ^{162a}, J. Hessler ¹¹², M. Hidaoui ^{36b}, N. Hidic ¹³⁶, E. Hill ¹⁶¹, T.S. Hillersoy ¹⁷,
 S.J. Hillier ²¹, J.R. Hinds ¹⁰⁹, F. Hinterkeuser ²⁵, M. Hirose ¹²⁷, S. Hirose ¹⁶³,
 D. Hirschbuehl ¹⁷⁷, T.G. Hitchings ¹⁰³, B. Hiti ⁹⁵, J. Hobbs ¹⁵¹, R. Hobincu ^{28e}, N. Hod ¹⁷⁵,
 A.M. Hodges ¹⁶⁸, M.C. Hodgkinson ¹⁴⁵, B.H. Hodgkinson ¹²⁹, A. Hoecker ³⁷, D.D. Hofer ¹⁰⁸,
 J. Hofer ¹⁶⁹, M. Holzbock ³⁷, L.B.A.H. Hommels ³³, V. Homsak ¹²⁹, B.P. Honan ¹⁰³,
 J.J. Hong ⁶⁸, T.M. Hong ¹³², B.H. Hooberman ¹⁶⁸, W.H. Hopkins ⁶, M.C. Hoppesch ¹⁶⁸,
 Y. Horii ¹¹³, M.E. Horstmann ¹¹², S. Hou ¹⁵⁴, M.R. Housenga ¹⁶⁸, J. Howarth ⁵⁹, J. Hoya ⁶,
 M. Hrabovsky ¹²⁵, T. Hryn'ova ⁴, P.J. Hsu ⁶⁵, S.-C. Hsu ¹⁴², T. Hsu ⁶⁶, M. Hu ^{18a}, Q. Hu ⁶²,
 S. Huang ³³, X. Huang ^{14,114c}, Y. Huang ¹³⁶, Y. Huang ^{114b}, Y. Huang ¹⁴, Z. Huang ⁶⁶,
 Z. Hubacek ¹³⁵, F. Huegging ²⁵, T.B. Huffman ¹²⁹, M. Hufnagel Maranhã De Faria ^{83a},
 C.A. Hugli ⁴⁸, M. Huhtinen ³⁷, S.K. Huiberts ¹⁷, R. Hulsken ¹⁰⁶, C.E. Hultquist ^{18a},
 D.L. Humphreys ¹⁰⁵, N. Huseynov ¹², J. Huston ¹⁰⁹, J. Huth ⁶¹, L. Huth ⁴⁸, R. Hyneman ⁷,
 G. Iacobucci ⁵⁶, G. Iakovidis ³⁰, L. Iconomidou-Fayard ⁶⁶, J.P. Iddon ³⁷, P. Iengo ^{72a,72b},
 R. Iguchi ¹⁵⁹, Y. Iiyama ¹⁵⁹, T. Iizawa ¹⁵⁹, Y. Ikegami ⁸⁴, D. Iliadis ¹⁵⁸, N. Ilic ¹⁶¹,
 H. Imam ^{36a}, G. Inacio Goncalves ^{83d}, S.A. Infante Cabanas ^{140c}, T. Ingebretsen Carlson ^{47a,47b},
 J.M. Inglis ⁹⁶, G. Introzzi ^{73a,73b}, M. Iodice ^{77a}, V. Ippolito ^{75a,75b}, R.K. Irwin ⁹⁴, M. Ishino ¹⁵⁹,
 W. Islam ¹⁷⁶, C. Issever ¹⁹, S. Istin ^{22a,ao}, K. Itabashi ⁸⁴, H. Ito ¹⁷⁴, R. Iuppa ^{78a,78b},
 A. Ivina ¹⁷⁵, V. Izzo ^{72a}, P. Jacka ¹³⁵, P. Jackson ¹, P. Jain ⁴⁸, K. Jakobs ⁵⁴, T. Jakoubek ¹⁷⁵,
 J. Jamieson ⁵⁹, W. Jang ¹⁵⁹, S. Jankovych ¹³⁶, M. Javurkova ¹⁰⁵, P. Jawahar ¹⁰³, L. Jeanty ¹²⁶,
 J. Jejelava ^{155a,ae}, P. Jenni ^{54,f}, C.E. Jessiman ³⁵, C. Jia ^{143a}, H. Jia ¹⁷⁰, J. Jia ¹⁵¹,
 X. Jia ^{112,114c}, Z. Jia ^{114a}, C. Jiang ⁵², Q. Jiang ^{64b}, S. Jiggins ⁴⁸, M. Jimenez Ortega ¹⁶⁹,
 J. Jimenez Pena ¹³, S. Jin ^{114a}, A. Jinaru ^{28b}, O. Jinnouchi ¹⁴¹, P. Johansson ¹⁴⁵, K.A. Johns ⁷,
 J.W. Johnson ¹³⁹, F.A. Jolly ⁴⁸, D.M. Jones ¹⁵², E. Jones ⁴⁸, K.S. Jones ⁸, P. Jones ³³,
 R.W.L. Jones ⁹³, T.J. Jones ⁹⁴, H.L. Joos ⁵⁵, R. Joshi ¹²², J. Jovicevic ¹⁶, X. Ju ^{18a},
 J.J. Junggeburth ³⁷, T. Junkermann ^{63a}, A. Juste Rozas ^{13,x}, M.K. Juzek ⁸⁸, S. Kabana ^{140f},
 A. Kaczmarzka ⁸⁸, S.A. Kadir ¹⁴⁹, M. Kado ¹¹², H. Kagan ¹²², M. Kagan ¹⁴⁹, A. Kahn ¹³¹,
 C. Kahra ¹⁰², T. Kaji ¹⁵⁹, E. Kajomovitz ¹⁵⁶, N. Kakati ¹⁷⁵, N. Kakoty ¹³, I. Kalaitzidou ⁵⁴,
 S. Kandel ⁸, N. Kanellos ¹⁰, N.J. Kang ¹³⁹, D. Kar ^{34h}, E. Karentzos ²⁵, K. Karki ⁸,

O. Karkout ¹¹⁷, S.N. Karpov ³⁹, Z.M. Karpova ³⁹, V. Kartvelishvili ⁹³, A.N. Karyukhin ³⁸, E. Kasimi ¹⁵⁸, J. Katzy ⁴⁸, S. Kaur ³⁵, K. Kawade ¹⁴⁶, M.P. Kawale ¹²³, C. Kawamoto ⁸⁹, T. Kawamoto ⁶², E.F. Kay ³⁷, F.I. Kaya ¹⁶⁴, S. Kazakos ¹⁰⁹, V.F. Kazanin ³⁸, J.M. Keaveney ^{34a}, R. Keeler ¹⁷¹, G.V. Kehris ⁶¹, J.S. Keller ³⁵, J.M. Kelly ¹⁷¹, J.J. Kempster ¹⁵², O. Kepka ¹³⁴, J. Kerr ^{162b}, B.P. Kerridge ¹³⁷, B.P. Kerševan ⁹⁵, L. Keszeghova ^{29a}, R.A. Khan ¹³², A. Khanov ¹²⁴, A.G. Kharlamov ³⁸, T. Kharlamova ³⁸, E.E. Khoda ¹⁴², M. Kholodenko ^{133a}, T.J. Khoo ¹⁹, G. Khorauli ¹⁷², Y. Khoulaki ^{36a}, J. Khubua ^{155b,*}, Y.A.R. Khwaira ¹³⁰, B. Kibirige ^{34h}, D. Kim ⁶, D.W. Kim ^{47a,47b}, Y.K. Kim ⁴⁰, N. Kimura ⁹⁸, M.K. Kingston ⁵⁵, A. Kirchhoff ⁵⁵, C. Kirfel ²⁵, F. Kirfel ²⁵, J. Kirk ¹³⁷, A.E. Kiryunin ¹¹², S. Kita ¹⁶³, O. Kivernyk ²⁵, M. Klassen ¹⁶⁴, C. Klein ³⁵, L. Klein ¹⁷², M.H. Klein ⁴⁵, S.B. Klein ⁵⁶, U. Klein ⁹⁴, A. Klimentov ³⁰, T. Klioutchnikova ³⁷, P. Kluit ¹¹⁷, S. Kluth ¹¹², E. Kneringer ⁷⁹, T.M. Knight ¹⁶¹, A. Knue ⁴⁹, M. Kobel ⁵⁰, D. Kobylanskii ¹⁷⁵, S.F. Koch ¹²⁹, M. Kocian ¹⁴⁹, P. Kodyš ¹³⁶, D.M. Koeck ¹²⁶, T. Koffas ³⁵, O. Kolay ⁵⁰, I. Koletsou ⁴, T. Komarek ⁸⁸, K. Köneke ⁵⁵, A.X.Y. Kong ¹, T. Kono ¹²¹, N. Konstantinidis ⁹⁸, P. Kontaxakis ⁵⁶, B. Konya ¹⁰⁰, R. Kopeliansky ⁴², S. Koperny ^{87a}, K. Korcyl ⁸⁸, K. Kordas ^{158,d}, A. Korn ⁹⁸, S. Korn ⁵⁵, I. Korolkov ¹³, N. Korotkova ³⁸, B. Kortman ¹¹⁷, O. Kortner ¹¹², S. Kortner ¹¹², W.H. Kostecka ¹¹⁸, M. Kostov ^{29a}, V.V. Kostyukhin ¹⁴⁷, A. Kotsokechagia ³⁷, A. Kotwal ⁵¹, A. Koulouris ³⁷, A. Kourkoumeli-Charalampidi ^{73a,73b}, C. Kourkoumelis ⁹, E. Kourlitis ¹¹², O. Kovanda ¹²⁶, R. Kowalewski ¹⁷¹, W. Kozanecki ¹²⁶, A.S. Kozhin ³⁸, V.A. Kramarenko ³⁸, G. Kramberger ⁹⁵, P. Kramer ²⁵, M.W. Krasny ¹³⁰, A. Krasznahorkay ¹⁰⁵, A.C. Kraus ¹¹⁸, J.W. Kraus ¹⁷⁷, J.A. Kremer ⁴⁸, N.B. Krengel ¹⁴⁷, T. Kresse ⁵⁰, L. Kretschmann ¹⁷⁷, J. Kretschmar ⁹⁴, P. Krieger ¹⁶¹, K. Krizka ²¹, K. Kroeninger ⁴⁹, H. Kroha ¹¹², J. Kroll ¹³⁴, J. Kroll ¹³¹, K.S. Krowpman ¹⁰⁹, U. Kruchonak ³⁹, H. Krüger ²⁵, N. Krumnack ⁸¹, M.C. Kruse ⁵¹, O. Kuchinskaia ³⁹, S. Kудay ^{3a}, S. Kuehn ³⁷, R. Kuesters ⁵⁴, T. Kuhl ⁴⁸, V. Kukhtin ³⁹, Y. Kulchitsky ³⁹, S. Kuleshov ^{140d,140b}, J. Kull ¹, E.V. Kumar ¹¹¹, M. Kumar ^{34h}, N. Kumari ⁴⁸, P. Kumari ^{162b}, A. Kupco ¹³⁴, A. Kupich ³⁸, O. Kuprash ⁵⁴, H. Kurashige ⁸⁶, L.L. Kurchaninov ^{162a}, O. Kurdysh ⁴, Y.A. Kurochkin ³⁸, A. Kurova ³⁸, M. Kuze ¹⁴¹, A.K. Kvam ¹⁰⁵, J. Kvita ¹²⁵, N.G. Kyriacou ¹⁴², C. Lacasta ¹⁶⁹, F. Lacava ^{75a,75b}, H. Lacker ¹⁹, D. Lacour ¹³⁰, N.N. Lad ⁹⁸, E. Ladygin ³⁹, A. Lafarge ⁴¹, B. Laforge ¹³⁰, T. Lagouri ¹⁷⁸, F.Z. Lahbabi ^{36a}, S. Lai ^{55,37}, W.S. Lai ⁹⁸, J.E. Lambert ¹⁷¹, S. Lammers ⁶⁸, W. Lampl ⁷, C. Lampoudis ^{158,d}, G. Lamprinoudis ¹⁰², A.N. Lancaster ¹¹⁸, E. Lançon ³⁰, U. Landgraf ⁵⁴, M.P.J. Landon ⁹⁶, V.S. Lang ⁵⁴, O.K.B. Langrekken ¹²⁸, A.J. Lankford ¹⁶⁵, F. Lanni ³⁷, K. Lantzsck ²⁵, A. Lanza ^{73a}, M. Lanzac Berrocal ¹⁶⁹, J.F. Laporte ¹³⁸, T. Lari ^{71a}, D. Larsen ¹⁷, L. Larson ¹¹, F. Lasagni Manghi ^{24b}, M. Lassnig ³⁷, S.D. Lawlor ¹⁴⁵, R. Lazaridou ¹⁶⁵, M. Lazzaroni ^{71a,71b}, E.T.T. Le ¹⁶⁵, H.D.M. Le ¹⁰⁹, E.M. Le Boulicaut ¹⁷⁸, L.T. Le Pottier ^{18a}, B. Leban ^{24b,24a}, F. Ledroit-Guillon ⁶⁰, T.F. Lee ^{162b}, L.L. Leeuw ^{34c}, M. Lefebvre ¹⁷¹, C. Leggett ^{18a}, G. Lehmann Miotto ³⁷, M. Leigh ⁵⁶, W.A. Leight ¹⁰⁵, W. Leinonen ¹¹⁶, A. Leisos ^{158,u}, M.A.L. Leite ^{83c}, C.E. Leitgeb ¹⁹, R. Leitner ¹³⁶, K.J.C. Leney ⁴⁵, T. Lenz ²⁵, S. Leone ^{74a}, C. Leonidopoulos ⁵², A. Leopold ¹⁵⁰, J.H. Lepage Bourbonnais ³⁵, R. Les ¹⁰⁹, C.G. Lester ³³, M. Levchenko ³⁸, J. Levêque ⁴, L.J. Levinson ¹⁷⁵, G. Levrini ^{24b,24a}, M.P. Lewicki ⁸⁸, C. Lewis ¹⁴², D.J. Lewis ⁴, L. Lewitt ¹⁴⁵, A. Li ³⁰, B. Li ^{143a}, C. Li ¹⁰⁸, C-Q. Li ¹¹², H. Li ^{143a}, H. Li ¹⁰³, H. Li ¹⁵, H. Li ⁶², H. Li ^{143a}, J. Li ^{144a}, K. Li ¹⁴, L. Li ^{144a}, R. Li ¹⁷⁸, S. Li ^{14,114c}, S. Li ^{144b,144a}, T. Li ⁵, X. Li ¹⁰⁶, Y. Li ¹⁴, Z. Li ¹⁵⁹, Z. Li ^{14,114c}, Z. Li ⁶², S. Liang ^{14,114c}, Z. Liang ¹⁴, M. Liberatore ¹³⁸, B. Liberti ^{76a}, G.B. Libotte ^{83d}, K. Lie ^{64c}, J. Lieber Marin ^{83e}, H. Lien ⁶⁸, H. Lin ¹⁰⁸, S.F. Lin ¹⁵¹, L. Linden ¹¹¹, R.E. Lindley ⁷, J.H. Lindon ³⁷, J. Ling ⁶¹, E. Lipeles ¹³¹, A. Lipniacka ¹⁷, A. Lister ¹⁷⁰, J.D. Little ⁶⁸, B. Liu ¹⁴, B.X. Liu ^{114b}, D. Liu ^{144b,144a},

D. Liu ¹³⁹, E.H.L. Liu ²¹, J.K.K. Liu ¹²⁰, K. Liu ^{144b}, K. Liu ^{144b,144a}, M. Liu ⁶², M.Y. Liu ⁶²,
 P. Liu ¹⁴, Q. Liu ^{144b,142,144a}, S. Liu ¹⁵¹, X. Liu ⁶², X. Liu ^{143a}, Y. Liu ^{114b,114c}, Y.L. Liu ^{143a},
 Y.W. Liu ⁶², Z. Liu ^{66,k}, S.L. Lloyd ⁹⁶, E.M. Lobodzinska ⁴⁸, P. Loch ⁷, E. Lodhi ¹⁶¹,
 K. Lohwasser ¹⁴⁵, E. Loiacono ⁴⁸, J.D. Lomas ²¹, J.D. Long ⁴², I. Longarini ¹⁶⁵, R. Longo ¹⁶⁸,
 A. Lopez Solis ¹³, N.A. Lopez-canelas ⁷, N. Lorenzo Martinez ⁴, A.M. Lory ¹¹¹, M. Losada ^{119a},
 G. Löschcke Centeno ⁴, X. Lou ^{47a,47b}, X. Lou ^{14,114c}, A. Lounis ⁶⁶, P.A. Love ⁹³, M. Lu ⁶⁶,
 S. Lu ¹³¹, Y.J. Lu ¹⁵⁴, H.J. Lubatti ¹⁴², C. Luci ^{75a,75b}, F.L. Lucio Alves ^{114a}, F. Luehring ⁶⁸,
 B.S. Lunday ¹³¹, O. Lundberg ¹⁵⁰, J. Lunde ³⁷, N.A. Luongo ⁶, M.S. Lutz ³⁷, A.B. Lux ²⁶,
 D. Lynn ³⁰, R. Lysak ¹³⁴, V. Lysenko ¹³⁵, E. Lytken ¹⁰⁰, V. Lyubushkin ³⁹, T. Lyubushkina ³⁹,
 M.M. Lyukova ¹⁵¹, H. Ma ³⁰, K. Ma ⁶², L.L. Ma ^{143a}, W. Ma ⁶², Y. Ma ¹²⁴,
 J.C. MacDonald ¹⁰², P.C. Machado De Abreu Farias ^{83e}, D. Macina ³⁷, R. Madar ⁴¹,
 T. Madula ⁹⁸, J. Maeda ⁸⁶, T. Maeno ³⁰, P.T. Mafa ^{34c,j}, H. Maguire ¹⁴⁵, M. Maheshwari ³³,
 V. Maiboroda ⁶⁶, A. Maio ^{133a,133b,133d}, K. Maj ^{87a}, O. Majersky ⁴⁸, S. Majewski ¹²⁶,
 R. Makhmanazarov ³⁸, N. Makovec ⁶⁶, V. Maksimovic ¹⁶, B. Malaescu ¹³⁰, J. Malamant ¹²⁸,
 Pa. Malecki ⁸⁸, V.P. Maleev ³⁸, F. Malek ^{60,o}, M. Mali ⁹⁵, D. Malito ⁹⁷, U. Mallik ^{80,*},
 A. Maloizel ⁵, S. Maltezos ¹⁰, A. Malvezzi Lopes ^{83d}, S. Malyukov ³⁹, J. Mamuzic ⁹⁵, G. Mancini ⁵³,
 M.N. Mancini ²⁷, G. Manco ^{73a,73b}, J.P. Mandalia ⁹⁶, S.S. Mandarry ¹⁵², I. Mandić ⁹⁵,
 L. Manhaes de Andrade Filho ^{83a}, I.M. Maniatis ¹⁷⁵, J. Manjarres Ramos ⁹¹, D.C. Mankad ¹⁷⁵,
 A. Mann ¹¹¹, T. Manoussos ³⁷, M.N. Mantinan ⁴⁰, S. Manzoni ³⁷, L. Mao ^{144a},
 X. Mapekula ^{34c}, A. Marantis ¹⁵⁸, R.R. Marcelo Gregorio ⁹⁶, G. Marchiori ⁵, C. Marcon ^{71a},
 E. Maricic ¹⁶, M. Marinescu ⁴⁸, S. Marium ⁴⁸, M. Marjanovic ¹²³, A. Markhoos ⁵⁴,
 M. Markovitch ⁶⁶, M.K. Maroun ¹⁰⁵, M.C. Marr ¹⁴⁸, G.T. Marsden ¹⁰³, E.J. Marshall ⁹³,
 Z. Marshall ^{18a}, S. Marti-Garcia ¹⁶⁹, J. Martin ⁹⁸, T.A. Martin ¹³⁷, V.J. Martin ⁵²,
 B. Martin dit Latour ¹⁷, L. Martinelli ^{75a,75b}, M. Martinez ^{13,x}, P. Martinez Agullo ¹⁶⁹,
 V.I. Martinez Outschoorn ¹⁰⁵, P. Martinez Suarez ³⁷, S. Martin-Haugh ¹³⁷, G. Martinovicova ¹³⁶,
 V.S. Martoiu ^{28b}, A.C. Martyniuk ⁹⁸, A. Marzin ³⁷, D. Mascione ^{78a,78b}, L. Masetti ¹⁰²,
 J. Masik ¹⁰³, A.L. Maslennikov ³⁹, S.L. Mason ⁴², P. Massarotti ^{72a,72b}, P. Mastrandrea ^{74a,74b},
 A. Mastroberardino ^{44b,44a}, T. Masubuchi ¹²⁷, T.T. Mathew ¹²⁶, J. Matousek ¹³⁶, D.M. Mattern ⁴⁹,
 J. Maurer ^{28b}, T. Maurin ⁵⁹, A.J. Maury ⁶⁶, B. Maček ⁹⁵, C. Mavungu Tsava ¹⁰⁴,
 D.A. Maximov ³⁸, A.E. May ¹⁰³, E. Mayer ⁴¹, R. Mazini ^{34h}, I. Maznas ¹¹⁸, S.M. Mazza ¹³⁹,
 E. Mazzeo ³⁷, J.P. Mc Gowan ¹⁷¹, S.P. Mc Kee ¹⁰⁸, C.A. Mc Lean ⁶, C.C. McCracken ¹⁷⁰,
 E.F. McDonald ¹⁰⁷, A.E. McDougall ¹¹⁷, L.F. Mcelhinney ⁹³, J.A. Mcfayden ¹⁵²,
 R.P. McGovern ¹³¹, R.P. Mckenzie ^{34h}, T.C. Mclachlan ⁴⁸, D.J. McLaughlin ⁹⁸, S.J. McMahon ¹³⁷,
 C.M. Mcpartland ⁹⁴, R.A. McPherson ^{171,ab}, S. Mehlhase ¹¹¹, A. Mehta ⁹⁴, D. Melini ¹⁶⁹,
 B.R. Mellado Garcia ^{34h}, A.H. Melo ⁵⁵, F. Meloni ⁴⁸, A.M. Mendes Jacques Da Costa ¹⁰³,
 L. Meng ⁹³, S. Menke ¹¹², M. Mentink ³⁷, E. Meoni ^{44b,44a}, G. Mercado ¹¹⁸, S. Merianos ¹⁵⁸,
 C. Merlassino ^{69a,69c}, C. Meroni ^{71a,71b}, J. Metcalfe ⁶, A.S. Mete ⁶, E. Meuser ¹⁰², C. Meyer ⁶⁸,
 J-P. Meyer ¹³⁸, Y. Miao ^{114a}, R.P. Middleton ¹³⁷, M. Mihovilovic ⁶⁶, L. Mijović ⁵²,
 G. Mikenberg ¹⁷⁵, M. Mikestikova ¹³⁴, M. Mikuž ⁹⁵, H. Mildner ¹⁰², A. Milic ³⁷,
 D.W. Miller ⁴⁰, E.H. Miller ¹⁴⁹, A. Milov ¹⁷⁵, D.A. Milstead ^{47a,47b}, T. Min ^{114a}, A.A. Minaenko ³⁸,
 I.A. Minashvili ^{155b}, A.I. Mincer ¹²⁰, B. Mindur ^{87a}, M. Mineev ³⁹, Y. Mino ⁸⁹, L.M. Mir ¹³,
 M. Miralles Lopez ⁵⁹, M. Mironova ^{18a}, M. Missio ¹¹⁶, A. Mitra ¹⁷³, V.A. Mitsou ¹⁶⁹,
 Y. Mitsumori ¹¹³, O. Miu ¹⁶¹, P.S. Miyagawa ⁹⁶, T. Mkrtychyan ^{63a}, M. Mlinarevic ⁹⁸,
 T. Mlinarevic ⁹⁸, M. Mlynarikova ¹³⁶, L. Mlynarska ^{87a}, C. Mo ^{144a}, S. Mobius ²⁰,
 M.H. Mohamed Farook ¹¹⁵, S. Mohapatra ⁴², M.F. Mohd Soberi ⁵², S. Mohiuddin ¹²⁴,
 G. Mokgatitwane ^{34h}, L. Moleri ¹⁷⁵, U. Molinatti ¹²⁹, L.G. Mollier ²⁰, B. Mondal ¹³⁴,
 S. Mondal ¹³⁵, K. Mönig ⁴⁸, E. Monnier ¹⁰⁴, L. Monsonis Romero ¹⁶⁹, J. Montejo Berlingen ¹³,

A. Montella ^{47a,47b}, M. Montella ¹²², F. Montereali ^{77a,77b}, F. Monticelli ⁹², S. Monzani ^{69a,69c},
 A. Morancho Tarda ⁴³, N. Morange ⁶⁶, A.L. Moreira De Carvalho ⁴⁸, M. Moreno Llácer ¹⁶⁹,
 C. Moreno Martinez ⁵⁶, J.M. Moreno Perez ^{23b}, P. Morettini ^{57b}, S. Morgenstern ³⁷, M. Morii ⁶¹,
 M. Morinaga ¹⁵⁹, M. Moritsu ⁹⁰, F. Morodei ^{75a,75b}, P. Moschovakos ³⁷, B. Moser ⁵⁴,
 M. Mosidze ^{155b}, T. Moskalets ⁴⁵, P. Moskvitina ¹¹⁶, J. Moss ³², P. Moszkowicz ^{87a},
 A. Moussa ^{36d}, Y. Moyal ¹⁷⁵, H. Moyano Gomez ¹³, E.J.W. Moyses ¹⁰⁵, T.G. Mroz ⁸⁸,
 O. Mtintsilana ^{34h}, S. Muanza ¹⁰⁴, M. Mucha ²⁵, J. Mueller ¹³², R. Müller ³⁷, G.A. Mullier ¹⁶⁷,
 A.J. Mullin ³³, J.J. Mullin ⁵¹, A.C. Mullins ⁴⁵, A.E. Mulski ⁶¹, D.P. Mungo ¹⁶¹, D. Munoz Perez ¹⁶⁹,
 F.J. Munoz Sanchez ¹⁰³, W.J. Murray ^{173,137}, M. Muškinja ⁹⁵, C. Mwewa ⁴⁸, A.G. Myagkov ^{38,a},
 A.J. Myers ⁸, G. Myers ¹⁰⁸, M. Myska ¹³⁵, B.P. Nachman ¹⁴⁹, K. Nagai ¹²⁹, K. Nagano ⁸⁴,
 R. Nagasaka ¹⁵⁹, J.L. Nagle ^{30,al}, E. Nagy ¹⁰⁴, A.M. Nairz ³⁷, Y. Nakahama ⁸⁴, K. Nakamura ⁸⁴,
 K. Nakkalil ⁵, A. Nandi ^{63b}, H. Nanjo ¹²⁷, E.A. Narayanan ⁴⁵, Y. Narukawa ¹⁵⁹, I. Naryshkin ³⁸,
 L. Nasella ^{71a,71b}, S. Nasri ^{119b}, C. Nass ²⁵, G. Navarro ^{23a}, A. Nayaz ¹⁹, P.Y. Nechaeva ³⁸,
 S. Nechaeva ^{24b,24a}, F. Nechansky ¹³⁴, L. Nedic ¹²⁹, T.J. Neep ²¹, A. Negri ^{73a,73b},
 M. Negrini ^{24b}, C. Nellist ¹¹⁷, C. Nelson ¹⁰⁶, K. Nelson ¹⁰⁸, S. Nemecek ¹³⁴, M. Nessi ^{37,g},
 M.S. Neubauer ¹⁶⁸, J. Newell ⁹⁴, P.R. Newman ²¹, Y.W.Y. Ng ¹⁶⁸, B. Ngair ^{119a},
 H.D.N. Nguyen ¹¹⁰, J.D. Nichols ¹²³, R.B. Nickerson ¹²⁹, R. Nicolaidou ¹³⁸, J. Nielsen ¹³⁹,
 M. Niemeyer ⁵⁵, J. Niermann ³⁷, N. Nikiforou ³⁷, V. Nikolaenko ^{38,a}, I. Nikolic-Audit ¹³⁰,
 P. Nilsson ³⁰, I. Ninca ⁴⁸, G. Ninio ¹⁵⁷, A. Nisati ^{75a}, R. Nisius ¹¹², N. Nitika ^{69a,69c},
 J-E. Nitschke ⁵⁰, E.K. Nkadimeng ^{34b}, T. Nobe ¹⁵⁹, D. Noll ^{18a}, T. Nommensen ¹⁵³,
 M.B. Norfolk ¹⁴⁵, B.J. Norman ³⁵, L.C. Nosler ^{18a}, M. Noury ^{36a}, J. Novak ⁹⁵, T. Novak ⁹⁵,
 R. Novotny ¹³⁵, L. Nozka ¹²⁵, K. Ntekas ¹⁶⁵, D. Ntounis ¹⁴⁹, N.M.J. Nunes De Moura Junior ^{83b},
 J. Ocariz ¹³⁰, I. Ochoa ^{133a}, S. Oerdek ^{48,y}, J.T. Offermann ⁴⁰, A. Ogrodnik ¹³⁶, A. Oh ¹⁰³,
 C.C. Ohm ¹⁵⁰, H. Oide ⁸⁴, M.L. Ojeda ³⁷, Y. Okumura ¹⁵⁹, L.F. Oleiro Seabra ^{133a},
 I. Oleksiyuk ⁵⁶, G. Oliveira Correa ¹³, D. Oliveira Damazio ³⁰, J.L. Oliver ¹, R. Omar ⁶⁸,
 Ö.O. Öncel ⁵⁴, A.P. O'Neill ²⁰, A. Onofre ^{133a,133e,e}, P.U.E. Onyisi ¹¹, M.J. Oreglia ⁴⁰,
 D. Orestano ^{77a,77b}, R. Orlandini ^{77a,77b}, R.S. Orr ¹⁶¹, L.M. Osojnak ⁴², Y. Osumi ¹¹³,
 G. Otero y Garzon ³¹, H. Otono ⁹⁰, M. Ouchrif ^{36d}, F. Ould-Saada ¹²⁸, T. Ovsiannikova ¹⁴²,
 M. Owen ⁵⁹, R.E. Owen ¹³⁷, V.E. Ozcan ^{22a}, F. Ozturk ⁸⁸, N. Ozturk ⁸, S. Ozturk ⁸²,
 H.A. Pacey ¹²⁹, K. Pachal ^{162a}, A. Pacheco Pages ¹³, C. Padilla Aranda ¹³, G. Padovano ^{75a,75b},
 S. Pagan Griso ^{18a}, G. Palacino ⁶⁸, A. Palazzo ^{70a,70b}, J. Pampel ²⁵, J. Pan ¹⁷⁸, T. Pan ^{64a},
 D.K. Panchal ¹¹, C.E. Pandini ⁶⁰, J.G. Panduro Vazquez ¹³⁷, H.D. Pandya ¹, H. Pang ¹³⁸,
 P. Pani ⁴⁸, G. Panizzo ^{69a,69c}, L. Panwar ¹³⁰, L. Paolozzi ⁵⁶, S. Parajuli ¹⁶⁸, A. Paramonov ⁶,
 C. Paraskevopoulos ⁵³, D. Paredes Hernandez ^{64b}, A. Pareti ^{73a,73b}, K.R. Park ⁴², T.H. Park ¹¹²,
 F. Parodi ^{57b,57a}, J.A. Parsons ⁴², U. Parzefall ⁵⁴, B. Pascual Dias ⁴¹, L. Pascual Dominguez ¹⁰¹,
 E. Pasqualucci ^{75a}, S. Passaggio ^{57b}, F. Pastore ⁹⁷, P. Patel ⁸⁸, U.M. Patel ⁵¹, J.R. Pater ¹⁰³,
 T. Pauly ³⁷, F. Pauwels ¹³⁶, C.I. Pazos ¹⁶⁴, M. Pedersen ¹²⁸, R. Pedro ^{133a}, S.V. Peleganchuk ³⁸,
 O. Penc ¹³⁴, E.A. Pender ⁵², S. Peng ¹⁵, G.D. Penn ¹⁷⁸, K.E. Penski ¹¹¹, M. Penzin ³⁸,
 B.S. Peralva ^{83d}, A.P. Pereira Peixoto ¹⁴², L. Pereira Sanchez ¹⁴⁹, D.V. Perepelitsa ^{30,al},
 G. Perera ¹⁰⁵, E. Perez Codina ³⁷, M. Perganti ¹⁰, H. Pernegger ³⁷, S. Perrella ^{75a,75b},
 K. Peters ⁴⁸, R.F.Y. Peters ¹⁰³, B.A. Petersen ³⁷, T.C. Petersen ⁴³, E. Petit ¹⁰⁴, V. Petousis ¹³⁵,
 A.R. Petri ^{71a,71b}, C. Petridou ^{158,d}, T. Petru ¹³⁶, A. Petrukhin ¹⁴⁷, M. Pettee ^{18a}, A. Petukhov ⁸²,
 K. Petukhova ³⁷, R. Pezoa ^{140g}, L. Pezzotti ^{24b,24a}, G. Pezzullo ¹⁷⁸, L. Pfaffenbichler ³⁷,
 A.J. Pflieger ⁷⁹, T.M. Pham ¹⁷⁶, T. Pham ¹⁰⁷, P.W. Phillips ¹³⁷, G. Piacquadio ¹⁵¹, E. Pianori ^{18a},
 F. Piazza ¹²⁶, R. Piegai ³¹, D. Pietreanu ^{28b}, A.D. Pilkington ¹⁰³, M. Pinamonti ^{69a,69c},
 J.L. Pinfeld ², B.C. Pinheiro Pereira ^{133a}, J. Pinol Bel ¹³, A.E. Pinto Pinoargote ¹³⁰,
 L. Pintucci ^{69a,69c}, K.M. Piper ¹⁵², A. Pirttikoski ⁵⁶, D.A. Pizzi ³⁵, L. Pizzimento ^{64b},

A. Plebani ³³, M.-A. Pleier ³⁰, V. Pleskot ¹³⁶, E. Plotnikova ³⁹, G. Poddar ⁹⁶, R. Poettgen ¹⁰⁰,
 L. Poggioli ¹³⁰, S. Polacek ¹³⁶, G. Polesello ^{73a}, A. Poley ¹⁴⁸, A. Polini ^{24b}, C.S. Pollard ¹⁷³,
 Z.B. Pollock ¹²², E. Pompa Pacchi ¹²³, N.I. Pond ⁹⁸, D. Ponomarenko ⁶⁸, L. Pontecorvo ³⁷,
 S. Popa ^{28a}, G.A. Popeneciu ^{28d}, A. Poreba ³⁷, D.M. Portillo Quintero ^{162a}, S. Pospisil ¹³⁵,
 M.A. Postill ¹⁴⁵, P. Postolache ^{28c}, K. Potamianos ¹⁷³, P.A. Potepa ^{87a}, I.N. Potrap ³⁹,
 C.J. Potter ³³, H. Potti ¹⁵³, J. Poveda ¹⁶⁹, M.E. Pozo Astigarraga ³⁷, R. Pozzi ³⁷,
 A. Prades Ibanez ^{76a,76b}, S.R. Pradhan ¹⁴⁵, J. Pretel ¹⁷¹, D. Price ¹⁰³, M. Primavera ^{70a},
 L. Primomo ^{69a,69c}, M.A. Principe Martin ¹⁰¹, R. Privara ¹²⁵, T. Procter ^{87b}, M.L. Proffitt ¹⁴²,
 N. Proklova ¹³¹, K. Prokofiev ^{64c}, G. Proto ¹¹², J. Proudfoot ⁶, M. Przybycien ^{87a},
 W.W. Przygoda ^{87b}, A. Psallidas ⁴⁶, J.E. Puddefoot ¹⁴⁵, D. Pudzha ⁵³, H.I. Purnell ¹,
 D. Pyatiizbyantseva ¹¹⁶, J. Qian ¹⁰⁸, R. Qian ¹⁰⁹, D. Qichen ¹²⁹, Y. Qin ¹³, T. Qiu ⁵²,
 A. Quadri ⁵⁵, M. Queitsch-Maitland ¹⁰³, G. Quetant ⁵⁶, R.P. Quinn ¹⁷⁰, G. Rabanal Bolanos ⁶¹,
 D. Rafanoharana ¹¹², F. Raffaelli ^{76a,76b}, F. Ragusa ^{71a,71b}, J.L. Rainbolt ⁴⁰, S. Rajagopalan ³⁰,
 E. Ramakoti ³⁹, L. Rambelli ^{57b,57a}, I.A. Ramirez-Berend ³⁵, K. Ran ^{48,114c}, D.S. Rankin ¹³¹,
 N.P. Rapheeha ^{34h}, H. Rasheed ^{28b}, D.F. Rassloff ^{63a}, A. Rastogi ^{18a}, S. Rave ¹⁰²,
 S. Ravera ^{57b,57a}, B. Ravina ³⁷, I. Ravinovich ¹⁷⁵, M. Raymond ³⁷, A.L. Read ¹²⁸,
 N.P. Readioff ¹⁴⁵, D.M. Rebuzzi ^{73a,73b}, A.S. Reed ⁵⁹, K. Reeves ²⁷, J.A. Reidelsturz ¹⁷⁷,
 D. Reikher ³⁷, A. Rej ⁴⁹, C. Rembser ³⁷, H. Ren ⁶², M. Renda ^{28b}, F. Renner ⁴⁸,
 A.G. Rennie ⁵⁹, M. Repik ⁵⁶, A.L. Rescia ^{57b,57a}, S. Resconi ^{71a}, M. Ressegotti ^{57b,57a},
 S. Rettie ¹¹⁷, W.F. Rettie ³⁵, M.M. Revering ³³, E. Reynolds ^{18a}, O.L. Rezanova ³⁹,
 P. Reznicek ¹³⁶, H. Riani ^{36d}, N. Ribaric ⁵¹, B. Ricci ^{69a,69c}, E. Ricci ^{78a,78b}, R. Richter ¹¹²,
 S. Richter ^{47a,47b}, E. Richter-Was ^{87b}, M. Ridel ¹³⁰, S. Ridouani ^{36d}, P. Rieck ¹²⁰, P. Riedler ³⁷,
 E.M. Riefel ^{47a,47b}, J.O. Rieger ¹¹⁷, M. Rijssenbeek ¹⁵¹, M. Rimoldi ³⁷, L. Rinaldi ^{24b,24a},
 P. Rincke ^{167,55}, G. Ripellino ¹⁶⁷, I. Riu ¹³, J.C. Rivera Vergara ¹⁷¹, F. Rizatdinova ¹²⁴,
 E. Rizvi ⁹⁶, B.R. Roberts ^{18a}, S.S. Roberts ¹³⁹, D. Robinson ³³, M. Robles Manzano ¹⁰²,
 A. Robson ⁵⁹, A. Rocchi ^{76a,76b}, C. Roda ^{74a,74b}, S. Rodriguez Bosca ³⁷, Y. Rodriguez Garcia ^{23a},
 A.M. Rodríguez Vera ¹¹⁸, S. Roe ³⁷, J.T. Roemer ³⁷, O. Røhne ¹²⁸, R.A. Rojas ³⁷,
 C.P.A. Roland ¹³⁰, A. Romaniouk ⁷⁹, E. Romano ^{73a,73b}, M. Romano ^{24b},
 A.C. Romero Hernandez ¹⁶⁸, N. Rompotis ⁹⁴, L. Roos ¹³⁰, S. Rosati ^{75a}, B.J. Rosser ⁴⁰,
 E. Rossi ¹²⁹, E. Rossi ^{72a,72b}, L.P. Rossi ⁶¹, L. Rossini ⁵⁴, R. Rosten ¹²², M. Rotaru ^{28b},
 B. Rottler ⁵⁴, D. Rousseau ⁶⁶, D. Rousso ⁴⁸, S. Roy-Garand ¹⁶¹, A. Rozanov ¹⁰⁴,
 Z.M.A. Rozario ⁵⁹, Y. Rozen ¹⁵⁶, A. Rubio Jimenez ¹⁶⁹, V.H. Ruelas Rivera ¹⁹, T.A. Ruggeri ¹,
 A. Ruggiero ¹²⁹, A. Ruiz-Martinez ¹⁶⁹, A. Rummler ³⁷, Z. Rurikova ⁵⁴, N.A. Rusakovich ³⁹,
 S. Ruscelli ⁴⁹, H.L. Russell ¹⁷¹, G. Russo ^{75a,75b}, J.P. Rutherford ⁷, S. Rutherford Colmenares ³³,
 M. Rybar ¹³⁶, P. Rybczynski ^{87a}, A. Ryzhov ⁴⁵, J.A. Sabater Iglesias ⁵⁶, H.F.W. Sadrozinski ¹³⁹,
 F. Safai Tehrani ^{75a}, S. Saha ¹, M. Sahinsoy ⁸², B. Sahoo ¹⁷⁵, A. Saibel ¹⁶⁹, B.T. Saifuddin ¹²³,
 M. Saimpert ¹³⁸, G.T. Saito ^{83c}, M. Saito ¹⁵⁹, T. Saito ¹⁵⁹, A. Sala ^{71a,71b}, A. Salnikov ¹⁴⁹,
 J. Salt ¹⁶⁹, A. Salvador Salas ¹⁵⁷, F. Salvatore ¹⁵², A. Salzburger ³⁷, D. Sammel ⁵⁴,
 E. Sampson ⁹³, D. Sampsonidis ^{158,d}, D. Sampsonidou ¹²⁶, J. Sánchez ¹⁶⁹,
 V. Sanchez Sebastian ¹⁶⁹, H. Sandaker ¹²⁸, C.O. Sander ⁴⁸, J.A. Sandesara ¹⁷⁶, M. Sandhoff ¹⁷⁷,
 C. Sandoval ^{23b}, L. Sanfilippo ^{63a}, D.P.C. Sankey ¹³⁷, T. Sano ⁸⁹, A. Sansoni ⁵³,
 M. Santana Queiroz ^{18b}, L. Santi ³⁷, C. Santoni ⁴¹, H. Santos ^{133a,133b}, A. Santra ¹⁷⁵,
 E. Sanzani ^{24b,24a}, K.A. Saoucha ^{85b}, J.G. Saraiva ^{133a,133d}, J. Sardain ⁷, O. Sasaki ⁸⁴,
 K. Sato ¹⁶³, C. Sauer ³⁷, E. Sauvan ⁴, P. Savard ^{161,ai}, R. Sawada ¹⁵⁹, C. Sawyer ¹³⁷,
 L. Sawyer ⁹⁹, C. Sbarra ^{24b}, A. Sbrizzi ^{24b,24a}, T. Scanlon ⁹⁸, J. Schaarschmidt ¹⁴²,
 U. Schäfer ¹⁰², A.C. Schaffer ^{66,45}, D. Schaile ¹¹¹, R.D. Schamberger ¹⁵¹, C. Scharf ¹⁹,
 M.M. Schefer ²⁰, V.A. Schegelsky ³⁸, D. Scheirich ¹³⁶, M. Schernau ^{140f}, C. Scheulen ⁵⁶,

C. Schiavi ^{57b,57a}, M. Schioppa ^{44b,44a}, B. Schlag ¹⁴⁹, S. Schlenker ³⁷, J. Schmeing ¹⁷⁷,
 E. Schmidt ¹¹², M.A. Schmidt ¹⁷⁷, K. Schmieden ¹⁰², C. Schmitt ¹⁰², N. Schmitt ¹⁰²,
 S. Schmitt ⁴⁸, N.A. Schneider ¹¹¹, L. Schoeffel ¹³⁸, A. Schoening ^{63b}, P.G. Scholer ³⁵,
 E. Schopf ¹⁴⁷, M. Schott ²⁵, S. Schramm ⁵⁶, T. Schroer ⁵⁶, H-C. Schultz-Coulon ^{63a},
 M. Schumacher ⁵⁴, B.A. Schumm ¹³⁹, Ph. Schune ¹³⁸, H.R. Schwartz ⁷, A. Schwartzman ¹⁴⁹,
 T.A. Schwarz ¹⁰⁸, Ph. Schwemling ¹³⁸, R. Schwienhorst ¹⁰⁹, F.G. Sciacca ²⁰, A. Sciandra ³⁰,
 G. Sciolla ²⁷, F. Scuri ^{74a}, C.D. Sebastiani ³⁷, K. Sedlaczek ¹¹⁸, S.C. Seidel ¹¹⁵, A. Seiden ¹³⁹,
 B.D. Seidlitz ⁴², C. Seitz ⁴⁸, J.M. Seixas ^{83b}, G. Sekhniaidze ^{72a}, L. Selem ⁶⁰,
 N. Semprini-Cesari ^{24b,24a}, A. Semushin ¹⁷⁹, D. Sengupta ⁵⁶, V. Senthilkumar ¹⁶⁹, L. Serin ⁶⁶,
 M. Sessa ^{72a,72b}, H. Severini ¹²³, F. Sforza ^{57b,57a}, A. Sfyrla ⁵⁶, Q. Sha ¹⁴, E. Shabalina ⁵⁵,
 H. Shaddix ¹¹⁸, A.H. Shah ³³, R. Shaheen ¹⁵⁰, J.D. Shahinian ¹³¹, M. Shamim ³⁷, L.Y. Shan ¹⁴,
 M. Shapiro ^{18a}, A. Sharma ³⁷, A.S. Sharma ¹⁷⁰, P. Sharma ³⁰, P.B. Shatalov ³⁸, K. Shaw ¹⁵²,
 S.M. Shaw ¹⁰³, Q. Shen ¹⁴, D.J. Sheppard ¹⁴⁸, P. Sherwood ⁹⁸, L. Shi ⁹⁸, X. Shi ¹⁴,
 S. Shimizu ⁸⁴, C.O. Shimmin ¹⁷⁸, I.P.J. Shipsey ^{129,*}, S. Shirabe ⁹⁰, M. Shiyakova ^{39,z},
 M.J. Shochet ⁴⁰, D.R. Shope ¹²⁸, B. Shrestha ¹²³, S. Shrestha ^{122,an}, I. Shreyber ³⁹,
 M.J. Shroff ¹⁷¹, P. Sicho ¹³⁴, A.M. Sickles ¹⁶⁸, E. Sideras Haddad ^{34h,166}, A.C. Sidley ¹¹⁷,
 A. Sidoti ^{24b}, F. Siegert ⁵⁰, Dj. Sijacki ¹⁶, F. Sili ⁹², J.M. Silva ⁵², I. Silva Ferreira ^{83b},
 M.V. Silva Oliveira ³⁰, S.B. Silverstein ^{47a}, S. Simion ⁶⁶, R. Simoniello ³⁷, E.L. Simpson ¹⁰³,
 H. Simpson ¹⁵², L.R. Simpson ⁶, S. Simsek ⁸², S. Sindhu ⁵⁵, P. Sinervo ¹⁶¹, S.N. Singh ²⁷,
 S. Singh ³⁰, S. Sinha ⁴⁸, S. Sinha ¹⁰³, M. Sioli ^{24b,24a}, K. Sioulas ⁹, I. Siral ³⁷, E. Sitnikova ⁴⁸,
 J. Sjölin ^{47a,47b}, A. Skaf ⁵⁵, E. Skorda ²¹, P. Skubic ¹²³, M. Slawinska ⁸⁸, I. Slazyk ¹⁷,
 I. Sliusar ¹²⁸, V. Smakhtin ¹⁷⁵, B.H. Smart ¹³⁷, S.Yu. Smirnov ^{140b}, Y. Smirnov ⁸²,
 L.N. Smirnova ^{38,a}, O. Smirnova ¹⁰⁰, A.C. Smith ⁴², D.R. Smith ¹⁶⁵, J.L. Smith ¹⁰³,
 M.B. Smith ³⁵, R. Smith ¹⁴⁹, H. Smitmanns ¹⁰², M. Smizanska ⁹³, K. Smolek ¹³⁵,
 P. Smolyanskiy ¹³⁵, A.A. Snesarev ³⁹, H.L. Snoek ¹¹⁷, S. Snyder ³⁰, R. Sobie ^{171,ab},
 A. Soffer ¹⁵⁷, C.A. Solans Sanchez ³⁷, E.Yu. Soldatov ³⁹, U. Soldevila ¹⁶⁹, A.A. Solodkov ^{34h},
 S. Solomon ²⁷, A. Soloshenko ³⁹, K. Solovieva ⁵⁴, O.V. Solovyanov ⁴¹, P. Sommer ⁵⁰,
 A. Sonay ¹³, A. Sopczak ¹³⁵, A.L. Soppio ⁵², F. Sopkova ^{29b}, J.D. Sorenson ¹¹⁵,
 I.R. Sotarriva Alvarez ¹⁴¹, V. Sothilingam ^{63a}, O.J. Soto Sandoval ^{140c,140b}, S. Sottocornola ⁶⁸,
 R. Soualah ^{85a}, Z. Soumami ^{36e}, D. South ⁴⁸, N. Soybelman ¹⁷⁵, S. Spagnolo ^{70a,70b},
 M. Spalla ¹¹², D. Sperlich ⁵⁴, B. Spisso ^{72a,72b}, D.P. Spiteri ⁵⁹, L. Splendori ¹⁰⁴, M. Spousta ¹³⁶,
 E.J. Staats ³⁵, R. Stamen ^{63a}, E. Stanecka ⁸⁸, W. Stanek-Maslouska ⁴⁸, M.V. Stange ⁵⁰,
 B. Stanislaus ^{18a}, M.M. Stanitzki ⁴⁸, B. Stapf ⁴⁸, E.A. Starchenko ³⁸, G.H. Stark ¹³⁹, J. Stark ⁹¹,
 P. Staroba ¹³⁴, P. Starovoitov ^{85b}, R. Staszewski ⁸⁸, C. Stauch ¹¹¹, G. Stavropoulos ⁴⁶,
 A. Steffl ³⁷, A. Stein ¹⁰², P. Steinberg ³⁰, B. Stelzer ^{148,162a}, H.J. Stelzer ¹³², O. Stelzer ^{162a},
 H. Stenzel ⁵⁸, T.J. Stevenson ¹⁵², G.A. Stewart ³⁷, J.R. Stewart ¹²⁴, G. Stoicea ^{28b},
 M. Stolarski ^{133a}, S. Stonjek ¹¹², A. Straessner ⁵⁰, J. Strandberg ¹⁵⁰, S. Strandberg ^{47a,47b},
 M. Stratmann ¹⁷⁷, M. Strauss ¹²³, T. Strebler ¹⁰⁴, P. Strizenec ^{29b}, R. Ströhmer ¹⁷²,
 D.M. Strom ¹²⁶, R. Stroynowski ⁴⁵, A. Strubig ^{47a,47b}, S.A. Stucci ³⁰, B. Stugu ¹⁷, J. Stupak ¹²³,
 N.A. Styles ⁴⁸, D. Su ¹⁴⁹, S. Su ⁶², X. Su ⁶², D. Suchy ^{29a}, A.D. Sudhakar Ponnu ⁵⁵,
 K. Sugizaki ¹³¹, V.V. Sulin ³⁸, D.M.S. Sultan ¹²⁹, L. Sultanaliyeva ²⁵, S. Sultansoy ^{3b},
 S. Sun ¹⁷⁶, W. Sun ¹⁴, O. Sunneborn Gudnadottir ¹⁶⁷, N. Sur ¹⁰⁰, M.R. Sutton ¹⁵²,
 M. Svatos ¹³⁴, P.N. Swallow ³³, M. Swiatlowski ^{162a}, T. Swirski ¹⁷², A. Swoboda ³⁷,
 I. Sykora ^{29a}, M. Sykora ¹³⁶, T. Sykora ¹³⁶, D. Ta ¹⁰², K. Tackmann ^{48,y}, A. Taffard ¹⁶⁵,
 R. Tafirout ^{162a}, Y. Takubo ⁸⁴, M. Talby ¹⁰⁴, A.A. Talyshev ³⁸, K.C. Tam ^{64b}, N.M. Tamir ¹⁵⁷,
 A. Tanaka ¹⁵⁹, J. Tanaka ¹⁵⁹, R. Tanaka ⁶⁶, M. Tanasini ¹⁵¹, Z. Tao ¹⁷⁰, S. Tapia Araya ^{140g},
 S. Tapprogge ¹⁰², A. Tarek Abouelfadl Mohamed ³⁷, S. Tarem ¹⁵⁶, K. Tariq ¹⁴, G. Tarna ³⁷,

G.F. Tartarelli ^{71a}, M.J. Tartarin ⁹¹, P. Tas ¹³⁶, M. Tasevsky ¹³⁴, E. Tassi ^{44b,44a}, A.C. Tate ¹⁶⁸, Y. Tayalati ^{36e,aa}, G.N. Taylor ¹⁰⁷, W. Taylor ^{162b}, R.J. Taylor Vara ¹⁶⁹, A.S. Tegetmeier ⁹¹, P. Teixeira-Dias ⁹⁷, J.J. Teoh ¹⁶¹, K. Terashi ¹⁵⁹, J. Terron ¹⁰¹, S. Terzo ¹³, M. Testa ⁵³, R.J. Teuscher ^{161,ab}, A. Thaler ⁷⁹, O. Theiner ⁵⁶, T. Theveneaux-Pelzer ¹⁰⁴, D.W. Thomas ⁹⁷, J.P. Thomas ²¹, E.A. Thompson ^{18a}, P.D. Thompson ²¹, E. Thomson ¹³¹, R.E. Thornberry ⁴⁵, C. Tian ⁶², Y. Tian ⁵⁶, V. Tikhomirov ⁸², Yu.A. Tikhonov ³⁹, S. Timoshenko ³⁸, D. Timoshyn ¹³⁶, E.X.L. Ting ¹, P. Tipton ¹⁷⁸, A. Tishelman-Charny ³⁰, K. Todome ¹⁴¹, S. Todorova-Nova ¹³⁶, L. Toffolin ^{69a,69c}, M. Togawa ⁸⁴, J. Tojo ⁹⁰, S. Tokár ^{29a}, O. Toldaiev ⁶⁸, G. Tolkachev ¹⁰⁴, M. Tomoto ⁸⁴, L. Tompkins ^{149,n}, E. Torrence ¹²⁶, H. Torres ⁹¹, D.I. Torres Arza ^{140g}, E. Torró Pastor ¹⁶⁹, M. Toscani ³¹, C. Tosciri ⁴⁰, M. Tost ¹¹, D.R. Tovey ¹⁴⁵, T. Trefzger ¹⁷², P.M. Tricarico ¹³, A. Tricoli ³⁰, I.M. Trigger ^{162a}, S. Trincaz-Duvoid ¹³⁰, D.A. Trischuk ²⁷, A. Tropina ³⁹, L. Truong ^{34c}, M. Trzebinski ⁸⁸, A. Trzuppek ⁸⁸, F. Tsai ¹⁵¹, M. Tsai ¹⁰⁸, A. Tsiamis ¹⁵⁸, P.V. Tsiareshka ³⁹, S. Tsigaridas ^{162a}, A. Tsigirotis ^{158,u}, V. Tsiskaridze ^{155a}, E.G. Tskhadadze ^{155a}, Y. Tsujikawa ⁸⁹, I.I. Tsukerman ³⁸, V. Tsulaia ^{18a}, S. Tsuno ⁸⁴, K. Tsuru ¹²¹, D. Tsybychev ¹⁵¹, Y. Tu ^{64b}, A. Tudorache ^{28b}, V. Tudorache ^{28b}, S.B. Tuncay ¹²⁹, S. Turchikhin ^{57b,57a}, I. Turk Cakir ^{3a}, R. Turra ^{71a}, T. Turtuvshin ^{39,ac}, P.M. Tuts ⁴², S. Tzamarias ^{158,d}, Y. Uematsu ⁸⁴, F. Ukegawa ¹⁶³, P.A. Ulloa Poblete ^{140c,140b}, E.N. Umaka ³⁰, G. Unal ³⁷, A. Undrus ³⁰, G. Unel ¹⁶⁵, J. Urban ^{29b}, P. Urrejola ^{140e}, G. Usai ⁸, R. Ushioda ¹⁶⁰, M. Usman ¹¹⁰, F. Ustuner ⁵², Z. Uysal ⁸², V. Vacek ¹³⁵, B. Vachon ¹⁰⁶, T. Vafeiadis ³⁷, A. Vaitkus ⁹⁸, C. Valderanis ¹¹¹, E. Valdes Santurio ^{47a,47b}, M. Valente ³⁷, S. Valentinetti ^{24b,24a}, A. Valero ¹⁶⁹, E. Valiente Moreno ¹⁶⁹, A. Vallier ⁹¹, J.A. Valls Ferrer ¹⁶⁹, D.R. Van Arneman ¹¹⁷, A. Van Der Graaf ⁴⁹, H.Z. Van Der Schyf ^{34h}, P. Van Gemmeren ⁶, M. Van Rijnbach ³⁷, S. Van Stroud ⁹⁸, I. Van Vulpen ¹¹⁷, P. Vana ¹³⁶, M. Vanadia ^{76a,76b}, U.M. Vande Voorde ¹⁵⁰, W. Vandelli ³⁷, E.R. Vandewall ¹²⁴, D. Vannicola ¹⁵⁷, L. Vannoli ⁵³, R. Vari ^{75a}, M. Varma ¹⁷⁸, E.W. Varnes ⁷, C. Varni ¹¹⁸, D. Varouchas ⁶⁶, L. Varriale ¹⁶⁹, K.E. Varvell ¹⁵³, M.E. Vasile ^{28b}, L. Vaslin ⁸⁴, M.D. Vassilev ¹⁴⁹, A. Vasyukov ³⁹, L.M. Vaughan ¹²⁴, R. Vavricka ¹³⁶, T. Vazquez Schroeder ¹³, J. Veatch ³², V. Vecchio ¹⁰³, M.J. Veen ¹⁰⁵, I. Veliscek ³⁰, I. Velkovska ⁹⁵, L.M. Veloce ¹⁶¹, F. Veloso ^{133a,133c}, S. Veneziano ^{75a}, A. Ventura ^{70a,70b}, A. Verbytskyi ¹¹², M. Verducci ^{74a,74b}, C. Vergis ⁹⁶, M. Verissimo De Araujo ^{83b}, W. Verkerke ¹¹⁷, J.C. Vermeulen ¹¹⁷, C. Vernieri ¹⁴⁹, M. Vessella ¹⁶⁵, M.C. Vetterli ^{148,ai}, A. Vgenopoulos ¹⁰², N. Viaux Maira ^{140g,af}, T. Vickey ¹⁴⁵, O.E. Vickey Boeriu ¹⁴⁵, G.H.A. Viehhauser ¹²⁹, L. Vigani ^{63b}, M. Vigi ¹¹², M. Villa ^{24b,24a}, M. Villaplana Perez ¹⁶⁹, E.M. Villhauer ⁴⁰, E. Vilucchi ⁵³, M. Vincent ¹⁶⁹, M.G. Vincter ³⁵, A. Visibile ¹¹⁷, A. Visive ¹¹⁷, C. Vittori ³⁷, I. Vivarelli ^{24b,24a}, M.I. Vivas Albornoz ⁴⁸, E. Voevodina ¹¹², F. Vogel ¹¹¹, J.C. Voigt ⁵⁰, P. Vokac ¹³⁵, Yu. Volkotrub ^{87b}, L. Vomberg ²⁵, E. Von Toerne ²⁵, B. Vormwald ³⁷, K. Vorobev ⁵¹, M. Vos ¹⁶⁹, K. Voss ¹⁴⁷, M. Vozak ³⁷, L. Vozdecky ¹²³, N. Vranjes ¹⁶, M. Vranjes Milosavljevic ¹⁶, M. Vreeswijk ¹¹⁷, N.K. Vu ^{144b,144a}, R. Vuillermet ³⁷, O. Vujanovic ¹⁰², I. Vukotic ⁴⁰, I.K. Vyas ³⁵, J.F. Wack ³³, S. Wada ¹⁶³, C. Wagner ¹⁴⁹, J.M. Wagner ^{18a}, W. Wagner ¹⁷⁷, S. Wahdan ¹⁷⁷, H. Wahlberg ⁹², C.H. Waits ¹²³, J. Walder ¹³⁷, R. Walker ¹¹¹, K. Walkingshaw Pass ⁵⁹, W. Walkowiak ¹⁴⁷, A. Wall ¹³¹, E.J. Wallin ¹⁰⁰, T. Wamorkar ^{18a}, K. Wandall-Christensen ¹⁶⁹, A. Wang ⁶², A.Z. Wang ¹³⁹, C. Wang ¹⁰², C. Wang ¹¹, H. Wang ^{18a}, J. Wang ^{64c}, P. Wang ¹⁰³, P. Wang ⁹⁸, R. Wang ⁶¹, R. Wang ⁶, S.M. Wang ¹⁵⁴, S. Wang ¹⁴, T. Wang ¹¹⁶, T. Wang ⁶², W.T. Wang ¹²⁹, W. Wang ¹⁴, X. Wang ¹⁶⁸, X. Wang ^{144a}, X. Wang ⁴⁸, Y. Wang ^{114a}, Y. Wang ⁶², Z. Wang ¹⁰⁸, Z. Wang ^{144b}, Z. Wang ¹⁰⁸, C. Wanotayaroj ⁸⁴, A. Warburton ¹⁰⁶, A.L. Warnerbring ¹⁴⁷, S. Waterhouse ⁹⁷, A.T. Watson ²¹, H. Watson ⁵², M.F. Watson ²¹, E. Watton ⁵⁹, G. Watts ¹⁴², B.M. Waugh ⁹⁸, J.M. Webb ⁵⁴, C. Weber ³⁰, H.A. Weber ¹⁹, M.S. Weber ²⁰, S.M. Weber ^{63a},

C. Wei ⁶², Y. Wei ⁵⁴, A.R. Weidberg ¹²⁹, E.J. Weik ¹²⁰, J. Weingarten ⁴⁹, C. Weiser ⁵⁴, C.J. Wells ⁴⁸, T. Wenaus ³⁰, T. Wengler ³⁷, N.S. Wenke ¹¹², N. Wermes ²⁵, M. Wessels ^{63a}, A.M. Wharton ⁹³, A.S. White ⁶¹, A. White ⁸, M.J. White ¹, D. Whiteson ¹⁶⁵, L. Wickremasinghe ¹²⁷, W. Wiedenmann ¹⁷⁶, M. Wielers ¹³⁷, R. Wierda ¹⁵⁰, C. Wiglesworth ⁴³, H.G. Wilkens ³⁷, J.J.H. Wilkinson ³³, D.M. Williams ⁴², H.H. Williams ¹³¹, S. Williams ³³, S. Willocq ¹⁰⁵, B.J. Wilson ¹⁰³, D.J. Wilson ¹⁰³, P.J. Windischhofer ⁴⁰, F.I. Winkel ³¹, F. Winklmeier ¹²⁶, B.T. Winter ⁵⁴, M. Wittgen ¹⁴⁹, M. Wobisch ⁹⁹, T. Wojtkowski ⁶⁰, Z. Wolffs ¹¹⁷, J. Wollrath ³⁷, M.W. Wolter ⁸⁸, H. Wolters ^{133a,133c}, M.C. Wong ¹³⁹, E.L. Woodward ⁴², S.D. Worm ⁴⁸, B.K. Wosiek ⁸⁸, K.W. Woźniak ⁸⁸, S. Wozniowski ⁵⁵, K. Wraight ⁵⁹, C. Wu ¹⁶¹, C. Wu ²¹, J. Wu ¹⁵⁹, M. Wu ^{114b}, M. Wu ¹¹⁶, S.L. Wu ¹⁷⁶, S. Wu ^{14.ak}, X. Wu ⁶², Y.Q. Wu ¹⁶¹, Y. Wu ⁶², Z. Wu ⁴, Z. Wu ^{114a}, J. Wuerzinger ¹¹², T.R. Wyatt ¹⁰³, B.M. Wynne ⁵², S. Xella ⁴³, L. Xia ^{114a}, M. Xia ¹⁵, M. Xie ⁶², A. Xiong ¹²⁶, J. Xiong ^{18a}, D. Xu ¹⁴, H. Xu ⁶², L. Xu ⁶², R. Xu ¹³¹, T. Xu ¹⁰⁸, Y. Xu ¹⁴², Z. Xu ⁵², R. Xue ¹³², B. Yabsley ¹⁵³, S. Yacoob ^{34a}, Y. Yamaguchi ⁸⁴, E. Yamashita ¹⁵⁹, H. Yamauchi ¹⁶³, T. Yamazaki ^{18a}, Y. Yamazaki ⁸⁶, S. Yan ⁵⁹, Z. Yan ¹⁰⁵, H.J. Yang ^{144a,144b}, H.T. Yang ⁶², S. Yang ⁶², T. Yang ^{64c}, X. Yang ³⁷, X. Yang ¹⁴, Y. Yang ¹⁵⁹, Y. Yang ⁶², W.-M. Yao ^{18a}, C.L. Yardley ¹⁵², J. Ye ¹⁴, S. Ye ³⁰, X. Ye ⁶², Y. Yeh ⁹⁸, I. Yeletsikh ³⁹, B. Yeo ^{18b}, M.R. Yexley ⁹⁸, T.P. Yildirim ¹²⁹, K. Yorita ¹⁷⁴, C.J.S. Young ³⁷, C. Young ¹⁴⁹, N.D. Young ¹²⁶, Y. Yu ⁶², J. Yuan ^{14,114c}, M. Yuan ¹⁰⁸, R. Yuan ^{144b,144a}, L. Yue ⁹⁸, M. Zaazoua ⁶², B. Zabinski ⁸⁸, I. Zahir ^{36a}, A. Zaid ^{57b,57a}, Z.K. Zak ⁸⁸, T. Zakareishvili ¹⁶⁹, S. Zambito ⁵⁶, J.A. Zamora Saa ^{140d}, J. Zang ¹⁵⁹, R. Zanzottera ^{71a,71b}, O. Zaplatilek ¹³⁵, C. Zeitnitz ¹⁷⁷, H. Zeng ¹⁴, J.C. Zeng ¹⁶⁸, D.T. Zenger Jr ²⁷, O. Zenin ³⁸, T. Ženiš ^{29a}, S. Zenz ⁹⁶, D. Zerwas ⁶⁶, M. Zhai ^{14,114c}, D.F. Zhang ¹⁴⁵, G. Zhang ^{14.ak}, J. Zhang ^{143a}, J. Zhang ⁶, K. Zhang ^{14,114c}, L. Zhang ⁶², L. Zhang ^{114a}, P. Zhang ^{14,114c}, R. Zhang ^{114a}, S. Zhang ⁹¹, T. Zhang ¹⁵⁹, Y. Zhang ¹⁴², Y. Zhang ⁹⁸, Y. Zhang ⁶², Y. Zhang ^{114a}, Z. Zhang ^{18a}, Z. Zhang ^{143a}, Z. Zhang ⁶⁶, H. Zhao ¹⁴², T. Zhao ^{143a}, Y. Zhao ³⁵, Z. Zhao ⁶², Z. Zhao ⁶², A. Zhemchugov ³⁹, J. Zheng ^{114a}, K. Zheng ¹⁶⁸, X. Zheng ⁶², Z. Zheng ¹⁴⁹, D. Zhong ¹⁶⁸, B. Zhou ¹⁰⁸, H. Zhou ⁷, N. Zhou ^{144a}, Y. Zhou ¹⁵, Y. Zhou ^{114a}, Y. Zhou ⁷, C.G. Zhu ^{143a}, J. Zhu ¹⁰⁸, X. Zhu ^{144b}, Y. Zhu ^{144a}, Y. Zhu ⁶², X. Zhuang ¹⁴, K. Zhukov ⁶⁸, N.I. Zimine ³⁹, J. Zinsser ^{63b}, M. Ziolkowski ¹⁴⁷, L. Živković ¹⁶, A. Zoccoli ^{24b,24a}, K. Zoch ⁶¹, A. Zografos ³⁷, T.G. Zorbas ¹⁴⁵, O. Zormpa ⁴⁶, L. Zwalinski ³⁷.

¹Department of Physics, University of Adelaide, Adelaide; Australia.

²Department of Physics, University of Alberta, Edmonton AB; Canada.

³(^a)Department of Physics, Ankara University, Ankara; (^b)Division of Physics, TOBB University of Economics and Technology, Ankara; Türkiye.

⁴LAPP, Université Savoie Mont Blanc, CNRS/IN2P3, Annecy; France.

⁵APC, Université Paris Cité, CNRS/IN2P3, Paris; France.

⁶High Energy Physics Division, Argonne National Laboratory, Argonne IL; United States of America.

⁷Department of Physics, University of Arizona, Tucson AZ; United States of America.

⁸Department of Physics, University of Texas at Arlington, Arlington TX; United States of America.

⁹Physics Department, National and Kapodistrian University of Athens, Athens; Greece.

¹⁰Physics Department, National Technical University of Athens, Zografou; Greece.

¹¹Department of Physics, University of Texas at Austin, Austin TX; United States of America.

¹²Institute of Physics, Azerbaijan Academy of Sciences, Baku; Azerbaijan.

¹³Institut de Física d'Altes Energies (IFAE), Barcelona Institute of Science and Technology, Barcelona; Spain.

- ¹⁴Institute of High Energy Physics, Chinese Academy of Sciences, Beijing; China.
- ¹⁵Physics Department, Tsinghua University, Beijing; China.
- ¹⁶Institute of Physics, University of Belgrade, Belgrade; Serbia.
- ¹⁷Department for Physics and Technology, University of Bergen, Bergen; Norway.
- ¹⁸(^a)Physics Division, Lawrence Berkeley National Laboratory, Berkeley CA;(^b)University of California, Berkeley CA; United States of America.
- ¹⁹Institut für Physik, Humboldt Universität zu Berlin, Berlin; Germany.
- ²⁰Albert Einstein Center for Fundamental Physics and Laboratory for High Energy Physics, University of Bern, Bern; Switzerland.
- ²¹School of Physics and Astronomy, University of Birmingham, Birmingham; United Kingdom.
- ²²(^a)Department of Physics, Bogazici University, Istanbul;(^b)Department of Physics Engineering, Gaziantep University, Gaziantep;(^c)Department of Physics, Istanbul University, Istanbul; Türkiye.
- ²³(^a)Facultad de Ciencias y Centro de Investigaciones, Universidad Antonio Nariño, Bogotá;(^b)Departamento de Física, Universidad Nacional de Colombia, Bogotá; Colombia.
- ²⁴(^a)Dipartimento di Fisica e Astronomia A. Righi, Università di Bologna, Bologna;(^b)INFN Sezione di Bologna; Italy.
- ²⁵Physikalisches Institut, Universität Bonn, Bonn; Germany.
- ²⁶Department of Physics, Boston University, Boston MA; United States of America.
- ²⁷Department of Physics, Brandeis University, Waltham MA; United States of America.
- ²⁸(^a)Transilvania University of Brasov, Brasov;(^b)Horia Hulubei National Institute of Physics and Nuclear Engineering, Bucharest;(^c)Department of Physics, Alexandru Ioan Cuza University of Iasi, Iasi;(^d)National Institute for Research and Development of Isotopic and Molecular Technologies, Physics Department, Cluj-Napoca;(^e)National University of Science and Technology Politehnica, Bucharest;(^f)West University in Timisoara, Timisoara;(^g)Faculty of Physics, University of Bucharest, Bucharest; Romania.
- ²⁹(^a)Faculty of Mathematics, Physics and Informatics, Comenius University, Bratislava;(^b)Department of Subnuclear Physics, Institute of Experimental Physics of the Slovak Academy of Sciences, Kosice; Slovak Republic.
- ³⁰Physics Department, Brookhaven National Laboratory, Upton NY; United States of America.
- ³¹Universidad de Buenos Aires, Facultad de Ciencias Exactas y Naturales, Departamento de Física, y CONICET, Instituto de Física de Buenos Aires (IFIBA), Buenos Aires; Argentina.
- ³²California State University, CA; United States of America.
- ³³Cavendish Laboratory, University of Cambridge, Cambridge; United Kingdom.
- ³⁴(^a)Department of Physics, University of Cape Town, Cape Town;(^b)iThemba Labs, Western Cape;(^c)Department of Mechanical Engineering Science, University of Johannesburg, Johannesburg;(^d)National Institute of Physics, University of the Philippines Diliman (Philippines);(^e)Department of Physics, Stellenbosch University, Matieland;(^f)University of South Africa, Department of Physics, Pretoria;(^g)University of Zululand, KwaDlangezwa;(^h)School of Physics, University of the Witwatersrand, Johannesburg; South Africa.
- ³⁵Department of Physics, Carleton University, Ottawa ON; Canada.
- ³⁶(^a)Faculté des Sciences Ain Chock, Université Hassan II de Casablanca;(^b)Faculté des Sciences, Université Ibn-Tofail, Kénitra;(^c)Faculté des Sciences Semlalia, Université Cadi Ayyad, LPHEA-Marrakech;(^d)LPMR, Faculté des Sciences, Université Mohamed Premier, Oujda;(^e)Faculté des sciences, Université Mohammed V, Rabat;(^f)Institute of Applied Physics, Mohammed VI Polytechnic University, Ben Guerir; Morocco.
- ³⁷CERN, Geneva; Switzerland.
- ³⁸Affiliated with an institute formerly covered by a cooperation agreement with CERN.
- ³⁹Affiliated with an international laboratory covered by a cooperation agreement with CERN.

- ⁴⁰ Enrico Fermi Institute, University of Chicago, Chicago IL; United States of America.
- ⁴¹ LPC, Université Clermont Auvergne, CNRS/IN2P3, Clermont-Ferrand; France.
- ⁴² Nevis Laboratory, Columbia University, Irvington NY; United States of America.
- ⁴³ Niels Bohr Institute, University of Copenhagen, Copenhagen; Denmark.
- ⁴⁴ ^(a) Dipartimento di Fisica, Università della Calabria, Rende; ^(b) INFN Gruppo Collegato di Cosenza, Laboratori Nazionali di Frascati; Italy.
- ⁴⁵ Physics Department, Southern Methodist University, Dallas TX; United States of America.
- ⁴⁶ National Centre for Scientific Research "Demokritos", Agia Paraskevi; Greece.
- ⁴⁷ ^(a) Department of Physics, Stockholm University; ^(b) Oskar Klein Centre, Stockholm; Sweden.
- ⁴⁸ Deutsches Elektronen-Synchrotron DESY, Hamburg and Zeuthen; Germany.
- ⁴⁹ Fakultät Physik, Technische Universität Dortmund, Dortmund; Germany.
- ⁵⁰ Institut für Kern- und Teilchenphysik, Technische Universität Dresden, Dresden; Germany.
- ⁵¹ Department of Physics, Duke University, Durham NC; United States of America.
- ⁵² SUPA - School of Physics and Astronomy, University of Edinburgh, Edinburgh; United Kingdom.
- ⁵³ INFN e Laboratori Nazionali di Frascati, Frascati; Italy.
- ⁵⁴ Physikalisches Institut, Albert-Ludwigs-Universität Freiburg, Freiburg; Germany.
- ⁵⁵ II. Physikalisches Institut, Georg-August-Universität Göttingen, Göttingen; Germany.
- ⁵⁶ Département de Physique Nucléaire et Corpusculaire, Université de Genève, Genève; Switzerland.
- ⁵⁷ ^(a) Dipartimento di Fisica, Università di Genova, Genova; ^(b) INFN Sezione di Genova; Italy.
- ⁵⁸ II. Physikalisches Institut, Justus-Liebig-Universität Giessen, Giessen; Germany.
- ⁵⁹ SUPA - School of Physics and Astronomy, University of Glasgow, Glasgow; United Kingdom.
- ⁶⁰ LPSC, Université Grenoble Alpes, CNRS/IN2P3, Grenoble INP, Grenoble; France.
- ⁶¹ Laboratory for Particle Physics and Cosmology, Harvard University, Cambridge MA; United States of America.
- ⁶² Department of Modern Physics and State Key Laboratory of Particle Detection and Electronics, University of Science and Technology of China, Hefei; China.
- ⁶³ ^(a) Kirchhoff-Institut für Physik, Ruprecht-Karls-Universität Heidelberg, Heidelberg; ^(b) Physikalisches Institut, Ruprecht-Karls-Universität Heidelberg, Heidelberg; Germany.
- ⁶⁴ ^(a) Department of Physics, Chinese University of Hong Kong, Shatin, N.T., Hong Kong; ^(b) Department of Physics, University of Hong Kong, Hong Kong; ^(c) Department of Physics and Institute for Advanced Study, Hong Kong University of Science and Technology, Clear Water Bay, Kowloon, Hong Kong; China.
- ⁶⁵ Department of Physics, National Tsing Hua University, Hsinchu; Taiwan.
- ⁶⁶ IJCLab, Université Paris-Saclay, CNRS/IN2P3, 91405, Orsay; France.
- ⁶⁷ Centro Nacional de Microelectrónica (IMB-CNM-CSIC), Barcelona; Spain.
- ⁶⁸ Department of Physics, Indiana University, Bloomington IN; United States of America.
- ⁶⁹ ^(a) INFN Gruppo Collegato di Udine, Sezione di Trieste, Udine; ^(b) ICTP, Trieste; ^(c) Dipartimento Politecnico di Ingegneria e Architettura, Università di Udine, Udine; Italy.
- ⁷⁰ ^(a) INFN Sezione di Lecce; ^(b) Dipartimento di Matematica e Fisica, Università del Salento, Lecce; Italy.
- ⁷¹ ^(a) INFN Sezione di Milano; ^(b) Dipartimento di Fisica, Università di Milano, Milano; Italy.
- ⁷² ^(a) INFN Sezione di Napoli; ^(b) Dipartimento di Fisica, Università di Napoli, Napoli; Italy.
- ⁷³ ^(a) INFN Sezione di Pavia; ^(b) Dipartimento di Fisica, Università di Pavia, Pavia; Italy.
- ⁷⁴ ^(a) INFN Sezione di Pisa; ^(b) Dipartimento di Fisica E. Fermi, Università di Pisa, Pisa; Italy.
- ⁷⁵ ^(a) INFN Sezione di Roma; ^(b) Dipartimento di Fisica, Sapienza Università di Roma, Roma; Italy.
- ⁷⁶ ^(a) INFN Sezione di Roma Tor Vergata; ^(b) Dipartimento di Fisica, Università di Roma Tor Vergata, Roma; Italy.
- ⁷⁷ ^(a) INFN Sezione di Roma Tre; ^(b) Dipartimento di Matematica e Fisica, Università Roma Tre, Roma; Italy.

- ⁷⁸(*a*) INFN-TIFPA; (*b*) Università degli Studi di Trento, Trento; Italy.
- ⁷⁹Universität Innsbruck, Department of Astro and Particle Physics, Innsbruck; Austria.
- ⁸⁰University of Iowa, Iowa City IA; United States of America.
- ⁸¹Department of Physics and Astronomy, Iowa State University, Ames IA; United States of America.
- ⁸²Istinye University, Sariyer, Istanbul; Türkiye.
- ⁸³(*a*) Departamento de Engenharia Elétrica, Universidade Federal de Juiz de Fora (UFJF), Juiz de Fora; (*b*) Universidade Federal do Rio De Janeiro COPPE/EE/IF, Rio de Janeiro; (*c*) Instituto de Física, Universidade de São Paulo, São Paulo; (*d*) Rio de Janeiro State University, Rio de Janeiro; (*e*) Federal University of Bahia, Bahia; Brazil.
- ⁸⁴KEK, High Energy Accelerator Research Organization, Tsukuba; Japan.
- ⁸⁵(*a*) Khalifa University of Science and Technology, Abu Dhabi; (*b*) University of Sharjah, Sharjah; United Arab Emirates.
- ⁸⁶Graduate School of Science, Kobe University, Kobe; Japan.
- ⁸⁷(*a*) AGH University of Krakow, Faculty of Physics and Applied Computer Science, Krakow; (*b*) Marian Smoluchowski Institute of Physics, Jagiellonian University, Krakow; Poland.
- ⁸⁸Institute of Nuclear Physics Polish Academy of Sciences, Krakow; Poland.
- ⁸⁹Faculty of Science, Kyoto University, Kyoto; Japan.
- ⁹⁰Research Center for Advanced Particle Physics and Department of Physics, Kyushu University, Fukuoka ; Japan.
- ⁹¹L2IT, Université de Toulouse, CNRS/IN2P3, UPS, Toulouse; France.
- ⁹²Instituto de Física La Plata, Universidad Nacional de La Plata and CONICET, La Plata; Argentina.
- ⁹³Physics Department, Lancaster University, Lancaster; United Kingdom.
- ⁹⁴Oliver Lodge Laboratory, University of Liverpool, Liverpool; United Kingdom.
- ⁹⁵Department of Experimental Particle Physics, Jožef Stefan Institute and Department of Physics, University of Ljubljana, Ljubljana; Slovenia.
- ⁹⁶Department of Physics and Astronomy, Queen Mary University of London, London; United Kingdom.
- ⁹⁷Department of Physics, Royal Holloway University of London, Egham; United Kingdom.
- ⁹⁸Department of Physics and Astronomy, University College London, London; United Kingdom.
- ⁹⁹Louisiana Tech University, Ruston LA; United States of America.
- ¹⁰⁰Fysiska institutionen, Lunds universitet, Lund; Sweden.
- ¹⁰¹Departamento de Física Teórica C-15 and CIAFF, Universidad Autónoma de Madrid, Madrid; Spain.
- ¹⁰²Institut für Physik, Universität Mainz, Mainz; Germany.
- ¹⁰³School of Physics and Astronomy, University of Manchester, Manchester; United Kingdom.
- ¹⁰⁴CPPM, Aix-Marseille Université, CNRS/IN2P3, Marseille; France.
- ¹⁰⁵Department of Physics, University of Massachusetts, Amherst MA; United States of America.
- ¹⁰⁶Department of Physics, McGill University, Montreal QC; Canada.
- ¹⁰⁷School of Physics, University of Melbourne, Victoria; Australia.
- ¹⁰⁸Department of Physics, University of Michigan, Ann Arbor MI; United States of America.
- ¹⁰⁹Department of Physics and Astronomy, Michigan State University, East Lansing MI; United States of America.
- ¹¹⁰Group of Particle Physics, University of Montreal, Montreal QC; Canada.
- ¹¹¹Fakultät für Physik, Ludwig-Maximilians-Universität München, München; Germany.
- ¹¹²Max-Planck-Institut für Physik (Werner-Heisenberg-Institut), München; Germany.
- ¹¹³Graduate School of Science and Kobayashi-Maskawa Institute, Nagoya University, Nagoya; Japan.
- ¹¹⁴(*a*) Department of Physics, Nanjing University, Nanjing; (*b*) School of Science, Shenzhen Campus of Sun Yat-sen University; (*c*) University of Chinese Academy of Science (UCAS), Beijing; China.
- ¹¹⁵Department of Physics and Astronomy, University of New Mexico, Albuquerque NM; United States of

America.

¹¹⁶Institute for Mathematics, Astrophysics and Particle Physics, Radboud University/Nikhef, Nijmegen; Netherlands.

¹¹⁷Nikhef National Institute for Subatomic Physics and University of Amsterdam, Amsterdam; Netherlands.

¹¹⁸Department of Physics, Northern Illinois University, DeKalb IL; United States of America.

¹¹⁹(^a)New York University Abu Dhabi, Abu Dhabi; (^b)United Arab Emirates University, Al Ain; United Arab Emirates.

¹²⁰Department of Physics, New York University, New York NY; United States of America.

¹²¹Ochanomizu University, Otsuka, Bunkyo-ku, Tokyo; Japan.

¹²²Ohio State University, Columbus OH; United States of America.

¹²³Homer L. Dodge Department of Physics and Astronomy, University of Oklahoma, Norman OK; United States of America.

¹²⁴Department of Physics, Oklahoma State University, Stillwater OK; United States of America.

¹²⁵Palacký University, Joint Laboratory of Optics, Olomouc; Czech Republic.

¹²⁶Institute for Fundamental Science, University of Oregon, Eugene, OR; United States of America.

¹²⁷Graduate School of Science, University of Osaka, Osaka; Japan.

¹²⁸Department of Physics, University of Oslo, Oslo; Norway.

¹²⁹Department of Physics, Oxford University, Oxford; United Kingdom.

¹³⁰LPNHE, Sorbonne Université, Université Paris Cité, CNRS/IN2P3, Paris; France.

¹³¹Department of Physics, University of Pennsylvania, Philadelphia PA; United States of America.

¹³²Department of Physics and Astronomy, University of Pittsburgh, Pittsburgh PA; United States of America.

¹³³(^a)Laboratório de Instrumentação e Física Experimental de Partículas - LIP, Lisboa; (^b)Departamento de Física, Faculdade de Ciências, Universidade de Lisboa, Lisboa; (^c)Departamento de Física, Universidade de Coimbra, Coimbra; (^d)Centro de Física Nuclear da Universidade de Lisboa, Lisboa; (^e)Departamento de Física, Escola de Ciências, Universidade do Minho, Braga; (^f)Departamento de Física Teórica y del Cosmos, Universidad de Granada, Granada (Spain); (^g)Departamento de Física, Instituto Superior Técnico, Universidade de Lisboa, Lisboa; Portugal.

¹³⁴Institute of Physics of the Czech Academy of Sciences, Prague; Czech Republic.

¹³⁵Czech Technical University in Prague, Prague; Czech Republic.

¹³⁶Charles University, Faculty of Mathematics and Physics, Prague; Czech Republic.

¹³⁷Particle Physics Department, Rutherford Appleton Laboratory, Didcot; United Kingdom.

¹³⁸IRFU, CEA, Université Paris-Saclay, Gif-sur-Yvette; France.

¹³⁹Santa Cruz Institute for Particle Physics, University of California Santa Cruz, Santa Cruz CA; United States of America.

¹⁴⁰(^a)Departamento de Física, Pontificia Universidad Católica de Chile, Santiago; (^b)Millennium Institute for Subatomic physics at high energy frontier (SAPHIR), Santiago; (^c)Instituto de Investigación Multidisciplinario en Ciencia y Tecnología, y Departamento de Física, Universidad de La Serena; (^d)Universidad Andres Bello, Department of Physics, Santiago; (^e)Universidad San Sebastian, Recoleta; (^f)Instituto de Alta Investigación, Universidad de Tarapacá, Arica; (^g)Departamento de Física, Universidad Técnica Federico Santa María, Valparaíso; Chile.

¹⁴¹Department of Physics, Institute of Science, Tokyo; Japan.

¹⁴²Department of Physics, University of Washington, Seattle WA; United States of America.

¹⁴³(^a)Institute of Frontier and Interdisciplinary Science and Key Laboratory of Particle Physics and Particle Irradiation (MOE), Shandong University, Qingdao; (^b)School of Physics, Zhengzhou University; China.

¹⁴⁴(^a)State Key Laboratory of Dark Matter Physics, School of Physics and Astronomy, Shanghai Jiao Tong

University, Key Laboratory for Particle Astrophysics and Cosmology (MOE), SKLPPC, Shanghai;^(b)State Key Laboratory of Dark Matter Physics, Tsung-Dao Lee Institute, Shanghai Jiao Tong University, Shanghai; China.

¹⁴⁵Department of Physics and Astronomy, University of Sheffield, Sheffield; United Kingdom.

¹⁴⁶Department of Physics, Shinshu University, Nagano; Japan.

¹⁴⁷Department Physik, Universität Siegen, Siegen; Germany.

¹⁴⁸Department of Physics, Simon Fraser University, Burnaby BC; Canada.

¹⁴⁹SLAC National Accelerator Laboratory, Stanford CA; United States of America.

¹⁵⁰Department of Physics, Royal Institute of Technology, Stockholm; Sweden.

¹⁵¹Departments of Physics and Astronomy, Stony Brook University, Stony Brook NY; United States of America.

¹⁵²Department of Physics and Astronomy, University of Sussex, Brighton; United Kingdom.

¹⁵³School of Physics, University of Sydney, Sydney; Australia.

¹⁵⁴Institute of Physics, Academia Sinica, Taipei; Taiwan.

¹⁵⁵^(a)E. Andronikashvili Institute of Physics, Iv. Javakhishvili Tbilisi State University, Tbilisi;^(b)High Energy Physics Institute, Tbilisi State University, Tbilisi;^(c)University of Georgia, Tbilisi; Georgia.

¹⁵⁶Department of Physics, Technion, Israel Institute of Technology, Haifa; Israel.

¹⁵⁷Raymond and Beverly Sackler School of Physics and Astronomy, Tel Aviv University, Tel Aviv; Israel.

¹⁵⁸Department of Physics, Aristotle University of Thessaloniki, Thessaloniki; Greece.

¹⁵⁹International Center for Elementary Particle Physics and Department of Physics, University of Tokyo, Tokyo; Japan.

¹⁶⁰Graduate School of Science and Technology, Tokyo Metropolitan University, Tokyo; Japan.

¹⁶¹Department of Physics, University of Toronto, Toronto ON; Canada.

¹⁶²^(a)TRIUMF, Vancouver BC;^(b)Department of Physics and Astronomy, York University, Toronto ON; Canada.

¹⁶³Division of Physics and Tomonaga Center for the History of the Universe, Faculty of Pure and Applied Sciences, University of Tsukuba, Tsukuba; Japan.

¹⁶⁴Department of Physics and Astronomy, Tufts University, Medford MA; United States of America.

¹⁶⁵Department of Physics and Astronomy, University of California Irvine, Irvine CA; United States of America.

¹⁶⁶University of West Attica, Athens; Greece.

¹⁶⁷Department of Physics and Astronomy, University of Uppsala, Uppsala; Sweden.

¹⁶⁸Department of Physics, University of Illinois, Urbana IL; United States of America.

¹⁶⁹Instituto de Física Corpuscular (IFIC), Centro Mixto Universidad de Valencia - CSIC, Valencia; Spain.

¹⁷⁰Department of Physics, University of British Columbia, Vancouver BC; Canada.

¹⁷¹Department of Physics and Astronomy, University of Victoria, Victoria BC; Canada.

¹⁷²Fakultät für Physik und Astronomie, Julius-Maximilians-Universität Würzburg, Würzburg; Germany.

¹⁷³Department of Physics, University of Warwick, Coventry; United Kingdom.

¹⁷⁴Waseda University, Tokyo; Japan.

¹⁷⁵Department of Particle Physics and Astrophysics, Weizmann Institute of Science, Rehovot; Israel.

¹⁷⁶Department of Physics, University of Wisconsin, Madison WI; United States of America.

¹⁷⁷Fakultät für Mathematik und Naturwissenschaften, Fachgruppe Physik, Bergische Universität Wuppertal, Wuppertal; Germany.

¹⁷⁸Department of Physics, Yale University, New Haven CT; United States of America.

¹⁷⁹Yerevan Physics Institute, Yerevan; Armenia.

^a Also at Affiliated with an institute formerly covered by a cooperation agreement with CERN.

^b Also at An-Najah National University, Nablus; Palestine.

^c Also at Borough of Manhattan Community College, City University of New York, New York NY; United States of America.

^d Also at Center for Interdisciplinary Research and Innovation (CIRI-AUTH), Thessaloniki; Greece.

^e Also at Centre of Physics of the Universities of Minho and Porto (CF-UM-UP); Portugal.

^f Also at CERN, Geneva; Switzerland.

^g Also at Département de Physique Nucléaire et Corpusculaire, Université de Genève, Genève; Switzerland.

^h Also at Departament de Física de la Universitat Autònoma de Barcelona, Barcelona; Spain.

ⁱ Also at Department of Financial and Management Engineering, University of the Aegean, Chios; Greece.

^j Also at Department of Mathematical Sciences, University of South Africa, Johannesburg; South Africa.

^k Also at Department of Modern Physics and State Key Laboratory of Particle Detection and Electronics, University of Science and Technology of China, Hefei; China.

^l Also at Department of Physics, Bolu Abant İzzet Baysal University, Bolu; Türkiye.

^m Also at Department of Physics, King's College London, London; United Kingdom.

ⁿ Also at Department of Physics, Stanford University, Stanford CA; United States of America.

^o Also at Department of Physics, Stellenbosch University; South Africa.

^p Also at Department of Physics, University of Fribourg, Fribourg; Switzerland.

^q Also at Department of Physics, University of Thessaly; Greece.

^r Also at Department of Physics, Westmont College, Santa Barbara; United States of America.

^s Also at Faculty of Physics, Sofia University, 'St. Kliment Ohridski', Sofia; Bulgaria.

^t Also at Faculty of Physics, University of Bucharest; Romania.

^u Also at Hellenic Open University, Patras; Greece.

^v Also at Henan University; China.

^w Also at Imam Mohammad Ibn Saud Islamic University; Saudi Arabia.

^x Also at Institutio Catalana de Recerca i Estudis Avancats, ICREA, Barcelona; Spain.

^y Also at Institut für Experimentalphysik, Universität Hamburg, Hamburg; Germany.

^z Also at Institute for Nuclear Research and Nuclear Energy (INRNE) of the Bulgarian Academy of Sciences, Sofia; Bulgaria.

^{aa} Also at Institute of Applied Physics, Mohammed VI Polytechnic University, Ben Guerir; Morocco.

^{ab} Also at Institute of Particle Physics (IPP); Canada.

^{ac} Also at Institute of Physics and Technology, Mongolian Academy of Sciences, Ulaanbaatar; Mongolia.

^{ad} Also at Institute of Physics, Azerbaijan Academy of Sciences, Baku; Azerbaijan.

^{ae} Also at Institute of Theoretical Physics, Ilija State University, Tbilisi; Georgia.

^{af} Also at Millennium Institute for Subatomic physics at high energy frontier (SAPHIR), Santiago; Chile.

^{ag} Also at National Institute of Physics, University of the Philippines Diliman (Philippines); Philippines.

^{ah} Also at The Collaborative Innovation Center of Quantum Matter (CICQM), Beijing; China.

^{ai} Also at TRIUMF, Vancouver BC; Canada.

^{aj} Also at Università di Napoli Parthenope, Napoli; Italy.

^{ak} Also at University of Chinese Academy of Sciences (UCAS), Beijing; China.

^{al} Also at University of Colorado Boulder, Department of Physics, Colorado; United States of America.

^{am} Also at University of Siena; Italy.

^{an} Also at Washington College, Chestertown, MD; United States of America.

^{ao} Also at Yeditepe University, Physics Department, Istanbul; Türkiye.

* Deceased